EFFECT OF SUBSTRATE MATERIAL AND ROUGHNESS ON THE PROPERTIES OF Mg AZ31-B ALLOY CAST ON HORIZONTAL SINGLE BELT CASTING SIMULATOR

AHMAD CHANGIZI

A Thesis

in

The Department

of

Mechanical and Industrial Engineering

Presented in Partial Fulfillment of the Requirements

for the Degree of Master of Applied Science (Mechanical Engineering) at

Concordia University

Montreal, Quebec, Canada

June 2009

Library and Archives
Canada

Published Heritage
Branch

395 Wellington Street
Ottawa ON K1A 0N4
Canada

Bibliothèque et
Archives Canada

Direction du
Patrimoine de l'édition

395, rue Wellington
Ottawa ON K1A 0N4
Canada

NOTICE:

The author has granted a non-
exclusive license allowing Library and
Archives Canada to reproduce,
publish, archive, preserve, conserve,
communicate to the public by
telecommunication or on the Internet,
loan, distribute and sell theses
worldwide, for commercial or non-
commercial purposes, in microform,
paper, electronic and/or any other
formats.

The author retains copyright
ownership and moral rights in this
thesis. Neither the thesis nor
substantial extracts from it may be
printed or otherwise reproduced
without the author's permission.

AVIS:

L'auteur a accordé une licence non exclusive
permettant à la Bibliothèque et Archives
Canada de reproduire, publier, archiver,
sauvegarder, conserver, transmettre au public
par télécommunication ou par l'Internet, prêter,
distribuer et vendre des thèses partout dans le
monde, à des fins commerciales ou autres, sur
support microforme, papier, électronique et/ou
autres formats.

L'auteur conserve la propriété du droit d'auteur
et des droits moraux qui protège cette thèse. Ni
la thèse ni des extraits substantiels de celle-ci
ne doivent être imprimés ou autrement
reproduits sans son autorisation.

In compliance with the Canadian
Privacy Act some supporting forms
may have been removed from this
thesis.

While these forms may be included
in the document page count, their
removal does not represent any loss
of content from the thesis.

Conformément à la loi canadienne sur la
protection de la vie privée, quelques
formulaires secondaires ont été enlevés de
cette thèse.

Bien que ces formulaires aient inclus dans
la pagination, il n'y aura aucun contenu
manquant.

Canada

Abstract

Effect of Substrate Material and Roughness on the Properties of Mg AZ31-B Alloy Cast on Horizontal Single belt Casting Simulator

Ahmad Changizi

Strips of magnesium alloy AZ31-B were cast on a single belt casting simulator with moving-mold system. A mixture of carbon dioxide (CO_2) and sulfur hexafluoride (SF_6) gases was used as a protective gas during melting and casting of the magnesium alloy. The castability of the magnesium alloy strips was investigated for different types of substrates: smooth low carbon steel substrate, copper with six different roughnesses, graphite-coated smooth steel and graphite-coated copper with different roughnesses. Moreover, the effect of strip thickness on the casting properties were investigated. The heat flux through the copper substrate was higher than that through the steel substrate, while coated substrates showed lower heat fluxes than the uncoated substrates. The highest heat flux was recorded for the grooved (rough) substrate with 0.15 mm depth, while further increasing the surface roughness (depth) resulted in a decrease in the heat flux. Decreasing the heat flux reduced the quality of the top surface of the strips. However, as the thickness of the strip decreased, although the heat flux decreased, the quality of the top surface increased. As the heat flux increased, the grain sizes of the strips were reduced while the secondary arm spacing (SDAS) decreased. The mechanical properties, TS, YS and HV increased when the heat flux increased. Although magnesium oxide normally appears in white, the black color of the outer MgO layer of the strips formed under unprotected conditions is due to the presence of sub-micron MgO particles.

Acknowledgements

I would like to dedicate this thesis to my parents and especially my father whom I wish had lived long enough to see this day. His memories will always be with me. I would not have been able to complete my study without the encouragements and emotional supports from my parents.

I wish to express here my deep and sincere gratitude to my professors: Dr. Mihaiela Isac, and Dr. Mamoun Medraj, for their valuable guidance and encouraging supports during this research.

I would also like to express my gratitude to Prof. R.I.L Guthrie for giving me an opportunity to be a member of his group and also for his valuable scientific support.

I would like to sincerely acknowledge McGill Metal Processing Center (MMPC) for providing the financial support for this work and for providing me access to facilities of laboratory for whole experiments.

I would also like to offer my especial thanks to Prof. Ali Shafyei for his benefited hints in analysis of the casting experiments results.

I would also like to thank my real true friends Dr. Arash Shahryari and Ms. Mahlegha Kazemi for their helps in editing my thesis.

I use this opportunity to appreciate all of my friends and laboratory's staff specially Dr. Donghui Li.

Finally, I would express my love and thanks to my family, my mother and brothers who have always been my great supports for their continuous inspiration and encouragements.

Table of Content

Chapter 1 - INTRODUCTION

Chapter 2 - LITERATURE REVIEW

Chapter 4 - RESULTS AND DISCUSSION

Chapter 5 - CONCLUSION, CONTRIBUTIONS and FUTURE WORK

List of Figures

xvi

List of Tables

INTRODUCTION

1.1. Continuous casting:

In the last forty years, continuous casting has become more and more important due to many economic advantages. Generally, continuous casting processes are used for the production of semi-fabricated strips, form cold rolling to foilstock building sheets and canstock[1]. These processes transfer molten metal alloys directly into a continuous coiled strip suitable for cold rolling or into wire-bars for wire-drawing. Consequently, the capital investment and operational costs are significantly lower than those in a conventional production process[2,3]. Because of higher productivity, continuous casting is the preferred casting method in modern plants. Among the continuous casting technologies, strip casting processes now remarkably account for approximately 30% of the world's output of rolled light metals semi-fabricated coilstock[4].

1.2. Magnesium strip casting:

The main advantage of magnesium compared to other metals is that magnesium has a very low density, 1.74 g/cm^2, which is 30% lower than Al. Another noticeable reason for producing magnesium parts is that magnesium has nearly inexhaustible natural resources. Magnesium alloys normally have very good castability and machinability as well as excellent specific strength and stiffness[5].

Strip casting is a near-net-shape casting process used for a number of years to produce a range of aluminum, copper, zinc and lead alloys. Large-scale production of other important metals is limited, but substantial progress on the pilot-plant scale has been made for magnesium[6,7].

Generally, most metals and alloys are amenable to direct casting into plates, strips or ribbons. However, a metallurgical understanding of these materials is needed to determine their suitability for casting into thin-gauge strips. Technically, the evaluation of a process must take into account the melting point of the alloy, the freezing range, the oxidation resistance in both liquid and solid states, the heat transfer behaviour, the fluidity of the melt and the number and type of the liquid-to-solid and the solid-state transformations, that may occur[1]. There is a particular emphasis on magnesium alloys as these are the major candidates for large-scale production by this processing route[8].

1.3. Objective of the present study:

The present study was carried out to evaluate strip casting of magnesium alloy, AZ31-B using a single belt casting techniques simulator. The main objective of the present thesis is to study the effects of heat flux and thermal contact resistivity of the strip quality.

This study attempted to cover the effect of substrate roughness and materials substrate on heat flux and thermal contact resistivity as well as quality of strip.

Effect of the coating on substrate and thickness of the strip on heat fluxes and thermal contact resistivity was part of this study.

This study also includes evaluating the quality, and mechanical behavior of magnesium AZ31-B alloy strips produced using horizontal single belt casting (HSBC) technique.

LITERATURE REVIEW

2.1. History of magnesium:

The history of elementary magnesium started when, in 1755, Joseph Black, a Scottish

chemist, discovered that magnesia contained a new element, magnesium. Black was not

able to isolate the metal. Magnesia was called "white stone" or "white earth". Sir

Humphrey Davy, the British chemist, isolated the metal in 1808, and has been honored as

the discoverer. Davy used a voltaic cell and a mercury cathode to decompose wet

magnesium sulphate by electrolysis. Antoine Alexandre Brutun Bussy isolated the metal

by fusing dehydrated magnesium chloride with potassium at elevated temperatures. Then

the former assistant to Sir Humphrey, Michael Faraday, obtained pure metallic

magnesium in 1833, by reducing dehydrated magnesium chloride by electrolysis.

Commercial production of magnesium by electrolysis is credited to Robert Bunsen, the

German scientist, who made a small laboratory cell for the electrolysis of fused

magnesium chloride in 1852 [5,9].

Germany was the only producer of magnesium in the world, in 1868. Commercial

electrolytic magnesium began in Germany in 1886, by using a modification of Bunsen's

cell. The Aluminum and Magnesium Farbik, Hemelingen (Germany) designed and built a plant for the dehydration and electrolysis of molten carnallite. In 1896, this process was further developed by Chemische Fabrik Griesheim-Elektron, who transferred the process to its Bitterfeld works and became the only magnesium producer in the world until 1916 [10]. Extraction remained based on electrolysis and thermal reductions were made such refinements as the internal heating of retorts which introduced in France in 1961. Extraction from dehydrated magnesium chloride prills introduced by the Norwegian company Norsk Hydro in 1974 [5,10].

Further developments varied considerably in different parts of the word[11].

2.1.1. Magnesium producers:

In early 2007, U.S. magnesium producer in Utah, Magcorp Company, announced that it would elevate its production capacity from 43,000 tons per year to more than 50,000 tons per year, while this increase in the production capacity would begin in the fourth quarter of 2007. Currently, the magnesium production capacity has reached approximately to 50,000 tons per year (by January 2009). The company had begun the construction of new electrolytic cells in 2004, but had not completed the expansion because of market conditions. The U.S. magnesium producer had signed a two year agreement, beginning in January 2008, to supply one of the U.S. automobile manufacturers with magnesium ingot for its North American parts production[10].

The Dow Chemical Company, producing 95 000 tons/year, is the largest in the U.S. located in Texas. Dow uses magnesium chloride as feedstock for the plant, derived from a seawater dolomite process[10,11].

China produced 700,000 tons of primary magnesium in 2008, compared to 627,000 tons in 2007, which is equivalent to a 11.64% increase in its production capacity. The growth rate, which saw an increase in 2006, continues the rising trend. Henan, Nigxian, Shanxi and Inner Mongolia are still the leading magnesium production based in China. However, due to the recent economical melt down and recession, the magnesium production cost has outweighed the market price and has thus resulted in a considerable cutoff in the production capacity. For instance, Taiyuan Yiwei Magnesium Industry Co. Ltd. (Taiyuan City, Shanxi Province, China), which is one of China's largest magnesium producers (capacity of 80,000 tons per year), decreased its production to about 12,000 tons/year, reported in November 2008 by Shair and McBeth[12,13].

Ube Industries Ltd, the last magnesium producer of Japan, stopped producing magnesium in its 8500-t/y plant in 1994, and started to import cheap supplies from China and Russia. This was the main reason for the closure. The high cost of electricity in Japan also affected Ube's competitiveness. The 17-year-old plant used the Pidgeon silicothermic process to produce magnesium. Ube also imported magnesium from Timminco of Canada and Norsk Hydro of Norway to continue supplying its customers[5,14].

2.2. Properties of pure magnesium

2.2.1. Physical properties of pure magnesium:

Pure magnesium is mainly used as an alloying element in aluminum, for steel desulphurization, for the production of nodular cast iron, as a reducing agent in titanium and zirconium production, and as a chemical in various processes. Table 2.1 lists some important physical properties of pure magnesium[5,9].

Table 2.1. Physical properties of pure magnesium (99.9 wt%)[5]

Property	Value
Melting point	$650^{\circ}C \pm 2$
Boiling point	$1107^{\circ}C \pm 10$
Latent heat of fusion	0.37 MJ/kg
Latent heat of evaporation	5.25 MJ/kg
Heat of combustion	25.1 MJ/kg
Specific heat	
at $20^{\circ}C$	1030 J/(kg K)
at $600^{\circ}C$	1178J/(kg K)
Electrical resistivity at $20^{\circ}C$	4.45 $\mu\Omega$ cm
Thermal conductivity at $25^{\circ}C$	155W/(kg K)
Linear coefficient of thermal expansion at $20^{\circ}C$	25.2×10^{-6} K^{-1}
Density	
at $20^{\circ}C$	1.738 g/cm^3
at $600^{\circ}C$	1.622 g/cm^3
at $650^{\circ}C$ (solid)	1.65 g/cm^3
at $650^{\circ}C$ (liquid)	1.58 g/cm^3
Volume change during solidification	4.2%
Volume change during cooling 650-$20^{\circ}C$	5%

Pure magnesium has a hexagonal crystal structure with lattice parameters a = 0.32092 nm and c = 0.52105 nm. The ideal c:a ratio for close-packed spheres is 1.633. For

magnesium at room temperature, the value is 1.6236. This shows that magnesium has a nearly perfect close-packed hexagonal structure with an atomic diameter of 0.32 nm[9].

2.2.2. Mechanical properties of pure magnesium:

Pure magnesium, 99.8 %, is used as ingot for remelting, and is used as powder, ribbon, wire, and extruded and rolled strip. Magnesium alloys are produced in several forms such as casting, sheet and plate, shapes, forgings, bars, and rods[15].

In sheet form, it is fabricated into many different articles by drawing, spinning or casting. Magnesium alloys are especially workable by hot forming methods. Structures are readily assembled by welding or riveting[17,18]. The excellent machinability of magnesium alloys has been reported. Parts composed of magnesium alloys can be machined at higher speeds and at lower costs than is the case in most other common metals. Table 2.2 lists some mechanical properties of magnesium AZ31 alloy versus steel[5,19,20].

Table 2.2. Mechanical properties of AZ31 alloy[5]

	Tensile strength MPa	Tensile yield strength MPa	Compressive yield stress MPa	Elongation 50mm	Brinell hardness 500kp/10 mm
Hard rolled Magnesium thickness 10 mm	290	220	180	15	73
Annealed Magnesium thickness 10 mm	255	150	110	21	56
Hard rolled steel	565	550	530	34	136
Annealed steel	385	285	280	37	111

2.3. Applications of magnesium alloys:

The Volkswagen Beetle used large magnesium alloy die-castings for the crankcase and the transmission housing. This car still contains around 20 kg of magnesium alloy. Volkswagen casts nearly 50,000 tons of magnesium each year[21].

Many applications of magnesium alloys that were developed during World War II could not be quickly converted to civilian uses. It was useful in aircraft wheels and aircraft engine casings, which could be modified for civilian industries[22]. Samsonite luggage was a very large user of magnesium sheet and extrusions. The original Samsonite hard luggage had a deep-drawn magnesium sheet for both sides and the frames were made of extruded magnesium[23]. Dow developed products for the magnesium sheet that it rolled. The Met Lab also designed alloy compositions to exploit the properties of magnesium for some industrial uses. Magnesium sheet was used on many rockets, including the Vanguard, Jupiter, Titan 1, Polaris, Thor-able Star, and the Atlas Agena. Moreover, the Dow group built Metro-Lite delivery bodies on an International truck frame. The floor and roof rails were 3.96 mm-thick magnesium sheet. The dent resistance of magnesium is higher than that of other metals used in construction. Magnesium sheeting for lithographic printing has been a mainstay of the magnesium sheet business[24].

2.3.1. Magnesium alloys in the automotive industry:

Magnesium has excellent mechanical and physical properties. It has a high specific strength and superior damping capacity. Magnesium alloys have a high potential for use as structural materials[25]. Previously, in order to reduce vehicle weight, aluminum was

the first choice for the automotive industry. However, when the price of magnesium fell, the automotive industry considered this light metal as a possible alternative[13]. Recently, the demand for low-cost magnesium sheet materials has significantly increased in the automotive and electronic industries[24]. Magnesium sheet metal components have great potential for application to automotive bodies. Generally, the automotive body makes up almost 25% of the vehicle weight and consists completely of sheet metal parts. Hence, the replacement of conventional sheet alloys by magnesium sheets would lead to considerable weight reduction[26,27].

Many parts of automobiles are made from magnesium: the steering column upper brackets, steering wheel cores, engine head cover, disk wheels, brake pedal brackets, meter panel housings, seat frames, air bag plates, oil pans, instrument panel reinforcement, and transmission cases[26].

2.3.2. Magnesium casting alloys in the automotive industry:

Currently, alloys made mostly of magnesium are produced by die casting for automotive applications. Volkswagen manufactured air-cooled engines and gearboxes housing with magnesium alloys AS41 and AZ81 in the 1970s, and they produced a gearbox housing made of AZ91 in 1990s. Moreover, the alloys AM50, AM60 and AZ91 are still being used to produce the interior components in the automotive industries[21,28].

2.3.3. Magnesium-wrought alloys in the automotive industry:

Wrought alloys account for 10-15% of all magnesium alloys despite their poor workability. The hot forming processes include rolling, extrusion, and forging are

10

performed at temperatures higher than 300°C – 350°C but below 500°C. Magnesium cold work forming is limited to prevent cracking.

Magnesium-wrought alloys come in seven different grades with approximately fifteen different chemistries. Typical extrusion grades include AZ80, ZK21, ZK60, ZC71, ZM21, ZM61, AZ21X1 and AZ31. The grades used for rolling are the following: AZ31, ZE10, ZM21, HM21, HK31, or ZK31. The following alloys are mainly used for forging: AZ80, ZK60, AZ61, and HM21[17,29,30].

2.3.3.1. Sheet alloys: AZ31 is the most common magnesium alloy for sheet production [24,26,31]. Volkswagen has produced a demonstrator hood from 1.3 mm Mg-sheet (inner) and 1.1mm Al-sheet (outer)[30].

2.3.3.2. Extrusion alloys: AZ31 is a major commercial extrusion alloy[30]. It could be possible to produce parts with a wall thickness of around 1.5 mm, depending on the section geometry. AZ61 and AZ80 because of higher level of aluminum have a higher strength than the AZ31 alloy. Recently, ZK60 with relatively high Zr-content resulting in high strength has been designed for car and bicycle applications. Due to much lower extrusion speeds for AZ61 and AM50 alloys, the production of tubing from these alloys is more expensive than that from AZ31[32]. It should be noted that magnesium extrusion parts are much more expensive than parts made from other materials and the maximum extrusion speed of the 6063 aluminum alloy is about twice the speed of AZ31. In order to have a good balance of strength, ductility, extrudability, and corrosion resistance, the extrusion alloy, AM30 (Mg-3%Al-0.4%Mn), was developed at GM[33,34]. Table 2.3

summarizes the potential application of wrought-magnesium components in automotive

interiors and body and chassis areas[33,35,36].

Table.2.3. Potential automotive application of wrought-magnesium components[33]

System	Component	Note
Interior	Instrument panel	Extrusion
	Seat components	Extrusion
	Trim plate	Sheet
Body	Body Door inner	Sheet
	Tailgate/liftgate inner	Sheet
	Roof frame	Extrusion
	Sunroof panel	Sheet
	Bumper beam	Extrusion
	Radiator support	Extrusion
	Shotgun	Sheet/extrusion
	A and B pillar	Sheet
	Decklid/hood inner	Sheet
	Hood outer/fender	Sheet
	Decklid/door outer	Sheet
	Dash panel	Sheet
	Frame rail	Extrusion
Chassis	Chassis Wheel	Forging
	Engine cradle	Extrusion
	Subframe	Extrusion
	Control arm	Forging

2.4. Processing of continuous casting:

Continuous strip casting has proved useful for the production of foil stock and strips for

deep-drawing processes. Magnesium alloys strips in a width of 700 mm and thicknesses

ranging from 4.5 to 7 mm have already been produced in weights of over four tones on a

pilot line[37].

Figure 2.1 represents the main aspect of continuous casting processes. Molten metal

exiting the nozzle, solidifies during its passage between the two drums, leaving them as a

strip. After casting, the strip is rolled directly. In the mass production of collapsible tubes

12

and rigid cans, the machines for the blanking of slugs or for extrusion are placed directly after the casting machines[37,38].
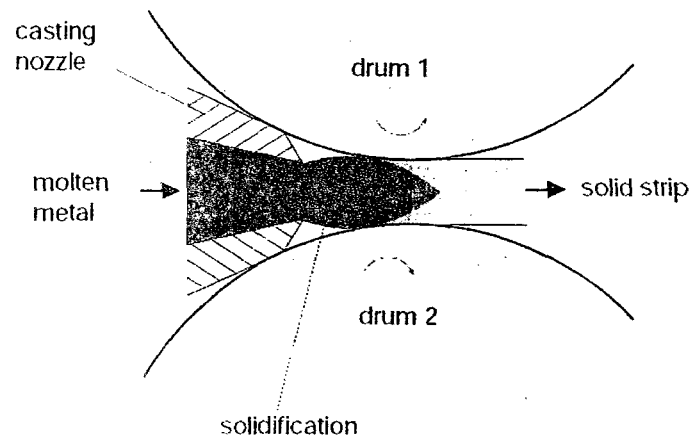
Figure.2.1 - Principle of Continuous Casting (for a twin drum caster)[38]

Direct Chill, known as DC, is the conventional method of producing rolling slabs in continuous casting. However, some slabs are produced using permanent moulds on a semi continuous basis. After DC casting, the rolling slabs are re-heated and hot rolled to a coilable thickness between 4 mm and 6 mm[38]. When continuous casting is used, it is possible to eliminate several production steps which are commonly involved in the production of the strip or foil using conventional technologies.

2.4.1. Conventional technology:

```
              ┌──────────────────┐
              │  Heat treatment  │
              └──────────────────┘
                       │
                       ▼
┌──────────┐    ┌──────────────┐    ┌─────────────┐    ┌──────────┐    ┌──────────────┐
│ Melting  │──▷ │  DC casting  │──▷ │ Hot rolling │──▷ │ Coiling  │──▷ │ Cold rolling │
└──────────┘    └──────────────┘    └─────────────┘    └──────────┘    └──────────────┘
                                                                              │
                                                                              ▼
                                                                    ┌──────────────────┐
                                                                    │  Foil or canstock │
                                                                    └──────────────────┘
```
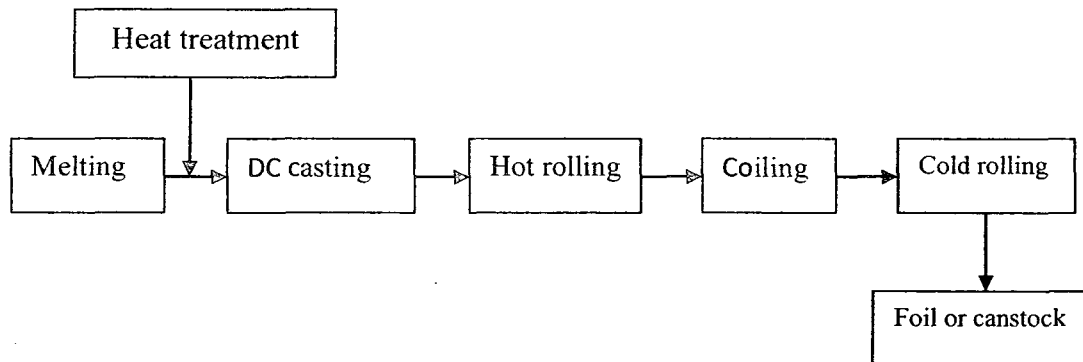
Figure 2.2 - Conventional technology for Mg alloys casting

In the conventional process of magnesium-alloy casting (Figure 2.2), the metal is direct chill-cast in the form of slabs. Then the slabs are homogenized at 400°C to 500°C for up to 2 hours. The slabs are scalped to a depth of about 3mm to achieve a smooth clean surface. The slabs are rolled to less than 1mm. Each step in the rolling reduces about 10% to 20% of the thickness of the strip. The rough hot-rolling process temperature range is between 400°C and 460°C. Hot rolling achieves a considerable reduction of about 20% in each pass. The final product thickness in rough hot rolling is about 5mm. Due to their low heat capacity, the slabs of magnesium alloys are reheated between passes. Because of the short preheating of the ingot before hot rolling, less energy is required. But, this process reduces the speed of production and so increases the price of magnesium sheets[39,40].

In order to reduce a flat plate to a strip about 1mm thick, rough hot rolling is followed by intermediate hot rolling, which is processed at 340 to 430°C. To keep the temperature of a slab above 340°C, reheating is performed after each pass. To achieve a final thickness of about 0.5 mm, the intermediate hot rolling, the warm rolling (from 190 to 400°C) or the cold rolling, is followed by the finish rolling. According to the intended application, a

14

rolled magnesium alloy sheet can be annealed. The final annealing may be tempered by heating to about 370°C for one hour, or a H24 temper that requires heating to about 260°C for one hour[39,40].

2.4.2. Continuous casting technology:

```
┌─────────┐     ┌──────────────┐     ┌─────────┐     ┌──────────────┐
│ Melting │ ──▷ │ Strip casting│ ──▷ │ Coiling │ ──▷ │ Cold rolling │
└─────────┘     └──────────────┘     └─────────┘     └──────────────┘
                                                             │
                                                             ▼
                                                     ┌──────────────┐
                                                     │   Foil or    │
                                                     │   Canstock   │
                                                     └──────────────┘
```
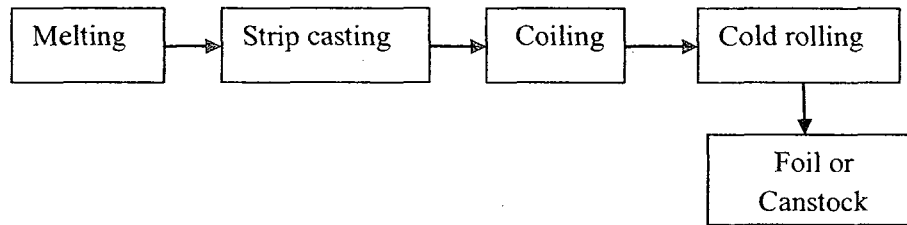
Figure 2.3 - Coutinouus casting technology for Mg alloys production

Continuous casting (Figure 2.3) allows for the skipping of certain production stages. Thus the processing costs are only a third to a half as high as those of traditional casting. Moreover, the investment costs are only a quarter to a third as high. Additionally, smaller spaces and labor requirements reinforce the cost advantages of continuous casting technology. The productivity is 15-20% higher and the material used is 1.5-2% less. Recent developments allows for production of very thin strips with less than 3 mm in thickness. This technology leads to production of strips via fewer rolling stages[41].

Technically, the ability to continuously cast a "semi finished" product close to near net shape minimizes the number of subsequent downstream operations required to produce the finished product. The quality of the semi finished product and its continuous production can significantly improve the production yield.

Commercially, the improved yield and reduced number of operations lowers the cost of production. Also the ability to continuous cast semi finished products can provide independence from outside suppliers, avoidance of extended delivery lead-times and close control of metal product quality.

When considering the specific production of precious metal medallions and coins where a fine grained, uniform, metal structure is requirement, the thickness of the "as cast" strip is determined by the reduction process deemed necessary to achieve the required metallurgical structure in the coinage strip.

The other serious disadvantage of continuous casting technology is that difficulties exist in casting alloys with high alloy content. There is a risk that cracks occur in the strip because of the wide freezing range of these alloys. This cracking is due to the fact that if the solidification of the melt does not happen at an early stage on the substrate, prior to the rolling process, all the metal is solidified at the rolling stage and liquid or semisolid metal can leave the casting substrate. With a lower casting rate, it is possible to avoid this problem, but, if the casting rate is too low, it is possible to have solidification in the direction of the casting nozzle. Generally, the casting rate of alloys is lower than that of commercially pure metal[42].

Continuously cast strips; inherently have a relatively large grain size. If there is insufficient reduction and recrystallisation of these grains during the processing of the strip defects will be apparent either at blanking or coining.

Therefore, only low element alloys, such as AZ31, ZE10, ZM21, HM21, HK31, and ZK31 can be cast. Other examples for this category of castable alloys are series 3000

AlMn alloy (max. 2% Mn) and series 5000 AlMg alloy (max. 2 to 3% Mg). Usually various strip casting technologies are categorized according to the physical dimensions of the finished product. Generally, the dimensions of strip casting for wide and narrow strips are 800-2150 mm[38].

2.4.3. Distinguishing features of continuous casting technologies:

The continuous casting technologies can be divided into horizontal and vertical casting direction methods. Moreover, on the basis of the mould type, it can be divided into fixed and mobile-wall mould processes. In the case of mobile-wall mould, the walls move with the molten metal. Fixed-wall moulds are not used in industrial production. Five types of casters for continuous casting of light metals are extensively used in industry. Most of them are used to produce aluminum and magnesium alloy strips or slabs[40,43].

2.4.3.1. Twin drum caster:

Figures 2.1 and 2.4 illustrate the twin drum caster, which has suitable commercial application for the production of foil stock. Immediately after leaving the casting nozzle, due to the contact with the water-cooled rolls, the molten metal solidifies. A homogeneous distribution of the melt must already occur in the casting nozzle. The casting direction can be horizontal or vertical. The solidification zone is 10 mm to 20 mm long and is started by a zone of hot rolling in the same gap. All such methods are in fact roll casting processes because the strip thickness can be reduced from 5% to 20% in situ by hot rolling[38,42,43].
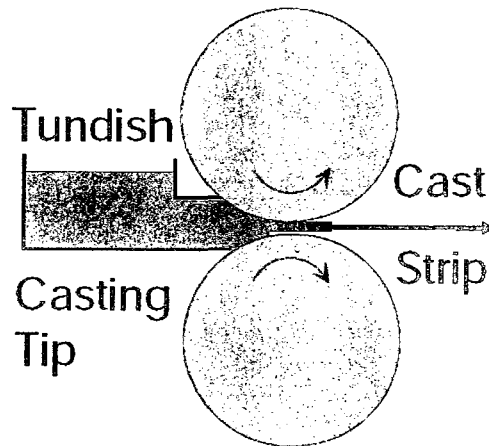
Figure.2.4 - Twin drum caster with horizontal casting direction[38]

2.4.3.2. Single drum casters:

Figure 2.5 shows a schematic of a single drum caster. Molten metal is delivered to the surface of a rotating drum, which is internally cooled by water. The molten metal is pulled onto the surface of the drum to form a thin strip of metal; it cools upon contact with the surface of the drum[38.45].
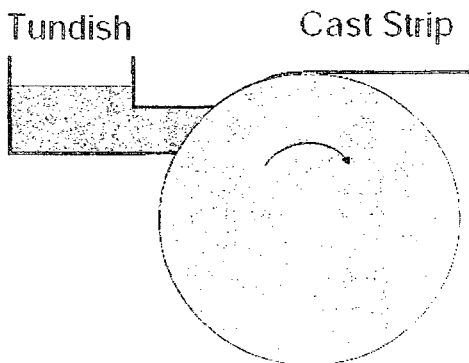
Figure.2.5 - Single drum caster[38]

2.4.3.3. Twin belt slab casting:

In this equipment, two moving thin metal belts are provided and create a moving mould for the metal to be cast as shown in Figure 2.6. There have been many ongoing studies to determine the heat flux and the thermal gradients of the molten metal that comes into contact with the belt on one side and a water coolant in contact with the belt on the other side[38,46].

Belt Quench System
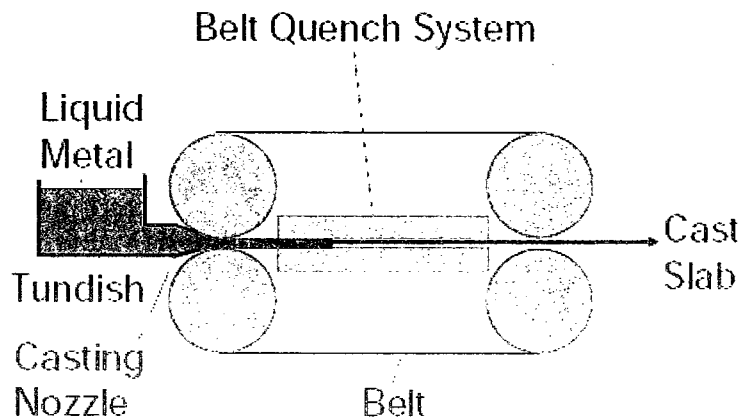
Figure.2.6 - Twin belt slab casting[38]

2.4.3.4. Block caster technique:

A number of chilling blocks mounted close to each other on a pair of opposing tracks, are shown in Figure 2.7. Block casters require exact dimensional control to avoid flashing caused by small gaps between the blocks. Such flashes can cause sliver defects when the strip is hot rolled[38,40].
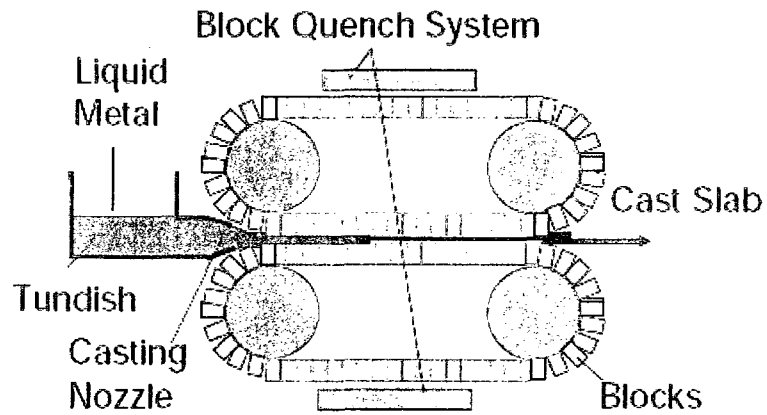
Figure.2.7 - Block caster[38]

2.4.3.5. Combination of a rotating steel belt and a water-cooled casting wheel:

In this method, a mould is formed between the belt and a sector on the outside of the casting wheel, as shown in Figure 2.8. There follows a description of some of the casters used for the commercial production of aluminum and other light metal slabs or strips[38.46].
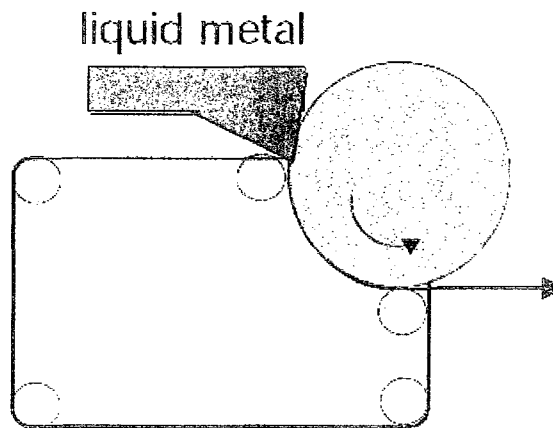
Figure.2.8 - Caster with a combination of steel belt and casting wheel[38]

2.4.3.6. Vertical casting direction:

2.4.3.6.1. Vertical strip casting machine, twin roll casting:

Vertical strip casting or twin-roll casting are established technology for the economical production of thin aluminum sheets directly from the melt. Recently, a similar technology has been applied to magnesium thin strip production[24,47].

POSCO and Magnesium Flachprodukte GmbH have already produced AZ31 magnesium alloy strips with 600 to 700 mm width and 3.0 to 7.0 mm thickness.

In twin roll casting, the melt flows through a nozzle to the gap between two rolls rotating toward each other. A melt bath is formed in the roll gap using side dams. A solidified metal shell is formed adjacent to each roll surface during the roll rotation so that these two shells meet and weld together before exiting the roll gap and thereby forming the strip[48].

The produced strip is annealed to obtain full or partial recrystallization to an appropriate grain size. The annealed strip is then rolled to produce a magnesium alloy sheet of a desired thickness, and the sheet is subjected to a final anneal[36]. The hot rolling and annealing usually are at a temperature from about 400 to 500°C. Further hot or cold rolling can be performed to obtain the desired microstructure and mechanical properties. Figure 2.9 represents a typical schematic of a twin-roll casting machine, which is used for producing magnesium strips[38,49,50].
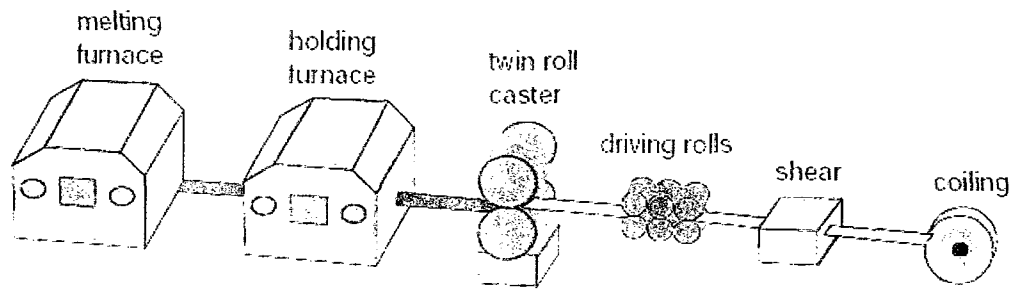
Figure 2.9 - Schematic view of strip caster[38]

The mechanical properties of commercial as-rolled AZ31 sheets of MEL and Osaka Fuji, which are produced by a twin roll caster, are compared in Table 2.4. The sheets of MEL and Osaka Fuji were produced by a DC casting/warm rolling process[27]. Results show that the mechanical properties of the final products depend on the thermo mechanical histories of the warm rolling process. The mechanical properties of an as-rolled sheet are compatible with or superior to those of commercial DC cast/warm rolled sheets. It should also be noted that the as-annealed AZ31 sheet shows a remarkably high elongation[9,27].

Table 2.4. Comparison of the mechanical properties of AZ31 sheet by different producers[27].

	0.2%Ys(MPa)	UTS(MPa)	Elongation (%)
RIST1	195-210	280-295	18-21
RIST2	250-265	305-310	13-15
MEL	246	295	20
Osaka Fuji	155	245	22

2.4.3.7. Casters with a horizontal casting direction:

Recently, horizontal feeding casters have been of great importance for the production of strips between 1000 mm and 2000 mm in width and with a gauge between 6 to 10 mm,

22

whereas in the latest developments a gauge of even 1 to 3 mm has been achieved. The casting rate usually depends on the alloy. It is between 0.8 m/min to 5 m/min. Horizontal feeding casters have been used to manufacture thin magnesium alloy sheets of AZ61, AZ91, and AZ31[46]. A pair consisting of a copper alloy roll and a pure copper roll is used. Figure 2.10 illustrates the horizontal twin roll strip casting process[50]. A source of molten metal feeds into the space between a pair of counter-rotating internally cooled rolls. Table 2.5 shows the principle dimensions of the horizontal feeding caster[38].
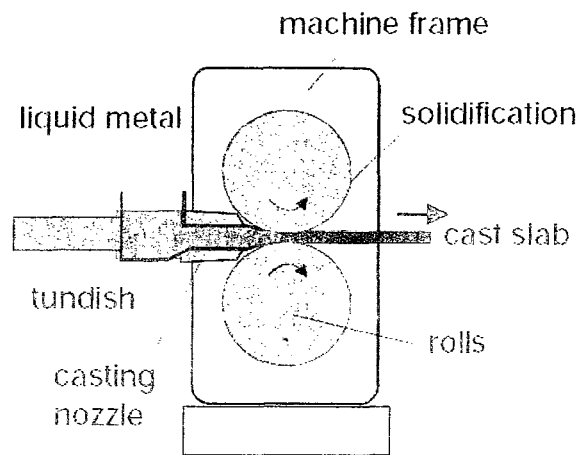
Figure.2.10 - Twin drum caster with horizontal casting direction[38]

Table.2.5: Dimensions of roll caster and tundish[38]

Rolls	
Materials	Pure copper, Copper alloys
Upper roll (mm)	Ø300×150
Lower roll (mm)	Ø300×150
Roll Speed (m/min)	0-60m/min (max)
Spring force (N/mm)	10009
Roll contacting length (mm)	50
Tundish	
Materials	Insulator, Mild steel

2.4.3.8. Single belt casting:

In the single belt casting process, the melt is fed on a moving steel conveyor belt via a nozzle. The belt is intensively water-cooled from below. In order to protect the melt, solidification takes place in a protective atmosphere such as Ar or CO_2/SF_6. Hence, material losses are reduced and deteriorative effects on product quality due to oxidation are avoided[52]. Afterwards, the yielded strip with 10-15mm thickness is carried into an in-line rolling mill with a 60-70% thickness reduction. In a typical hot-rolling mill, it is possible to achieve the desired thickness range, which is 90% of the original thickness (Figure 2.11)[53].

The mould moves horizontally. The increase of productivity requires only an increase of the length of the cooling belt[53].
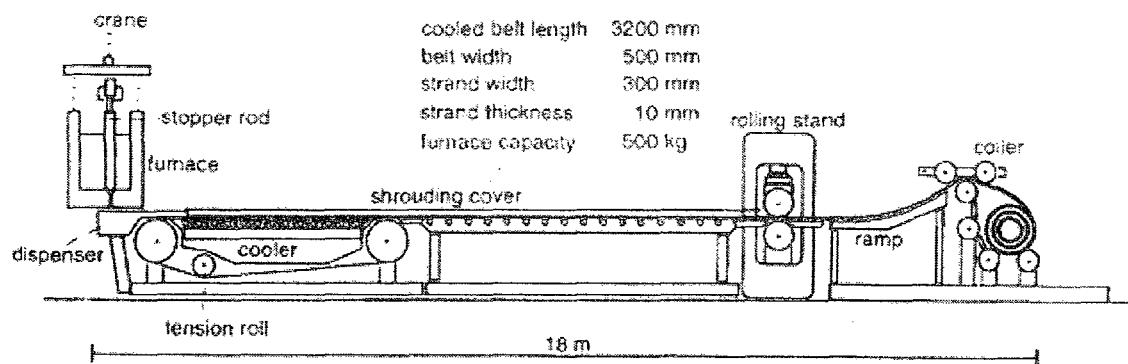
Figure.2.11 - Single belt casting machine at Institut fur Allgemeine Metallurgie[53]

The single belt casting process has the following operational advantages compared to other competitive near- net-shape casting processes[54]:

➢ High productivity strip production

➢ Low investment and operational cost

➢ Facilitated melt feeding and low sensitivity to breakouts of liquid metal

This process also has some difficulties, which should be solved. The main problem seems to be that of the non-uniform thickness of the strand[54]. There are other major problems related to the surfaces and edges. In principle, it is the same as in conventional continuous casting, but the strand surface and edges are much larger. Because of the material loss, scale formation with a similar thickness as in conventional continuous casting is completely intolerable. Therefore, the cooling length of the caster and the roller table are covered to keep the strip under the protection of an inert gas[55].

2.5. Heat transfer in the casting process:

2.5.1. Resistances to heat transfer:

The hot liquid metal takes time to lose its heat and to solidify. Resistances to heat flow from the interior of the casting are caused by the following:[55]

➢ The liquid

➢ The solidified metal

➢ The metal/mould interface

All these resistances add up, as if they were in series. This is shown schematically in Figure 2.12[56-58].
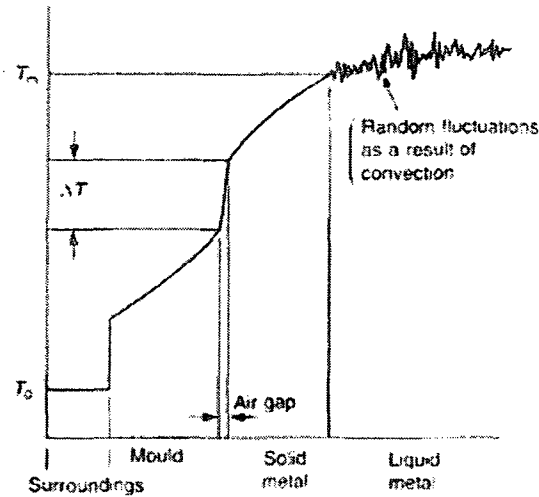
Figure.2.12 - Temperature profile across the casting freezing resistances that control the rate of heat loss[58]

2.5.1.1. The liquid resistance:

In actual fact, in nearly all cases of interest, the liquid resistance is negligible, as a result of flow by forced convection during filling and thermal convection during cooling. The mixing quickly was transported heat and so smooth out the temperature gradients[59].

2.5.1.2. The solidified metal resistance:

2.5.1.2.1. Effect of conduction heat transfer:

For the unidirectional flow of heat from a metal poured with zero superheat, at its melting point T_m, against a mould wall initially at temperature T_0, the transient heat flow problem is described by the following partial differential equation, at the solidifying interface, where α_s is the thermal diffusivity of the solidified melt, LH is Latent heat of solidification[58].

Heat conducted away through solidified shell of magnesium = release of latent heat + heat input from the melt

$$-k\frac{\partial T}{\partial t}\Big|_{\substack{x=s\\t=t}} = +\rho LH\frac{dx}{dt} + h(T^{Bulk} - T_m) \qquad (2.1)$$

Where, T_m=melting/freezing point of Mg, x=0 is mould/metal interface, x=s is liquid/solid interface of Mg.

The boundary conditions are x = 0, T = T_0; at x = S, T = T_m and at the solidification front the rate of heat evolution must balance the rate of conduction down the temperature gradient as illustrated by Figure 2.13[52,59]:
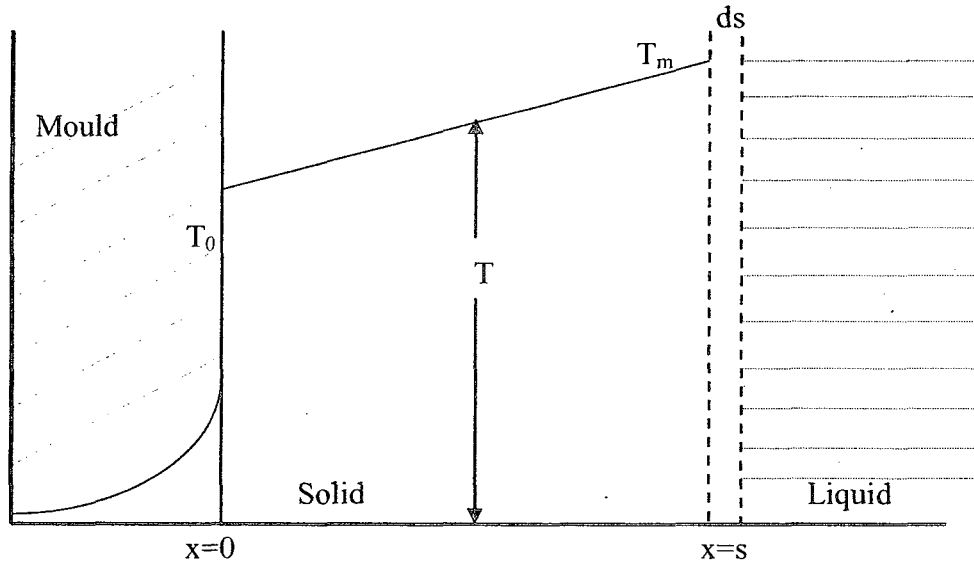
Figure.2.13 - Temperature profile in a solidifying melt and a cooling mould without temperature gradient within the solidified[52.59].

$$\rho_s LH\left(\frac{\partial x}{\partial t}\right) = -k_s\left(\frac{\partial T}{\partial x}\right)_{\substack{x=s\\t=t}} \qquad (2.2)$$

where k_s is the thermal conductivity of the solid, LH is the latent heat of solidification. .

Heat conducted away from solidification front $\approx K \frac{(T_m - T_0)}{x}$, neglecting accumulation of

heat front, and x=s at T=T_m

$$\frac{kA(T_m - T_0)}{s} = \rho \, LH \, A \, \frac{ds}{dt} - h_L A (T^{Super \ heat} - T_m) \qquad (2.3)$$

where h_L is heat transfer coefficient of liquid.

If $T_{Superheat \ temp}$ =$T_{Melting \ temp}$, and 3th term is zero

$$\frac{kA(T_m - T_0)}{\rho LHA} \int_0^t dt = \int_{s=0}^{s=s} s dt \qquad (2.4)$$

and

$$\frac{k(T_m - T_0)}{\rho LH} \cdot t = \frac{1}{2} s^2 \qquad (2.5)$$

and

$$s \cong \sqrt{\frac{2k(T_m - T_0) t}{\rho \, LH}} \qquad (2.6)$$

or

$$s \cong a \cdot t^{\frac{1}{2}} \qquad (2.7)$$

28

The important result to note is the parabolic time law for the thickening of the solidified shell. This agrees well with the experimental observations. For instance, the thickness S of steel solidifying against a cast iron ingot mould is found to be:

$$S = a.t^{\frac{1}{2}}(-b) \qquad (2.8)$$

where the constants a and b are of the order of 3 and 25, respectively, when the units are millimeters and seconds. (-b) refers to loss of melt superheat before freezing starts. The apparent delay in the beginning of solidification presented by the appearance of the constant b is a consequence of the following[58,59]:

> The finite interface resistance further slows the initial rate of heat loss. Initially the solidification rate will be linear. Then, the resistance of the solidifying metal becomes dominant for thick casting, giving the parabolic relation[58].

Figure 2.14 shows experimental data for shell thickness (half the total strip thickness) as a function of solidification time during vertical TRC of AISI 304 stainless steel. The solid line in this figure is the predicted shell thickness using following equation:

$$d_t = \frac{k}{h}\left[\left(\frac{2h^2 t_s (T_m - T_M)}{\rho a k L_f} + 1\right)^{1/2} - 1\right] \qquad (2.9)$$

where d_t is the thickness of a solidifying shell, L_f is the latent heat of fusion, t_s is the contact time between the melt and the mould wall (solidification time), k is the solidification rate constant and a is a constant

This relation shows a good agreement with the experimental data. This research used this relation to control the solidification conditions required to generate the desired strip thickness. For a given roll diameter, t, is related to casting velocity which allows Eq. 2.9 to be used to predict strip thickness of a given metal based on casting velocity as well as melt superheat and thermophysical properties of the metal and mould. It must be assumed, however, that the roll separating force is not sufficient to significantly modify the final gauge of the strip.
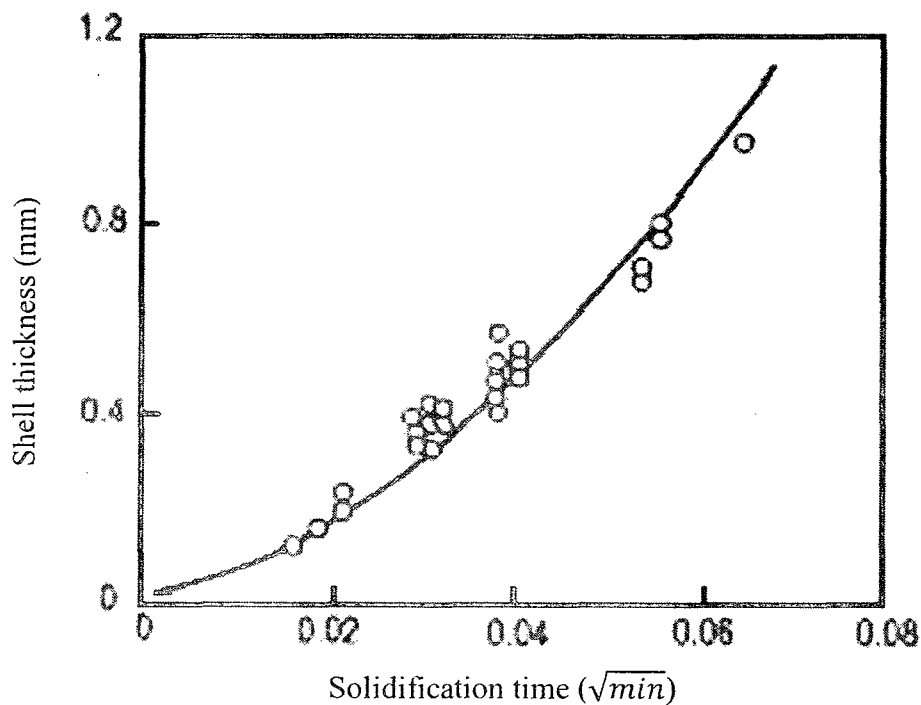
Figure 2.14 – Relation between shell thickness and solidification time for AISI 304 stainless steel strips[58].

2.5.1.2.2. Effect of convection heat transfer:

The heat flow from the solidifying metal is often limited by metal/substrate thermal resistance in the form of the entrapped gasses. The rate of heat transfer across the gas

interface by convection for a metal at temperature T_m , to the surface of a mould of temperature, T_M, is given by Newton's law of cooling:

$$q = hA(T_m - T_M) \qquad (2.10)$$

where h is the convective heat transfer coefficient. This mode of heat transfer is different to conduction and is a result of the movement of fluid relative to the substrate surface. Nevertheless, interfacial thermal conductance can also be quantified using a relation of the same form as equation 2.10[51].

2.5.1.2.3. Effect of radiation heat transfer:

Heat may also be transferred by the process of thermal radiation if a gap exists between the metal and the substrate during casting. The rate of heat transfer is given as

$$q = F_\delta F_G \sigma A(T_m^4 - T_M^4) \qquad (2.11)$$

where σ is the Stefan-Boltzamann constant (5.669×10^{-8} W/m^{2}K^4), F_δ is an emissivity function that takes into account the non-ideality of the radiating surfaces and F_G a geometric factor due to the linear nature of propagation of radiation such that not all radiation leaving one surface may reach the surface.

The three modes of the heat transfer play a role in direct strip casting. Heat transfer at the metal/substrate interface can occur by conduction thorough the points of intimate contact, together with radiation, convection and conduction across any entrapped gas in the interfacial gap or through any surface films that may be present on the substrate. It was pointed out in the literature that thermal conductance through a gaseous interfacial film corresponds to more than 98% of the heat flux with only minor contributions from radiation and convective heat transfer[59,61].

2.5.1.3. The metal/mould interface resistance:

In casting process, heat flow is controlled to an important degree by the thermal resistance at the metal/mould interface. If both the metal and the mould have reasonable thermal conductivity, then the boundary between the two is the dominant thermal resistance. When an insulating mould coat is applied, the interface becomes even more significant than in other cases, and also when the casting cools and shrinks away from the mould and the mould heats up, expanding away from the metal, an air gap is left, separating the two. These circumstances are common in the casting of light alloys. For unidirectional heat flow, the rate of heat released during solidification of a solid of density ρ_s and latent heat of solidification H is [58,59,61]:

$$\dot{q} = \rho_s H A \frac{\partial S}{\partial t} \qquad (2.12)$$

where s= location of solid/liquid interface at x=s (referenced x=0 at the mould/cast metal interface).

This released heat has to be transferred to the mould. The heat transfer coefficient h across the metal/mould interface is simply defined as the rate of transfer of energy q (usually measured in watts) across unit area (usually a square meter) of the interface, per unit temperature difference across the interface. The rate of heat transfer across the gases, interfacial gap between the casting and mould interface of conduction, for a metal at temperature T_m to the surface of a mould of temperature, T_M^* is given by Newton's law of cooling:

$$\dot{q} = hA(T_m^* - T_M^*) \tag{2.13}$$

where * denotes interface and h is the heat transfer coefficient for conduction, h is a function of the thermal conductivity and the material thickness.

$$h = \frac{k}{\Delta x} \tag{2.14}$$

Hence, combining equations 2.12 and 2.13 and integrating from s = 0 at t = t_0 and, s=S at t=t gives:

$$s = \frac{h(T_m^* - T_M^*)}{\rho_s H} \times t \tag{2.15}$$

It is immediately apparent that the shape of the strip does not alter the heat transfer across the interface,[58,61,62].

2.5.2. The air gap:

The strong cooling on the belt side by water, masses the strip to solidify and to conduct as it cools. During casting, strip may distort due to the steep thermal gradients and air gap formed between strip and substrate due to shrinkage of strip. This air gap has been determined to be the greatest single resistance to heat removal.

The air gap acts as a reinforce to the withdrawal of heats leading to lower casting rates and to casting defects such as segregation, shell bending, surface cracks, and cell size variations of a continuously cast strip[59].

2.5.3. The heat transfer coefficient:

When the metal first pours into the mould, the macroscopic contact is good because of the conformance of the molten metal. Gaps exist on a microscale between high spots as shown in Figure 2.16. At the high spots themselves, the high initial heat flux causes nucleation of the metal by local severe maximum 2°C undercooling[59]. The solid covers most of the surface of the casting. Conformance and overall contact between the surfaces is expected to remain during all of this early period, even though the mould will now be starting to move rapidly because of the deformation of both the casting and the mould. After the creation of a solidified layer with sufficient strength, further movements of both the casting and the mould are likely to cause the good fit to be broken, so that contact is maintained across only a few widely spaced random high spots[59,62,63].
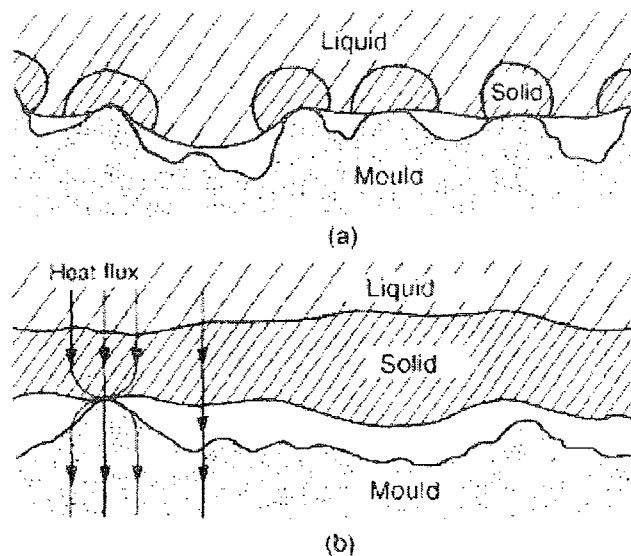
Figure 2.15 – Metal/mould interface when solid is nucleating at points of good thermal contact. In general, macroscopic contact is good at this stage (a). Later (b) the casting gains strength, and casting and mould both deform, reducing contact to isolated points at greater separations on non-conforming rigid surfaces[59].

The total heat transfer coefficient of heat across the interface can be written as the sum of three components[64]:

$$h_t = h_s + h_c + h_r \qquad (2.16)$$

where h_s is the conduction heat transfer coefficient (W/m^{2}K) through the solid contacts, h_c, is the convection heat transfer coefficient (W/m^{2}K) through the gas phase, and h_r is the heat transfer coefficient (W/m^{2}K) that is transferred by radiation. Ho and Pehlke[64] reported analytical equations for each of these contributions to the total heat flux. The results can be explained as following:

1- While the casting surface can conform; the contribution of solid-solid conduction is the most important.

2- When the interfacial gap starts to open, conduction through the solid contacts becomes negligible. The rapid decrease of the casting surface temperature is suddenly halted, and reheating of the surface starts to occur. An interesting mirror image behavior can be noted in the surface temperature of the chill, which is now out of contact with the casting and starts to cool[64].

3- After solid conduction diminishes, the important mechanism for heat transfer becomes the conduction of heat through the gas phase. This is calculated from:

$$h_c = k/d \qquad (2.17)$$

where k is the thermal conductivity of the gas and d is the thickness of the gap. Ho and Pehlke[64] have developed formulas for small gas gaps when the gap is smaller than the

mean free path of the gas molecules, thereby effectively reducing the gaps thermal conductivity. Hence, heat transfer is a strong function of gap thickness. Moreover, it is also a strong function of the composition of the gas. Even a small component of hydrogen will greatly increase the conductivity of interfacial layers of the gaps between the casting and the mould.[39,49]

2.5.4. Thermal contact resistivity:

In order to explain this concept, let us consider the example of heat transfer through two metal rods of cross-sectional area A that are pressed against each other. Heat transfer through the interface of these two rods is the sum of the heat transfers through the solid contact spots and the gaps in the noncontact areas and can be expressed as[64]:

$$\dot{Q} = \dot{Q}_{contact} + \dot{Q}_{gap} \tag{2.18}$$

It can also be expressed in an analogous manner to Newton's law of cooling as:

$$\dot{Q} = h_c \, A \, \Delta T_{interface} \tag{2.19}$$

where A is the apparent interface area (which is the same as the cross-sectional area of the rods) and $\Delta T_{interface}$ is the effective temperature difference at the interface. The quantity h_c, which corresponds to the convection heat transfer coefficient, is called the thermal contact conductance and is expressed as[64]:

$$h_c = \frac{\dot{Q}/A}{\Delta T_{interface}} \qquad (\text{W/m}^2 . \,^\circ\text{C}) \tag{2.20}$$

It is related to thermal contact resistance by[64]:

$$R_c = \frac{1}{h_c} = \frac{\Delta T_{interface}}{\dot{Q}/A} \qquad (\text{m}^2 . \,^\circ\text{C/W}) \tag{2.21}$$

That is, the thermal contact resistance is the inverse of the thermal contact conductance. Usually, thermal contact conductance is reported in the literature, but the concept of thermal contact resistance serves as a better vehicle for explaining the effect of an interface on heat transfer. Note that R_c represents thermal contact resistance per unit area. The thermal resistance for the entire interface is obtained by dividing R_c by the apparent interface area A. The thermal contact resistance can be determined from equation 21 by measuring the temperature drop at the interface and dividing it by the heat flux under steady conditions. The value of thermal contact resistance depends on the surface roughness and the material properties as well as the temperature and pressure at the interface and the type of fluid trapped at the interface[26,58,64].

2.5.6. Variations in heat transfer during strip casting:

Interfacial heat transfer during solidification strongly depends on the interfacial heat transfer coefficient varying during the process. In this regard, many studies have been conducted by Isac et al. 1997[51] and J.Kim et al. 2004[54]. During casting, the molten metal cools and solidifies and any thermal expansion or contraction of both the metal and the mould will change the contact configuration at the interface and result in a variation in heat transfer. Moreover, when molten metal makes contact with the mould, there is an initial increase in mould temperature with both the metal and mould finally decreasing in temperature over time. It is clear that a single value for heat transfer coefficient is not realistic, although average values are almost exclusively reported. Careful measurements and analysis are therefore necessary if one is to achieve acceptable transient heat transfer coefficients during the whole process of solidification. The time evolution of heat flux

can be readily determined by careful thermocouple measurements and numerical solutions of the heat flow equations [58].

2.5.6. Mould surface topography (roughness):

One of the important substrate properties influencing the average heat flux during strip casting or any near net shape casting process is the substrate topography. Figure 2.16a shows that the average heat flux is inversely proportional to the surface roughness. These results are consistent with the splat cooling of liquid on different substrate materials of different roughnesses, as shown in Figure 2.16b. The relationship between the heat transfer coefficient (kW/m^{2}K) and the arithmetic average roughness, R_a (μm) of a substrate surface is as follows[63]:

$$\bar{h} = c_1 + c_2 R_a^{-n} \tag{2.22}$$

The coefficients c_1 and c_2 for various metals and substrates have been presented in Table 2.6. These values with $c_2 \neq 0$ indicate that heat flux reaches an asymptotic value when the surface roughness increases, as shown in Figure 2.17[63]. Increasing the surface roughness results in a decrease in A_c and, thus reduces the heat transfer coefficient. This decrease is, in turn, due to a decrease in the thermal conductivity through the interfacial voids. Moreover, a decrease in the wettability of liquid metal as a result of increasing the surface roughness (R_a) has been shown by Hitchcock et al.[66]; this is expected to decrease interfacial heat transfer[57,62].
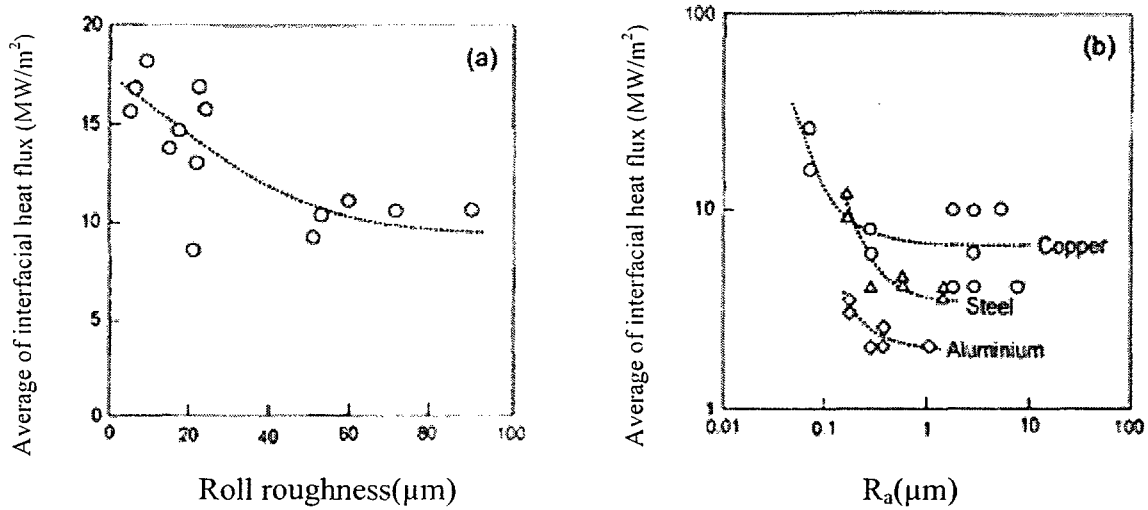
Figure 2.16 - Effect of substrate surface roughness on interfacial heat transfer coefficient for (a) twin roll casting of steel, (b) splat quenching of Ni[63]

Table 2.6. Coefficient in equation 2.17 for various casting conditions[58]

Molten Materials	Substrate	C_1	C_2
Al-5%Cu	Copper	0	9.1
Nickel	Copper	67	0.7
	Aluminum	33.8	1.98
	Steel	19.7	0.42
Copper	Copper	0	65.2

The transient heat flux data reported by Strezov and Herbertson[63] for a range of substrate surface profiles, have been shown in Figure 2.17a. The substrate topography directly influences the time dependence behavior of the heat flux; it has been shown that a smooth substrate generates a markedly different heat flux profile compared with a textured substrate. The effect of ridge pitch (for a constant depth of 30 μm) on both the maximum heat flux and heat flux after 50 ms immersion time is given in Figure 2.17b. It is obvious that the ridged substrate manifests a higher q_{max}, while the maximum occurs at a pitch range of 100-200 μm. However, this trend is reversed after 50 ms of exposure, as

39

the heat flux on smooth substrate is higher than that on the ridged substrate. In the stage, where a solid shell has already formed on both types of substrates and, in the case of ridged substrates, heat transfer occurs through the peaks. On the other hand, due to substantial gas entrapment, the valleys are expected to lead to a much lower heat flux. Subsequently, the heat transfer after substantial shell formation is different from that before the point of nucleation (<10 ms)[58]. This implies that the major interfacial heat flux is concentrated through the peaks of either the ridges or pyramids. Despite the large transient heat fluxes associated with textured substrates, it is observed that the average heat flux over the entire immersion period is in fact larger for a smooth substrate (compared to the rough substrate) resulting in thicker as-cast coupons. This is well in agreement with Figure 2.17[61-63].
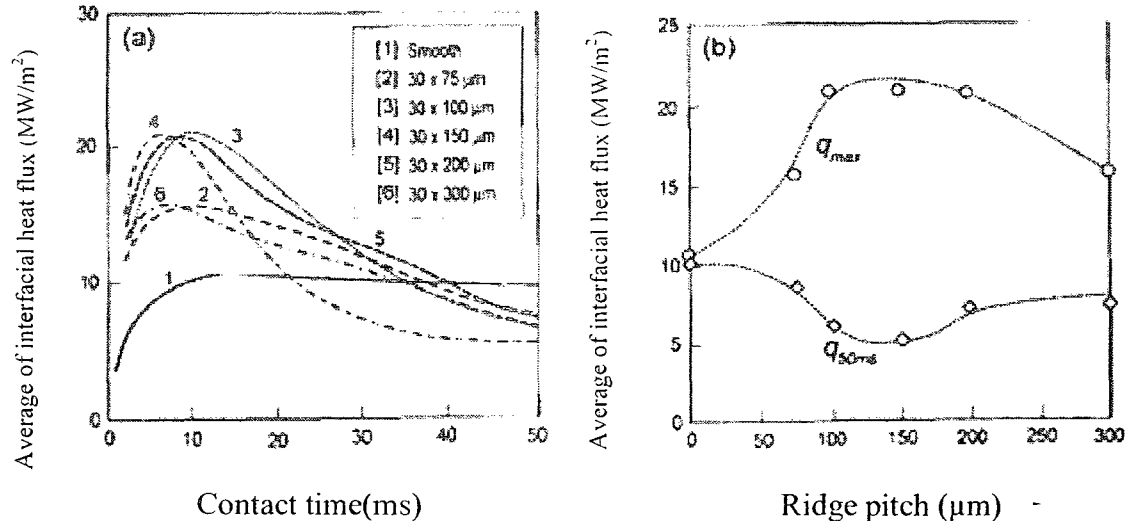
Figure 2.17 - (a) Effect surface topography on interfacial heat flux during casting of AISI304 stainless steel onto copper substrates. (b) Effect of ridge spacing on maximum heat flux and heat flux after 50 ms contact time[63]

40

2.5.7. Transient heat flux:

The transient interface heat flux patterns during the initial stages of solidification for a range of metals have been determined by various experimental and modeling techniques. Strezov and Herbertson[63] have measured the change in substrate temperature at a location of 0.8 mm below the mould surface during the solidification of AISI 304 stainless steel. From those data, they calculated the transient heat fluxes. They used the twin roll caster shown in Figure 2.18.
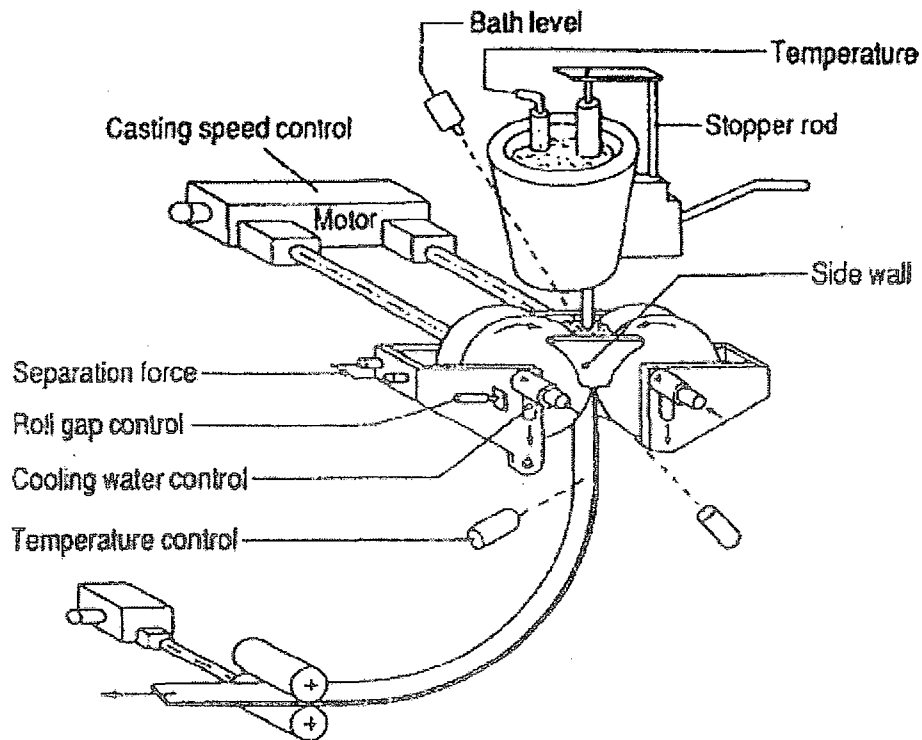
Figure 2.18 - Schematic representation of a twin roll caster[63].

Figure 2.19 represents typical results of calculated heat flux history for the first 50 ms of contact between the molten metal and a copper substrate. The peak is attributed to

nucleation at the melt/substrate interface during solidification, with its effect on nucleation behavior. The peak also represents the quantitative reflection of the effectiveness of initial melt/substrate contact with its magnitude influenced by various casting parameters: mould topography, melt superheat and atmosphere, immersion velocity and melt composition[58.63].
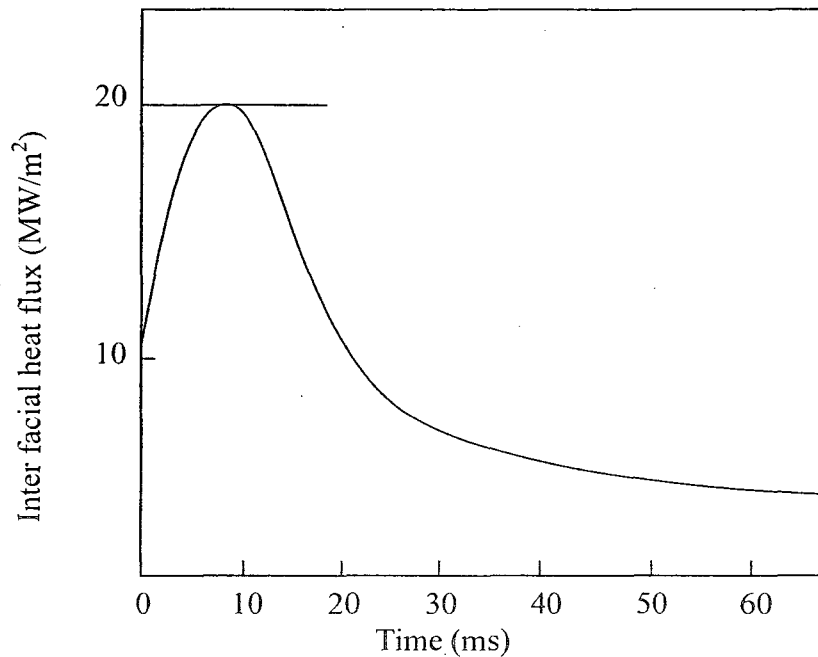
Figure 2.19 - Calculated interfacial heat flux as a function of contact time during solidification of AISI 304 stainless steel on a copper substrate[58].

2.5.8. Interfacial heat transfer at single belt caster:

The rate of interfacial heat transfer between the liquid metal and the substrate beneath plays a valuable role in the strip casting process. The interfacial heat flux has a great effect on the quality of the strips and the underlying microstructures[66,68].

42

Many casting process variables can affect the interfacial heat transfer between a solidifying strip and substrate. These include the thermo physical properties of the liquid metal and the substrate; melt superheat and the roughness of the substrate. When two substances at different temperatures contact each other perfectly, the interfacial heat flux is infinite for the first moment of contact. Perfect contact corresponds to zero thermal resistance at the interface[69-71].

The thermal resistances are explained in Section 2.5.1; these resistance factors greatly decrease the value of heat flux and completely change the actual interfacial flows of heat[72].

At the moment that the liquid metal comes into contact with the substrate, the liquid metal begins to feed onto the moving substrate and liquid/solid contact enhances the heat transfer to the interface. A considerable amount of heat is transferred at this stage[73].

The transient is attributed to nucleation at the melt/substrate interface during solidification with its effect on nucleation behavior. The peak is also thought to be a quantitative reflection of the effectiveness of initial melt/substrate contact with its magnitude influenced by various casting parameters, substrate topography, thickness of strip and coating thickness.

The drop in the heat flux thereafter is caused by the contraction of the solidified layer and by the consequent formation of an "air gap" between the coating and the solidified shell. The influence of air gaps on the heat flux has been confirmed by monitoring the temperature of the bottom surface of the strip[74].

The solidification begins on the substrate, and the interfacial heat transfer is dominated by the sensible heat release of the metal's superheat and the latent heat. Heat is transferred through the strip/substrate interface because of the small thickness of the strip. Heat conduction from the interface to the substrate and the heat transferred by the release of latent heat are comparable and result in the constant value of heat transfer resistance during a certain period of time. After the release of latent heat, the increase of the solidified shell in the strip continuously changes the interfacial heat transfer from the liquid/solid to solid/solid[75].

2.5.9. Inverse heat transfer technique:

Direct heat conduction problems determine the interior temperature distribution within a body for a given set of boundary conditions. Thus, it is possible to solve the internal temperature distribution based on heat transfer boundary conditions such as a specific surface temperature or heat flux. The inverse problem, or inverse heat conduction problem (IHCP), is aimed at determining the surface temperature and/or interfacial heat flux for particular subsurface transient temperature distributions measured at subsurface points close to the surface. This inverse heat transfer calculation is a well known analytical method and is identified by the following[61]:

1- Existence of a solution

2- Uniqueness

3- Continuous dependence on the data given

44

The third condition tabs with account small variations in the input subsurface transient temperature data. It produces only small changes in the solution, a condition which can be termed as stability. However, the IHCP is not applicable in this area and small errors in the temperature data can result in large oscillations of the values of heat flux. To address this problem, more complicated algorithms needs to be developed [62].

2.5.9.1. Beck's IHCP non-linear estimation technique:

Beck[68] put forward a non-linear estimation method to deal with phase changes and temperature dependent thermal properties of the solidification process used for solving the IHCP. To treat experimental data, statistical principles and the concept of amplitudes temperatures are applied to the thermal capacity and heat conduction of the substrate during subsurface temperature measurements. This application is performed using a non-linear estimation method to solve the delayed and diminished thermal response problems. The heat flux is taken to be a constant or a linear function of time within a given time interval. This is the principle of Beck's non-linear estimation technique, according to which the heat flux is then determined for that period according to the following function

$$F(q) = \sum_i^{N_1} \sum_j^{N_2(N_3+1)} (T_{ij} - Y_{ij})^2 \qquad (2,23)$$

Where N_1 which is the number of internal points in the temperature measurement excluding those used for boundary condition. N_2 is the number of temperature measurements per time interval. N_3 is the future number of time intervals considered for the heat flux calculation at each time interval. T_{ij}, Y_{ij} are the calculated and measured temperatures of location i and the time instant j, respectively[61].

To minimize equation 2.16, the condition $\frac{\partial F}{\partial q} = 0$ can be applied:

$$\sum_i^{N_1} \sum_j^{N_2(N_3+1)} \left(T_{ij} - Y_{ij}\right) \frac{\partial T_{ij}}{\partial q_{ij}} = 0 \qquad (2.24)$$

The first derivative of the calculated temperature (dependent variable) with respect to the heat flux (the unknown) is called the sensitivity coefficient and is denoted as $\varnothing_{ij}$. Using the taylor series expansion of $T_{ij}(q)$,

$$T_{ij}(q_{l+1}) \approx T_{ij}(q_{\_l}) + \varnothing_{ij}\, \delta q_{l+1} \qquad (2.25)$$

The following iterative expression for soling the heat at each time interval can be obtained[61,62]:

$$\delta q_{l+1} = \frac{\sum_i^{N_1} \sum_j^{N_2(N_3+1)}\left(T_{ij} - Y_{ij}\right)\varnothing_{ij}}{\sum_i^{N_1} \sum_j^{N_2(N_3+1)} \varnothing_{ij}^2} \qquad (2.26)$$

The subscript l of the heat flux denotes the time when it was applied. The sensitivity coefficients are zero wherever $l > j$ since the temperature at time j at any point does not depend on the future heat flux.

By repeatedly applying the expression $q_{i+1} = q_1 + \delta q_{l+1}$ to correct the heat flux at location $q = q_0 (l = 0)$, the heat flux q at the time interval can be obtained when $\delta q_{l+1}/q_1$ is small enough, less than 0.1[62].

2.6. Macroscopic quality:

Most defects at the top side of the strip are a consequence of the melt flow. The defects could be related to the distribution of the melt over the substrate width, melt, and the reaction with protection gases or the formation of oxide layers. Carefully controlling oxygen level using a protective gas, controlling casting temperature and using modified casting nozzles, can solve some of these problems. The partial plugging of the casting nozzle and too high casting speeds lead to a turbulent melt flow that can deteriorate the surface quality[75].

In order to obtain a uniform melt distribution between the side dams, Ditze and Schwerdtfeger[67] studied different nozzle exits. These are shown in Figure 2.20, where types 1, 3 and 6 achieved satisfactory results. Initially, nozzles 4 and 5 worked fine, but then made a strand only in the center of the belt that had no contact with the side dams. Because the feeding streams did not combine, Nozzle 2 produced a strand of ninth strands [47.55]. Figure 2.21 shows a picture of strands with this defect. The strand in Figure 2.21a was produced with Nozzle 2 shown in Figure 2.21b. Figure 2.21b presents a strand with bad sticking defects and incomplete combining of the melt. Some of the strands become black during cooling Figure 2.21c. The strand of Figure 2.21d resulted in no contact with the side walls[47]. A better macroscopic quality of strip surface was obtained with an increase in superheat, but at the expense of a coarser microstructure[69.70].

Spitzer et al[50] investigated the relationship between some of the defects at the lower surface and the liquid steel metal flow. They have suggested that the defects can be avoided by delivering molten metal to the moving belt uniformly over the width, and

with a velocity as close as possible to that of the belt. This is very hard to achieve[55]. On other hand, Schwerdtfeger suggested that the cooling zone of the steel caster and the first part of the roller table be encapsulated under protective gas to minimize the scaling of the surface[53].

Many small pits are observed distributed on the magnesium strip bottom surface when the substrate is not coated[52]. Because of these pits, it is possible to find, on the top surface of the strips, pitted regions vertically above those pits or holes in the bottom surface. These pitted regions on the strip's top surfaces are due to the extra thermal resistance of the air gap between the strip and substrate. At uniform thermal Vegetable oil and Graphite coatings can improve the strip surface quality remarkably for casting of aluminum alloys[57] Using graphite coating on the substrate the strip's bottom surface was flattened exhibiting no obvious surface defects. This surface quality ensured that the strip sample made uniform thermal contact with the copper substrate during solidification, resulting in a uniform heat extraction from the strip's bottom[47.72].
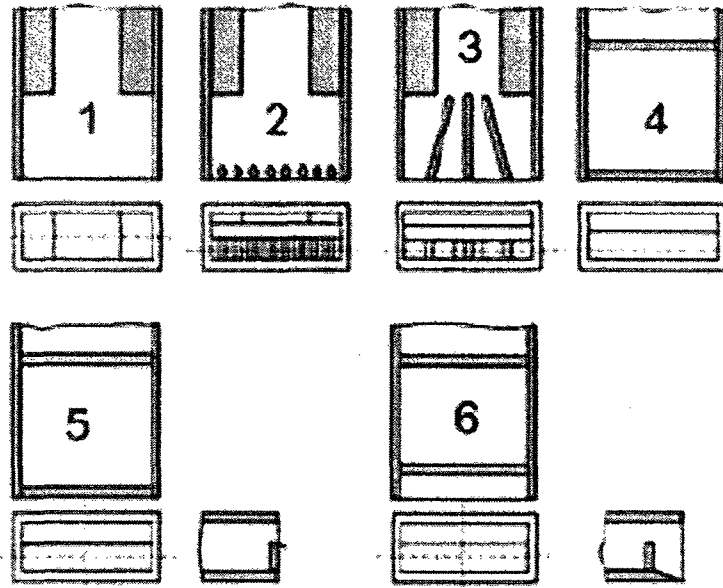
Figure 2.20 – Flow views of nozzles used for feeding the magnesium melt to the belt[47]
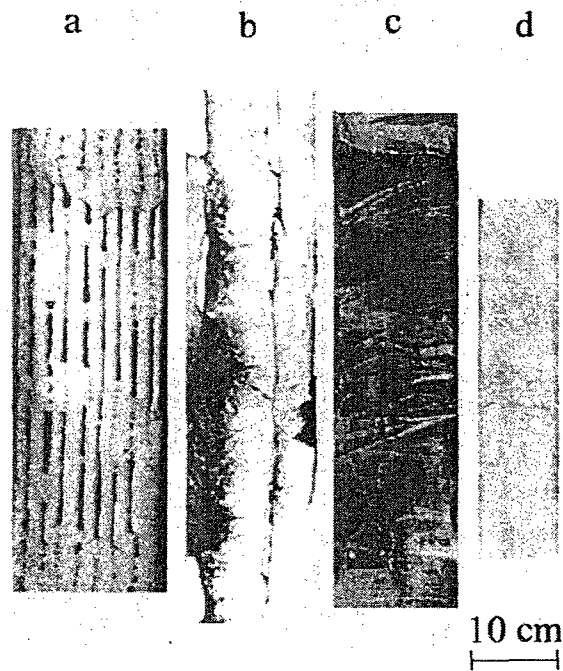
Figure 2.21 - Strands of magnesium with versus casting defects. (a) Strand cast with Nozzle 2 in Figure.218. The various feeding streams did not re-combine. (b) Strand with bad side defect caused by sticking to the side dam and with non-complete combining of the melt. (c) Strand with black blackened lower surface. (d) Strand cast without contact with the side dams[47].

49

2.7. Microstructure:

The dendrite arm spacing of the steel strip produced by a single belt casting is smaller than that of conventionally cast slabs[58]. In magnesium alloys, the microsegregation was in the same range of conventionally cast slabs but macrosegregation was very low. Due to the different cooling rates at the lower and upper surfaces of the strip, the dendrite structure and microsegregation is not symmetrical with respect to the center plane[76.77]. Figure 2.22 is for the structure close to the lower and upper surfaces of the strand, respectively. It is clear that the dendrite arm spacing increases with the increasing distance from the lower side of the strip[49,78].

Figure 2.23 illustrates the grain size distribution over the thickness of the strip. The grain size follows the temperature profile with the largest grain sizes near the center and the smallest near the bottom of the strip. The difference in cooling conditions between the bottom and the top surface of the strip cause a larger grain size at the top[72,79]. However, the mechanical behavior of the upper and lower halves of the strip did not reveal significant differences between the mechanical properties of the single belt cast strands compared with the conventionally cast slabs[79,80].

a)   b)
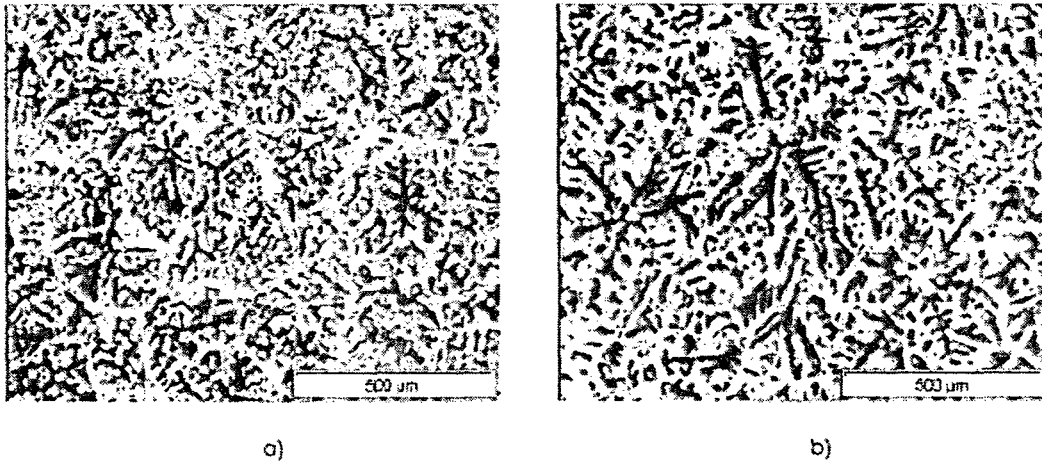
Figure 2.22 - Micrograph demonstrating the pronounced dendritic structure of the 0.8 mm thickness AZ91 strip cast on low carbon steel substrate with 660°C using temperature. Transverse sections close to the (a) lower (b) upper surfaces of the strands[48].
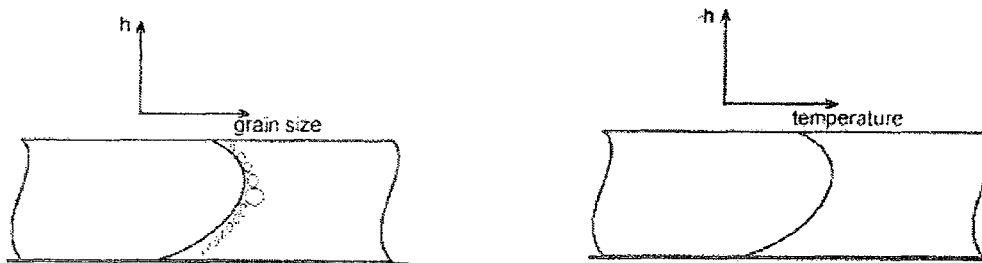
Figure 2.23 - Grain size distribution and temperature spread over the thickness of strip [72].

Palkowski *et al*[72] have observed interdenderitic porosity in regions close to the upper surface of strip cast AZ91 and AM50 magnesium alloys. The amount of porosity in AM50 was less than in AZ91. It was mentioned that the porosity formation is due to the shrinkage of molten metal during solidification. The higher level of interdendritic porosity in AZ91 is due to its larger freezing range compared to AM50. Also, they reported that as the superheat of molten metal decreases, smaller secondary dendrite arm spacing (SDAS) are obtained.

51

They reported that increasing the cooling rate, results in a decrease in the grain size. The SDAS increased with an increase in strip thickness owing to extending the solidification time[81-84].

2.7.1. Dendrite Arm Spacing of single belt:

A convenient measure of the effects of solidification conditions on dendrite structure is dendrite arm spacing, which is the average spacing between dendrite arms. Figure 2.24 represent secondary dendrite arm spacing (SDAS) definition. SDAS is usually the most useful parameter.

Solid   **Liquid**

- - Secondary dendrite
arm spacing (SDAS)
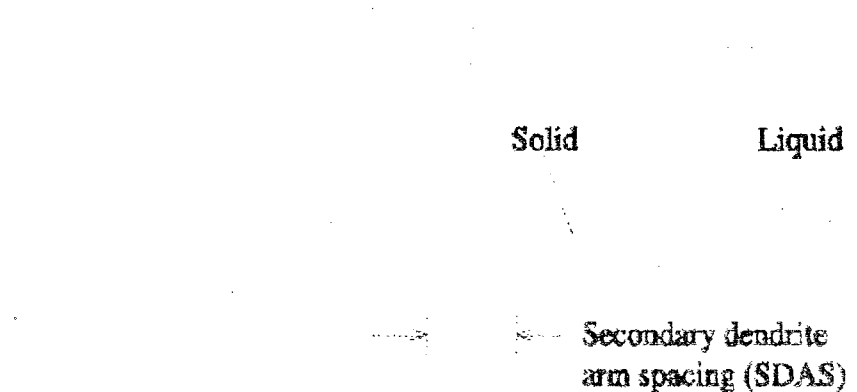
Figure 2.24 -The secondary dendrite arm spacing (SDAS)[85]

Numerous experiments have confirmed that secondary spacing, d_s, is closely dependent on the total time, t_f, during which liquid and solid have coexisted:

$$ds = a.t_f^n \tag{2.27}$$

where a and n are constants for specific conditions. Measured values of n range between 0.25 and 0.4, the lower values relating to earlier stages of dendrite growth, when the fraction of solid, f_s, is small, while higher values occur when, f_s, is high. However, d_s

represent the distance between the centers of two adjacent secondary dendrite arms[79,81,85].

2.7.2. Fluid flow in strip casting:

A popular approach to calculating convective transfer rates in turbulent flow is to assume that close to the solid-liquid interface, but sufficiently away from it for the effects of molecular transport to be negligible, the velocity and temperatures profiles are given by the so-called universal logarithmic laws. This is particularly true in problems that involve solidification, in which the solid-liquid interface normally has a complex morphology, usually with dendrites, whose spacing depend on the cooling rate. This virtually excludes the possibility of applying the wall function in solidification problems, other than those involving planar freezing. Casting nozzles were improved for single belt casting machines. The nozzle includes a sloped surface which reduces molten metal turbulence during the casting process[60.62].

CHAPTER

3

EXPERIMENTAL PROCEDURE

3.1. Raw materials and melting unit:

Commercial magnesium alloy AZ31 grade B bar ingots obtained from Magnesium Electron Co. were used as raw material in the present experiments. The ingot materials were cut into smaller pieces.

A graphite coating obtained from Asbury Carbons Co. was used as coating for the substrate. The median particle size of graphite is 0.5-0.6µm. The graphite particles are flake shaped and have wide aspect ratio.

The melting of magnesium alloy AZ3-1B was carried out in an Inductotherm induction furnace, shown in Figure 3.1. The raw materials were melted in a mild steel crucible shown in Figure 3.2. A hand-held digital thermometer closely monitored the temperature of the melt. To minimize the temperature drop, the molten metal was poured directly from the crucible into the tundish.
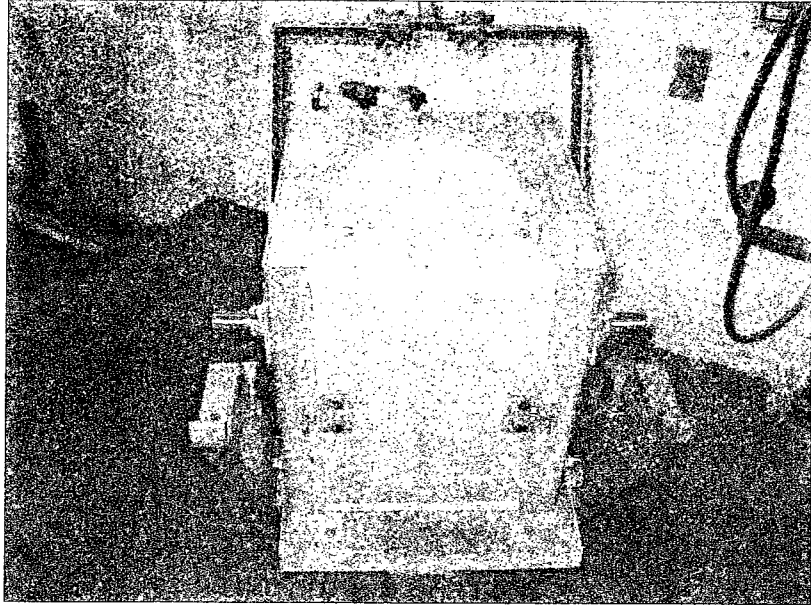
Figure 3.1 - Inductotherm induction furnace

Figure 3.2 - Mild steel crucible

3.2. Strip casting simulator:

A schematic overview and photo of the strip cast simulator are shown in Figure 3.3. As can be seen, the instrument includes the following: a containment mould, a substrate onto which the melt can be poured, a tundish, a motor that drags the substrate at pre-selected casting speeds, and a data acquisition system. The simulator can be set to produce strips of (w×l×t) of 80×1100× (1-5) mm, dimensions. The substrate can be coated with different coatings such as graphite, zirconia, nickel oxide, alumina, etc. Graphite powders used as a coating of substrate in the present study. In order to measure local heat fluxes, two thermocouples were placed in each segment of the substrate. For that purpose two holes were drilled along the longitudinal axis of each segment of the substrate at chosen depths.

The thermocouples were K type, which were bonded to the substrate by screws. The data from the thermocouples were acquired at the rate of 100/sec by an Omega data acquisition system set at a low noise option. The speed of the substrates is one of the important parameters to be considered and was fixed at 0.5 m/sec for most experiments. The calibration of the substrate's speed was performed by recording the substrate motion using a video camera followed by a subsequent analysis of the recorded videos.
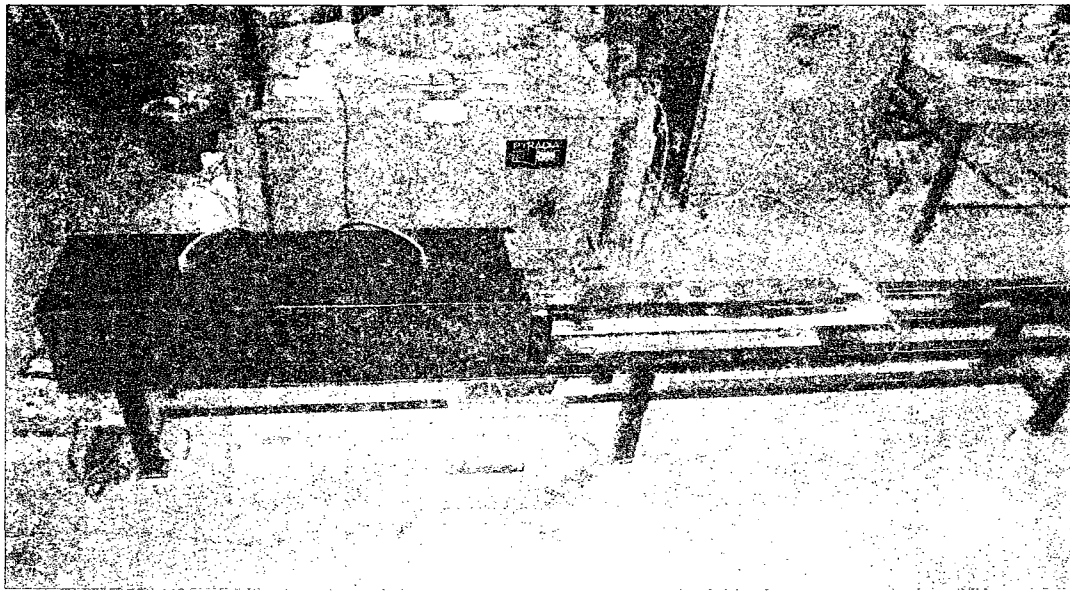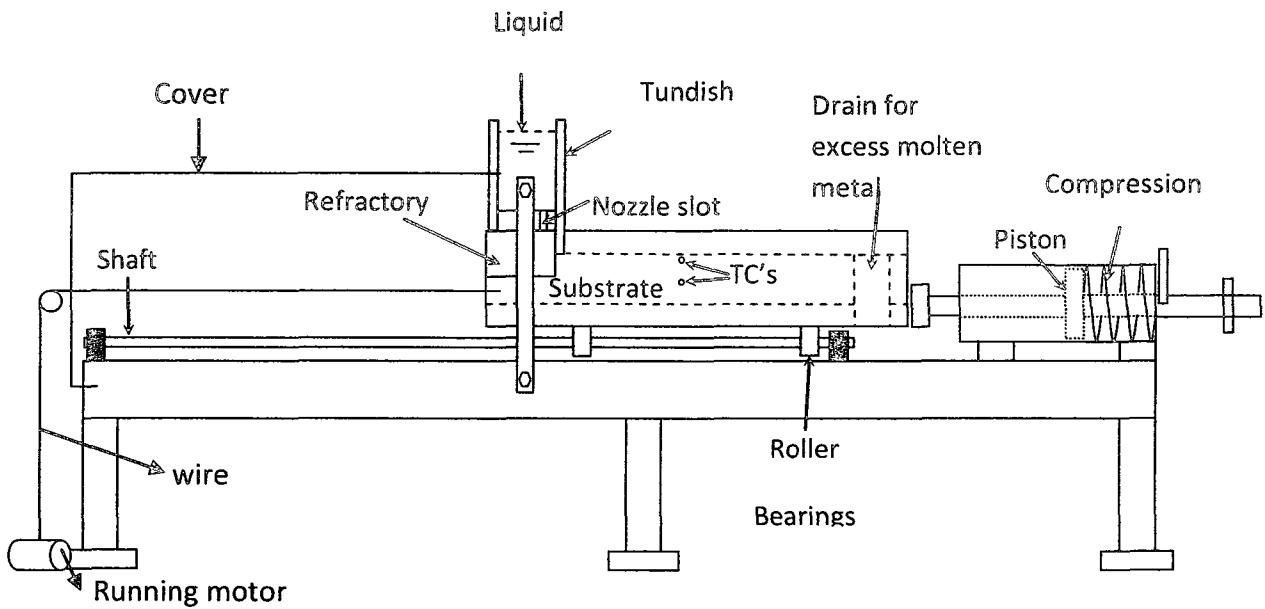
Figure 3.3 - Schematic and photo of the strip casting single belt simulator with a copper substrate fitted with six different copper inserts of various textures and roughensses

3.3. Substrate specification:

Two types of substrate were used in the experiments: steel with a polished surface and pure copper with six differently textured inserts. Figure 3.4 illustrates the schematics along with photos and dimensional specifications for the six copper substrate having 2×2

inch segments. Each segment has a different roughness and texture according to references[86,87].

Photo	Schematic	Specification
Segment(I)		$R_a \approx 0$
Segment(II)		$a = 64.4\ \mu m$ $x = 477.7\ \mu m$ $y = 90\ \mu m$ $z = 7\ mm$
Segment(III)		$z = 150\ \mu m$ $a = 8\ mm$ $b = 825\ \mu m$ $c = 78.5\ \mu m$
Segment(IV)		$z = 240\ \mu m$ $a = 320\ mm$ $b = 1103\ \mu m$ $c = 317\ \mu m$
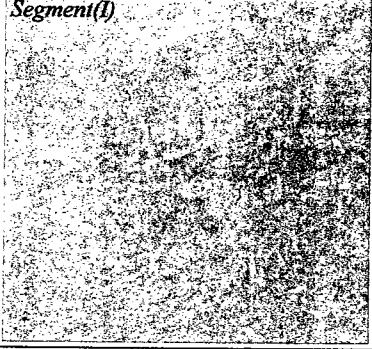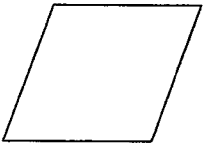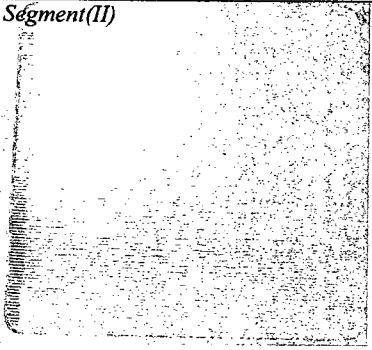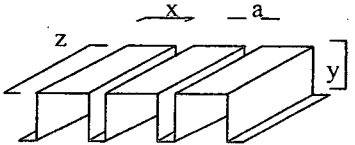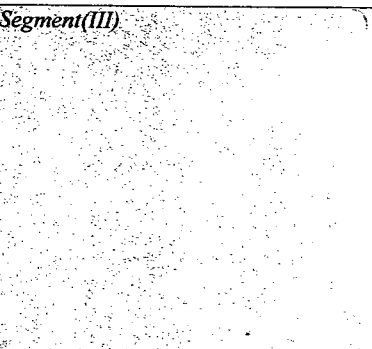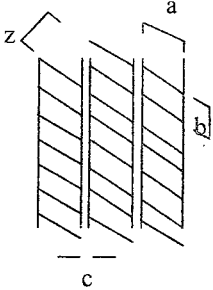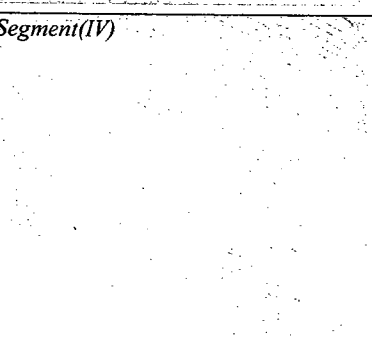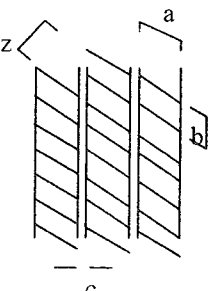
Figure 3.4 - Different segment areas of substrate
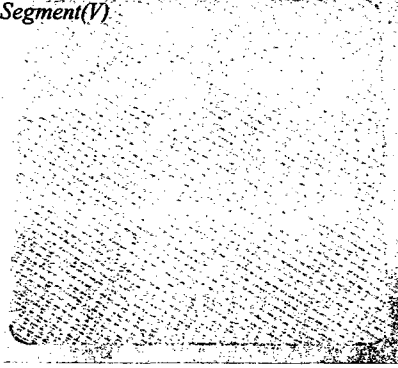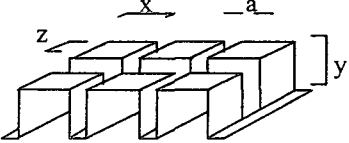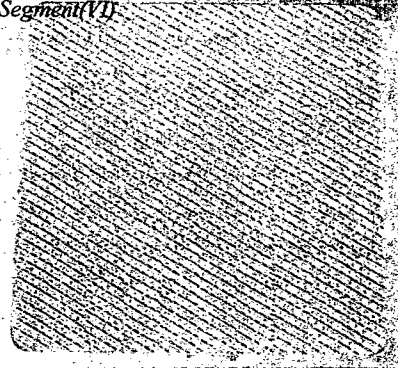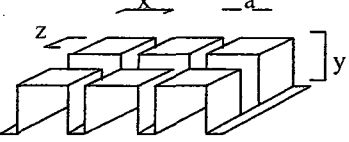
Photo	Schematic	Specification
Segment(V)		$a = 488$ μm $x = 998$ μm $y = 300$ μm $z = 998$ μm
Segment(VI)		$a = 451$ μm $x = 1074$ μm $y = 600$ μm $z = 1074$ μm

Figure 3.4 continued - Different areas of substrate

3.4. Melting and pouring of molten metal:

The melt was prepared in a steel crucible in which the atmosphere of the melt was protected from any excessive oxidation or possible burning, using a mixture of sulfur hexafluoride, 0.5% SF_6, in a carrier gas of carbon dioxide, 99.5% CO_2.

The molten metal was heated by using an induction furnace heating it to a temperature of 710°C, which is higher than the pouring temperature, 700°C, in order to provide sufficient superheat for skimming and metal transferring purposes. Once the melt had reached the desired temperature, the crucible was moved out of the induction furnace and transferred to the tundish. The molten metal was poured directly from the crucible into the tundish to avoid any large temperature drops. Before pouring, the tundish was preheated up to 150

°C for drying the refractory walls inside the tundish. At the same time, the substrate were preheated to 30°C for avoiding moisture. Transferring and pouring of the molten metal were done manually.

After pouring the molten melt into the tundish, a period of 2-3 second was allowed before releasing and pouring onto the substrate. The substrate was propelled by a motor to run at a constant speed of 0.5 m/sec.

To protect the melt during pouring and solidification, the substrate and tundish were protected with the gas mixture (0.5% SF_6, 99.5% CO_2). Alumina refractories were used to prepare the nozzle and to cover the inside walls of the tundish.

The preparation of the simulator for casting can be summarized in the following steps:

1- Cleaning and lubricating the substrate rails

2- Fixing the thermocouples

3- Fixing the substrate with screws

4- Leveling the substrate

5- Fixing the tundish

6- Adjusting the nozzle and refractory on the tundish

7- Checking if there was any friction during the movement of the substrate

8- Sealing the liner to avoid the melt's splashing out

9- Installing a cover over the strip

10- Preheating the substrate and tundish

11- Turning on the protection gas on the substrate and the tundish

3.5. Casting condition and procedure:

As noted in the literature review, the substrate coating, the substrate material, the substrate roughness, and the casting thickness, greatly influence strip quality. For these reasons, the experiments were designed to investigate the effect of these parameters on heat fluxes, microstructures and mechanical properties of the cast AZ31-B sheet products.

3.5.1. The effect of substrate material:

According to previous investigations[61,63], substrate materials have a great effect on the quality of a single belt casting. Moreover, the effect of the substrate material on the heat flux and microstructure is important. In order to investigate the effect of substrate materials on the strip's microstructure, surface quality, heat flux, and the mechanical properties, two kinds of substrates (steel and copper) were used.

3.5.2. The effect of substrate texture:

The roughness of the substrate has an effect on the quality of the surface and the microstructure of strip cast AZ31-B[62,88]. In this regard, the effect of the substrate surface textures were investigated by dividing the copper substrate to six different roughnesses. The heat flux was measured by twelve thermocouples (two thermocouples per segment). All castings with a copper substrate were done with this type of substrate.

3.5.3. The effect of substrate coating:

It has been shown that the coating of the substrate has a great effect on the surface quality, heat flux, and also the microstructure and the mechanical behavior of single belt casting AZ31-B[61,71]. To investigate the effect of coating on the above-mentioned

parameters, the substrate was coated with graphite to a 60.51±5 μm thickness. In order to determine the coating thickness, a cross section of the substrate was analyzed using optical microscopy and Clemex image analyzer.

3.5.4. The effect of strip thickness:

It is known that the casting thickness has a significant effect on microstructure, heat flux and mechanical properties[62]. Therefore, to investigate the effect of thickness on strip casting, the strip thicknesses of 1 and 3 mm were studied in the case of copper substrate with a graphite coating.

3.5.5. Summary of casting condition:

A summary of the experimental conditions for casting strips of magnesium alloys is given in Table 3.1. To achieve reasonable results (for good reproductively), each condition was repeated at least three times. For all the castings, the pouring temperature and the casting speed were kept constant at, 700°C and 0.50 m/sec.

Table 3.1. Summary of casing conditions.

Substrate Material	Coating	Thickness
Steel	No	3mm
Steel	Graphite	3mm
Copper	No	3mm
Copper	Graphite	3mm
Copper	Graphite	1mm

3.6. Metallographic examination:

The microstructures were investigated by means of optical and scanning electron microscopy. Optical microscopy was conducted on both polished and etched samples. Samples were mounted and mechanically ground using standard SiC sanding papers with

240, 320, 400, 600, and 1200 grit. The samples were rinsed and dried with ethanol and blasts of hot air[89].

The residual visible scratches after rough polishing were removed using 0.3 microns alumina powder in water on a polishing cloth. The samples were cleaned with distilled water and cotton, rinsed in ethanol, and dried using a stream of hot air. In order to prepare the samples for scanning electron microscopy (SEM), the samples were further polished with a silica colloid suspension, OP-U. The samples were then cleaned in the sonication bath for 10 minutes. Moreover, to investigate the non-conductive MgO powder it was coated with gold. A Struers polishing machine was used for the grinding and polishing of the samples.

In order to differentiate various secondary phases, the samples were etched with a liquid solution (10% HNO_3 – 90% Ethanol) for a duration of ten seconds. A different solution was used for etching the samples to observe grain boundaries (5gr picric acid, 0.5 ml nitric acid, 5 ml water, 25 ml ethanol) carried out for a period of 2 seconds. Finally, for better microstructural observation, etching of the samples was further continued with (1% HNO_3 – 99% Ethanol) for another 2 seconds. It should be noted that, after each step the samples were rinsed with ethanol and dried with hot air. The samples were examined and photographed using Optical microscopy, equipped with Clemex image analyzer. The grain size was measured using the linear intercept method, as described in ASTM E 112-88. The secondary dendrite arm spacing (SDAS) were measured using Clemex image analyzer. For microstructural and phase distribution a HITACHI 3000N scanning electron microscopy (SEM) was used[90,91].

3.7. Mechanical properties examination:

Vickers microhardness measurements were carried out according to ASTM standard E384-99 using a CM-100AT CLARK-microhardness tester shown in Figure 3.5. All the tests were performed under 10g loads for 15 seconds indentation time. The hardness of the strips was ascertained using a pyramidal diamond indenter. More than ten tests were made on a polished part of the bottom side of the strip and on cross sections of the specimens. The average value of the tests was used.

It should be noted that, microstructure of the AZ31-B had a secondary phase and microhardness test were carried out on matrix structure. The average microhardness measured is related to the tensile strength and the yield strength according to the equations presented.
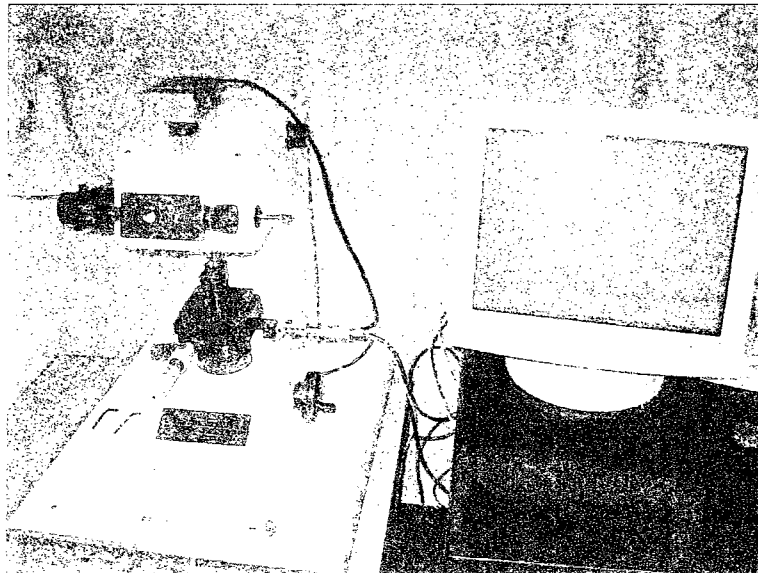
Figure 3.5 – CLARK microhardness tester

The hardness of metals is its resistance to surface indentation under standard test condition. Both hardness and tensile strength are indicators of a metal's resistance to plastic deformation. Consequently, they are roughly proportional. Commonly a correlation between hardness and tensile strength is given by following formula for approximately estimating the tensile strength of a metal from its hardness value:

$$TS\ (MPa) = 3.4 \times BHN \tag{3.1}$$

The correlation of hardness with tensile strength is generally good (difference usually less than ± 10 %)[92].

The 0.2 percent offset yield strength can be determined with good precision from the Vickers hardness measurements according to the following relation[93]:

$$\sigma_0 = \frac{DPH}{3}(0.1)^{n'-2} \tag{3.2}$$

Where σ_0 is the 0.2 percent offset yield strength, kgf mm^{-2} (=0.81 MPa), DPH is the Vickers hardness number and n' is a material constant related to strain hardening exponent of the metal[93].

The hardness can be related to the yield stress of the material, σ_y, by an expression based on the theory of indentation of rigid perfectly plastic solid.

$$HV = \frac{Indenter\ \ Force\ (kg)}{Surface\ \ Area\ \ of\ \ the\ Inprint\ (mm^2)} \tag{3.3}$$

65

For non-strain hardening materials the Vickers hardness number, which is defined as in the above formula, can be related to the constant yield stress, σ_y, by[93,94]:

$$H = 3\sigma_y \qquad\qquad (3.4)$$

where H is hardness (Tables are available to relate H to H_v) and σ_y is the yield strength.

Hardening and tempering heat-treating process for metals will give rise to microstructural change in the metal. Undoubtedly, the difference in yield strength was led mainly by the differential microstructures resulted from the different heat treating parameters used by the heat treatment providers. The major adjustable parameters in heat treatment comprise tempering temperature and time. They affect the microstructure, grain size, and eventually mechanical properties of the parts, including the yield strength and hardness. It is estimated that the major differences in processing parameters used by the heat treatment providers are of tempering temperature.

The grain size, one of the microstructural measurements, has particularly significant influence on the yield strength. Yield strength will generally tend to decrease with increasing grain size much the same as toughness does.

In general, as the average grain size decreases, the metal becomes stronger (more resistant to plastic flow) and as the grain size increases, the opposite effect on strength occurs. The difference in grain size is caused mainly by the differential heat treating parameters and/or possibly original grain size of the material before hardening.

The effect of grain size on yield strength, σ_y, is given by the Hall-Petch equation:

$$\sigma_{y=} \sigma_0 + kd^{-1/2} \qquad (3.5)$$

Where σ_0 is the lattice resistance, i.e. friction stress which opposes dislocation motion and k is a constant, sometimes called the dislocation locking term and d is the grain size[93,94].

3.8. Calculation of heat fluxes:

3.8.1. Applying IHCP to a single strip caster belt simulator:

If the IHCP applied for the interface between the single belt simulator shown schematically in Figure 3.6, the boundary conditions for the governing differential equations can be expressed as[61] :

$$\rho C_p \left(\frac{\partial T}{\partial t} \right) = k \frac{\partial^2 T}{\partial x^2} \qquad (3.6)$$

$$-k \frac{\partial T}{\partial t} \Big|_{x=0} = q_1 \qquad \text{t>t}_{l\text{-}1} \qquad (3.7)$$

$$T(x_1, t = t_{l-1}) = F(x_1) \qquad (3.8)$$

$$T(x_2, t = t_{l-1}) = F(x_2) \qquad (3.9)$$

The corresponding differential equation and boundary conditions for sensitivity coefficients are:[62]:

$$\rho C_p \frac{\partial \emptyset}{\partial t} = k \frac{\partial^2 \emptyset}{\partial x^2} \qquad (3.10)$$

$$-k\frac{\partial \emptyset}{\partial x}\Big|_{x=0} = 1 \qquad l > t_{l-1} \qquad\qquad (3.11)$$

$$\emptyset(x_1, t = t_{l-1}) = 0 \qquad\qquad (3.12)$$

$$\emptyset(x_2, t = t_{l-1}) = 0 \qquad\qquad (3.13)$$

Where $\emptyset$ is sensitivity coefficient and subscript l denotes the time when it was applied. In this investigation, temperatures are recorded using two thermocouples for each segment of the substrate connected to an omega data acquisition system. In order to convert the time vs. temperature data to time vs. heat flux, an IHCP software was developed by R.Tavares[51]. The software was presented in this work is elaborated in details in Appendix (I). Software principles are explained in chapter 2 section 2.5.8.1[51,61].
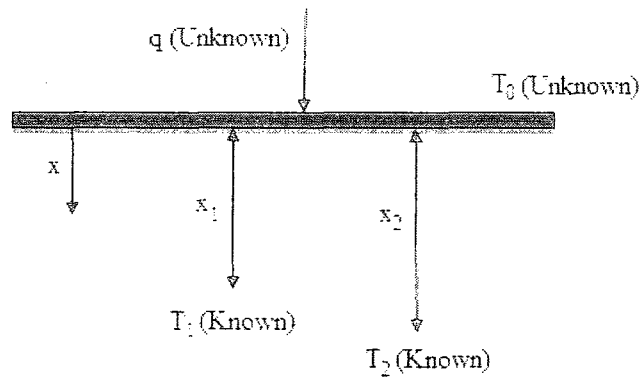
Figure 3.6 – Schematic of applying IHCP to deduce interfacial heat fluxes for the single belt strip casting simulator[61.62]

3.8.2. Filtering of noise:

Because of the electrical noise produced by the other equipments in the experimental area, noise on the time vs. temperature curve were observed. To alleviate this problem, a lowpass filter, Hamming Filter, was developed and programmed using MATLAB

(Appendix II) and was applied to the data. The applied software significantly filtered the noise and smoothened the curves (noise reduction).

This filter has a magnitude one at all frequencies with a magnitude less than ω_0, and magnitude zero at frequencies with magnitude between ω_0 and π. Its impulse response sequence $h(n)$ is:

$$h(n) = \frac{1}{2\pi} \int_{-\pi}^{\pi} H(\omega)e^{i\omega n}\, d\omega = \frac{1}{2\pi} \int_{-\omega_0}^{\omega_0} e^{j\omega n}\, d\omega = \frac{\omega_0}{\pi} sinc\left(\frac{\omega_0}{\pi} n\right) \quad (3.14)$$

Where ω is the frequency and n is the order of frequency while $H(\omega)$ is the complex frequency response of a filter.

Sensibility and range of data could be celebrated by changing cut off frequency and the filter is not implementable if the data which are dealt with are infinite or outside a sensible range. By retaining the central section of the impulse response in this truncation, a linear phase filter was obtained. The graphs are represented by datasheet of numbers corresponding to both coordinates. The noise-modification of the graphs were carried out by applying the noise filtration over the groups of numbers in order, each comprising 51 data element. The low-pass cut-off frequency were 0 of 0.4π rad/s[95.96].

RESULTS AND DISCUSSION

4.1. Heat flux analysis:

4.1.1. The effect of the substrate material on heat flux:

One of the important issues in strip casting is the material of the substrate. Figure 4.1 and Figure 4.1 show the plot of the calculated heat fluxes versus contact time and the maximum values obtained. The casting conditions (speed, superheat, thickness) were the same at each time. Only the substrate was changed from steel to copper (coated and uncoated).
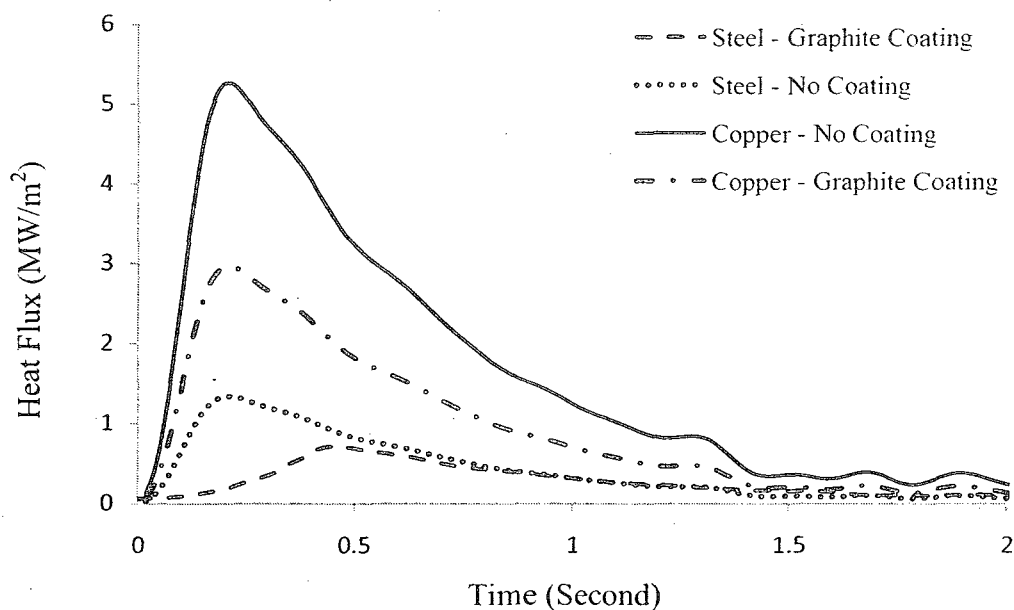
Figure 4.1 - Comparing Heat flux in Steel and Copper substrate

Table 4.1. Value of maximum heat flux in different materials of substrate[97]

Substrate Materials	Coating	R_a	Max Heat Flux MW/m^2
Steel	No	0	1.29
Copper	No	0	5.06
Steel	Yes	0	0.71
Copper	Yes	0	2.85

According to Fourier's law of heat conduction:

$$q = -kA\frac{\partial T}{\partial x} \tag{4.1}$$

The thermal conductivity of various metals is plotted against temperature in Figure 4.2, and the thermophysical properties are summarized in Table 4.2. The results match the values given in Figure 4.1, that is, the conductivity of copper is about twenty times higher than the conductivity of steel.
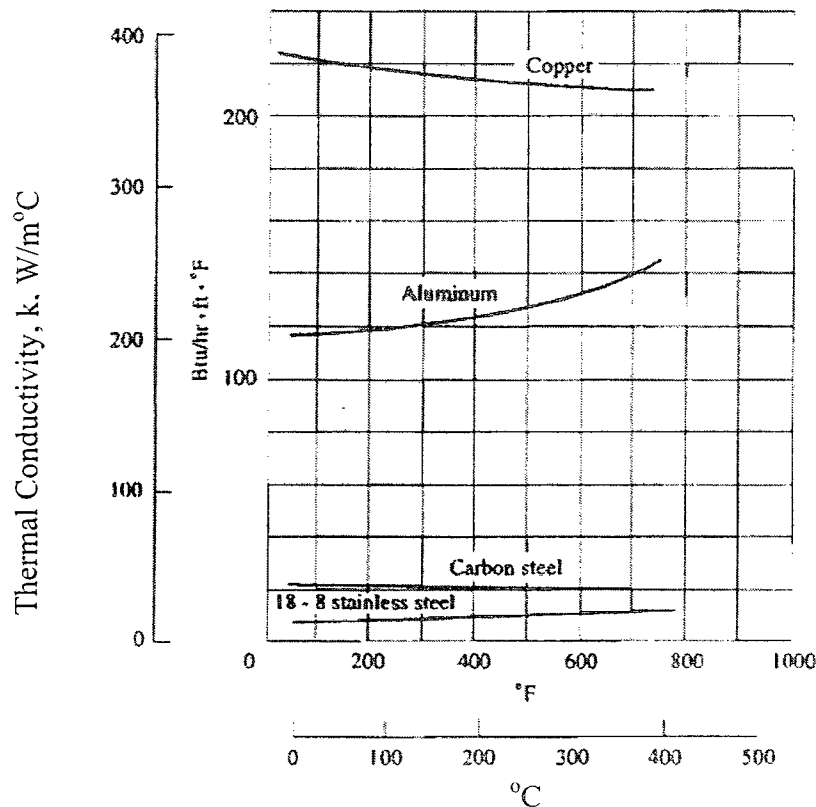
Figure 4.2 – Thermal conductivity of different substrate materials[97]

Table 4.2. Thermophysical properties of the substrates used[98.99]

Substrate materials	C_p (kJ/kg °C)	k (W/m °K)	ρ (kg/m^3)	α cm^2/sec
Carbon steel	0.486	48	7753	0.081
Copper	0.383	386	8954	0.415
Graphite	0.71	24	2200	0.0024

The heat flux is related to the thermal conductivity and thermal diffusivity (cm^2/s). Hence, the great difference between thermal conductivity, k, of steel and copper is reflected on the heat flux vs. time curves. The copper substrate without graphite coating has the highest thermal conductivity, and it has the highest heat flux at the mould/melt interface. Because of the poor thermal conductivity of graphite and steel, the steel substrate with graphite layer coat has a small heat flux at the mould/melt interface.

4.1.2. The effect of the surface topology of the substrate on the heat flux:

According to previous explanation in chapter 2 section 2.5.3, in the real casting procedure, metal/mould interface has no perfect contact. Localized heat flows through the real contact points between the metal/mould interfaces. Figure 4.3 shows the real interface of the mould/melt. That is the most significant cause for the thermal resistance at the interface[54.59.99].
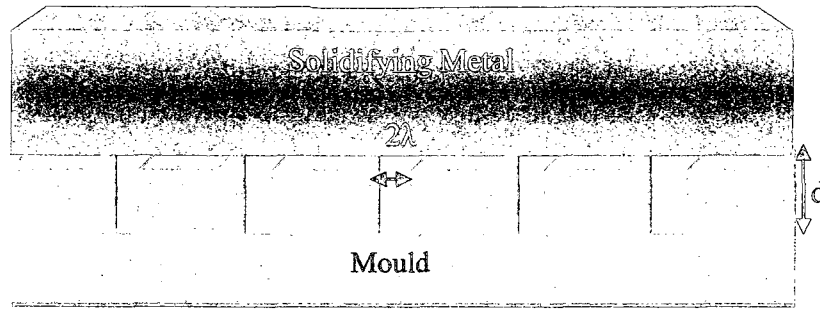
Figure 4.3 - Real interface of mould – melt[59]

When the melt "hangs" between two parallel-running peaks separated at distance of 2λ, the melt sag (d_{sag}) depends on the melt surface tension (σ) and the metallostatic pressure (ΔP). In the case of a non-wetting substrate, the radius of the metal's curvature, R, is[63]

$$R = \frac{\sigma}{\Delta P} = \frac{\sigma}{\rho g h} \qquad (4.2)$$

where σ is the melt surface tension, ρ is the melt density, g is the gravity constant, and h is the melt height. As illustrated in Figure 4.4, the melt sag can be calculated as[62,63]:

$$d_{sag} = R - \sqrt{R^2 - \lambda^2} \qquad (4.3)$$
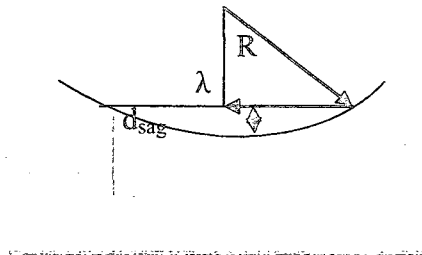
Figure 4.4 - Radius of curvature and melt sag[62]

On the other hand, when two materials at different temperatures contact each other perfectly, the interfacial heat flux is infinite for the first moment of contact. There is no thermal resistance at the interface, if the contact is perfect. In ideal perfect thermal

73

contact, the interfacial heat flux at the moment of contact would begin to drop off exponentially from a value of infinity. However, in real experiments many thermal resistances exist at the interface. These include thin films of trapped air, oxide layers, gaps made by shrinkage of the solidifying shell from the interface, that would reduce any air gap. These factors reduce the value of the heat flux and change the interfacial heat flux from that achieved with a perfect thermal contact. Figure 4.5 illustrates that there are many initial air pockets at the interface. Together with the development of an air gap as the solidifying metal shrinks, these gaps greatly hinder melt/mould heat transfer[54].

────▷ : Heat flux through contact point   ⇒ : Heat flux through air pocket
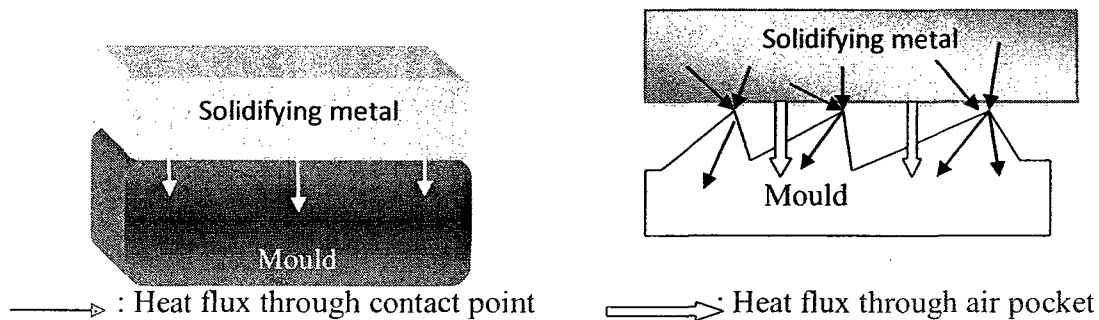
Figure 4.5 - Perfect versus real contact melt-mould[54]

Moreover, as noted in chapter 2, macroscopically, the thermal resistance effect can be obtained by measuring the temperature profile of the contacting bodies along their centerline, and extrapolating the resulting one-dimensional line to the contact interface, as illustrated in Fatigue 4.5. The thermal contact resistance, R_c, is then defined as the ratio between the temperate and heat transferred[97,98].

Figure 4.6 shows the specification of the substrate in deferent segments based on the depths of the grooves, however, the more detail of the substrate topography presented in section 3.3.

74
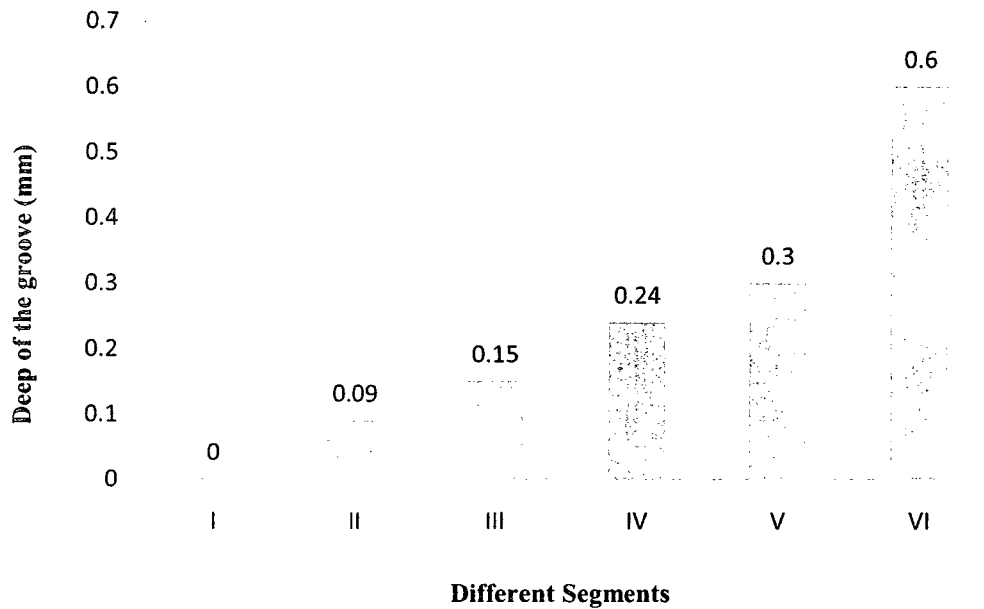
Figure 4.6- Specifying the deferent segments of substrate by deeps of grooves

Figure 4.7, illustrates the heat flux notation with time for different surface topologies, where a,b,c,d,e and f represent deferent segments of substrate form I to VI respectively. However, the figures indicate that increasing the surface roughness leads to a decrease in the heat flux. Table 4.3 shows that the heat transfer through the air pockets at the mould/melt interface was lower than that at the contact points.

The maximum heat flux was achieved in segment (III), c, in the coated and non-coated substrates while the minimum heat flux was recorded in segment (VI), f. Therefore, segment (III), c, is associated with maximum surface contact of melt/mould, while the highest numbers of air pockets are present in segment (VI), f.
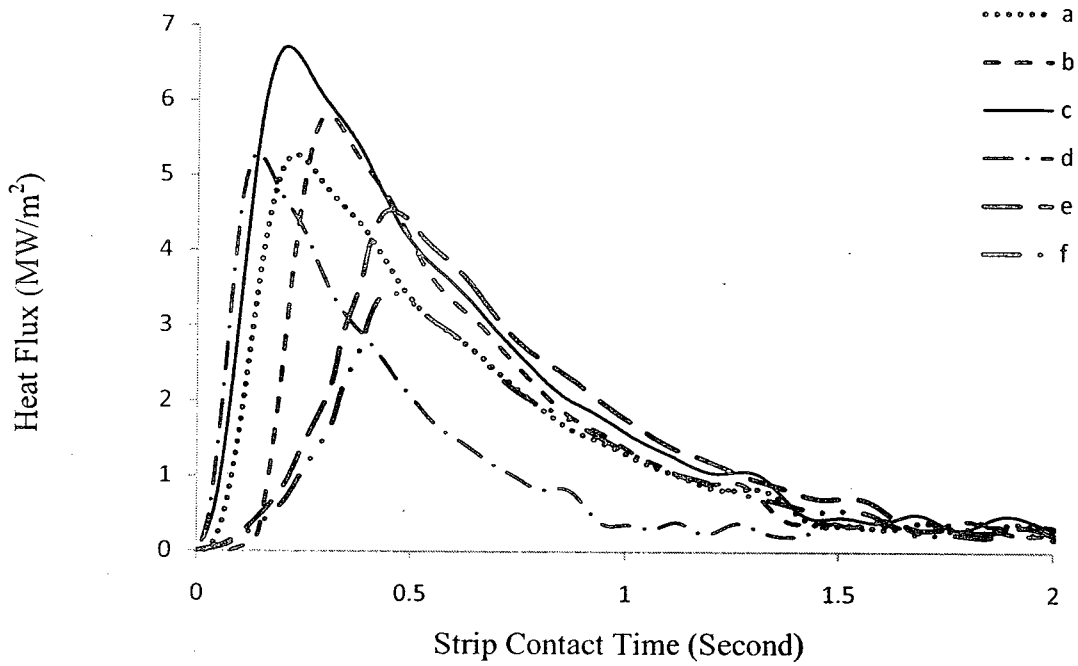
a) Uncoated copper substrate for six types of macro-texturing
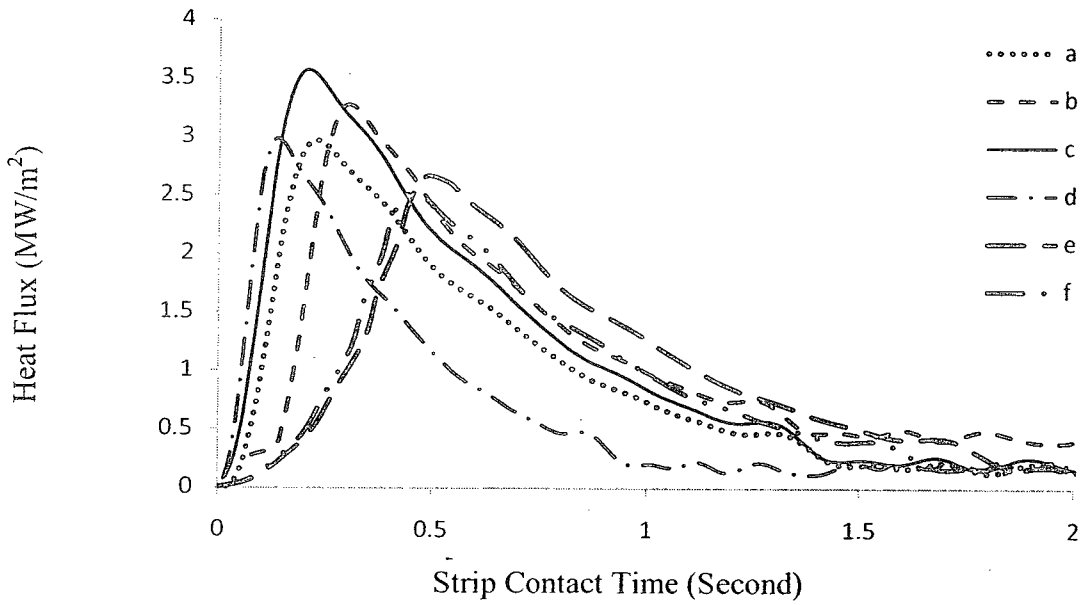
b) Copper substrate with graphite coating for six types of macro-texturing

Figure 4.7 - Effect of surface topology of substrate on heat flux with 3mm thickness of magnesium alloy strip

Table 4.3. Maximum values of heat flux from 3mm strips of magnesium cast on macro textured copper substrate

Segment No.	Coating	Depth of grooves (mm)	Max.Heat Flux (MW/m^2)
I	No	0	5.06
II	No	0.09	5.78
III	No	0.15	6.60
IV	No	0.24	5.18
V	No	0.3	4.38
VI	No	0.6	3.35
I	YES	0	2.85
II	YES	0.09	3.20
III	YES	0.15	3.53
IV	YES	0.24	2.93
V	YES	0.3	2.58
VI	YES	0.6	2.50

4.1.3. The effect of the substrate coating on heat flux:

According to the proposed mechanisms of interfacial heat transfer, given in the last sections, several parameters, such as surface rigidity, materials type, etc., affect the heat flow from the hot melt to the mould. Taking into account the poor thermal conductivity of graphite (Table 4.2), it can be assumed that the heat flux might be reduced using graphite coating. On the other hand, Figure 4.8 shows that coating a mould with fine graphite powders could increase the interface of the substrate/melt.
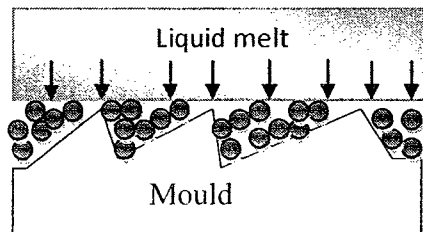
Figure 4.8 — Interface of coated mould/melt surface

Figure 4.9 illustrates the heat flux of the magnesium AZ31-B alloy for different surface

roughnesses, with and without graphite coating on the substrate. Maximum heat fluxes for graphite-coated substrates were less than those for un-coated substrates. Additionally, the influence of surface roughness on heat fluxes was more pronounced for un-coated substrate compared to the graphite coated substrate. However, graphite coating, due to its poor thermal conductivity, decreased the heat flux at the melt/mould interface.
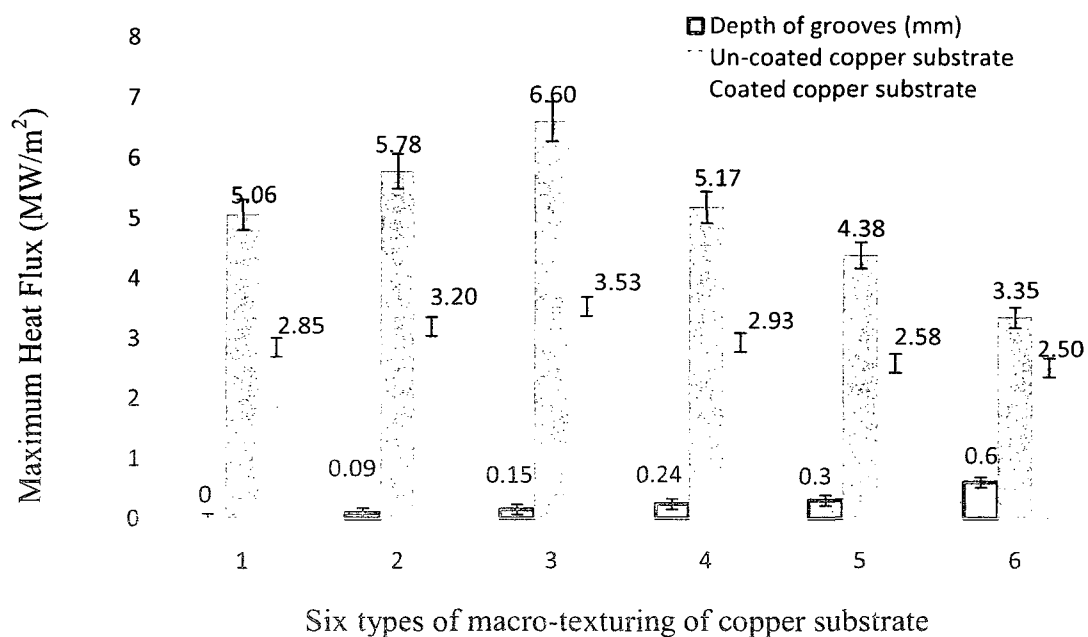
Figure 4.9 - Effect of surface topology of substrate on heat flux with and without coating

4.1.4. The effect of strip thickness on heat flux:

The distance between the nozzle and the substrate was decreased, and this variation reduced the thickness of the produced strips from 3 to 1mm. Figure 4.10 shows the evaluation of the heat flux versus temperature according to different textures of substrate for a strip of 1mm thickness. The substrate was coated with fine graphite. For evaluating thickness of coating on substrate, small coated part's of the substrate was investigated

under the optical microscope, image analyser, and thickness of the fine graphite was

evaluated of 60.51±5 μm.
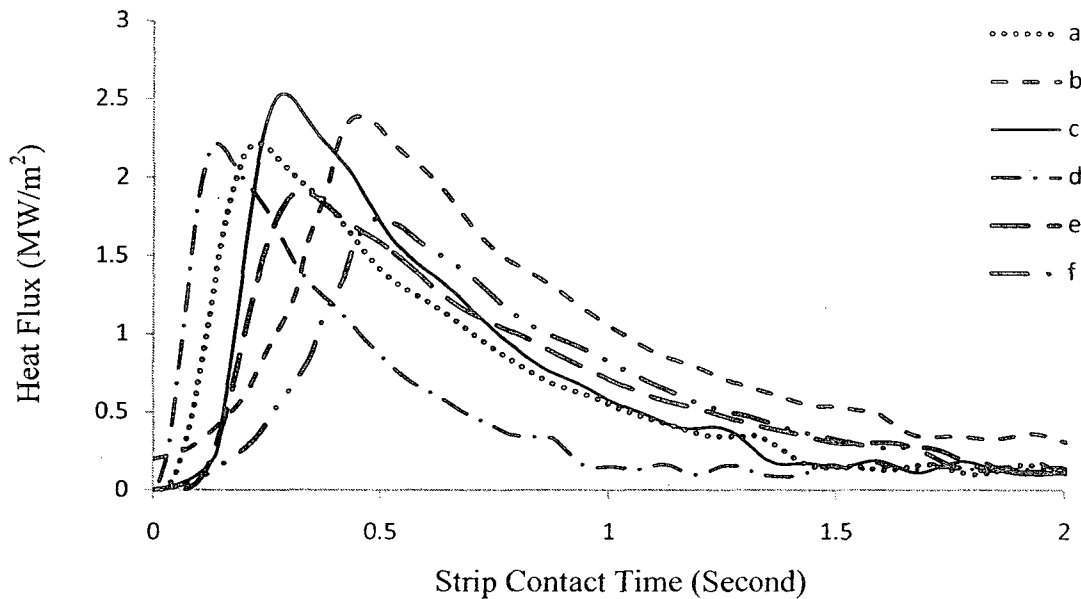
Figure 4.10 - Heat fluxes for 1mm of magnesium strip being cast on different textures of copper chill substrates

From Figure 4.9, one can divide the transient data into two regions:

➢ Initial increase of q curves with time of contact

➢ Exponential decrease of q with contact time

Based on the small solidification thickness in this work, at the first moment of the liquid metal comes into contact with the substrate, the liquid metal begins to feed onto the substrate and this contact liquid/solid contact enhances the heat transfer to the interface. A considerable amount of heat is transferred in this stage. Then, the solidification starts on the surface of substrate, and the interfacial heat transfer is dominated by the sensible heat release of the melt's superheat and evaluation latent heat. Because of the small

thickness of the strip, this released heat is transferred into the strip/substrate interface. Through the interface, the heat conduction from the interface to the interface to the substrate and the transferred heat by the release of latent heat come to be comparable and result in the constant value of heat transfer resistance during a certain amount of the time.

Consequently, after the release of heat, the increase of the solidified shell in the strip changes the interfacial heat transfer from a liquid/solid to a solid/solid contact causing, the value of the heat flux being to decrease exponentially due to the shrinkage of the solidified shell and the formation of an air gap at the interface. An idealized curve of the heat flux is shown in Figure 4.11.

Based on figure 4.10 texture IV, d, behavior appears close to ideal in the comparison with other textures.
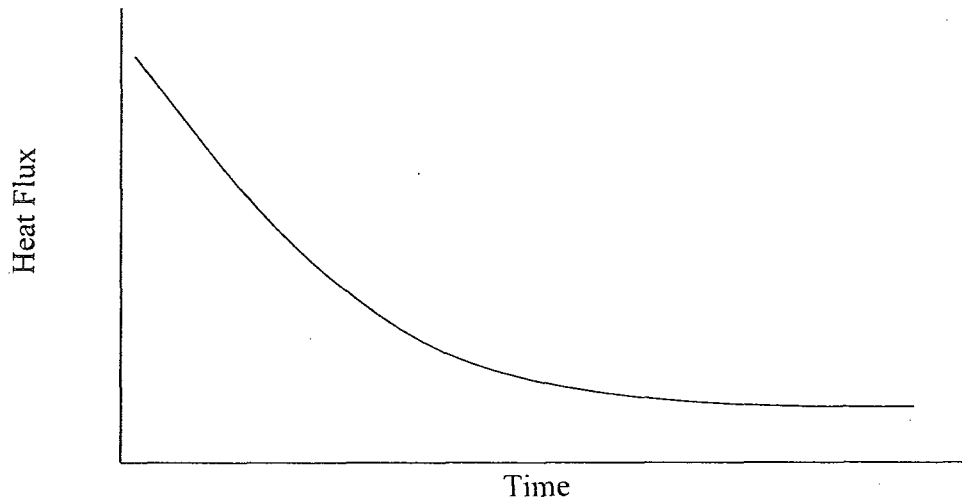
Figure 4.11 - Ideal curve of heat flux[57]

Changes in the maximum heat flux measured versus the strip thickness were observed. In Figure 4.12 and in the following equations, it is evident that if one increases the strip thickness, the amount of heat transferred from the strip to substrate should increase.

Essentially, the total amount of the heat loss per unit area required to complete solidification of liquid metal is:

$$\Delta Q_t = \rho \cdot d\{C_p(T_c - T_M) + \Delta H\} \tag{4.4}$$

Where ρ is the density of liquid metal, d is the thickness of strip produced, C_p is the specific heat, T_C is the casting temperature, T_M is the melting point, and ΔH is the latent heat of fusion. Note that $\rho \cdot d\{C_p(T_c - T_M)\}$ is sensible heat and $\rho \cdot d \cdot \Delta H$ is a latent heat component.

A heat balance relates the total loss necessary to complete solidification with the heat loss to the air by radiation ΔQ_r, and the solid by conduction ΔQ_c. The heat loss due to radiation from the upper surface of the strip can be described by the equation:

$$\Delta Q_r = \int_0^\tau q_r \, dt \tag{4.5}$$

where

$$q_r = \varepsilon \sigma T_M^T \tag{4.6}$$

Where ε is the emissivity, and σ is the Stefan-Boltzmann constant, 5.6703×10^{-8} W/m^{2}K^4.

The heat loss by conduction to the substrate is:

$$\Delta Q_r = \int_0^\tau q_c \, dt \qquad (4.7)$$

where

$$q_c = -k \frac{\partial T(x,t)}{\partial x} \Big|_{x=0} \qquad (4.8)$$

where k is the conductivity.

Therefore, subsutition of expressions for ΔQ_t, ΔQ_r and ΔQ_c into the heat balance equation yields a formula from which the total time to complete solidification, τ, can be calculated.

$$\Delta Q_t = \Delta Q_r + \Delta Q_c \qquad (4.9)$$

gives

$$\rho \cdot d \{ C_p (T_c - T_M) + \Delta H \} = \varepsilon \cdot \sigma \cdot \tau \cdot T_M^4 - \int_0^\tau k \frac{\partial T(x,t)}{\partial x} \Big|_{x=0} d_t \qquad (4.10)$$

Here, the heat loss by conduction includes the radiation of heat transfer due to air gap formation. Interface heat loss by radiation is negligible owing to its much lower order of magnitude versus conduction. Moreover, the thinner the strip production, the lower the heat flux dissipated, and the strip thickness, d, is very sensitive factor for evaluating the time of solidification[62].
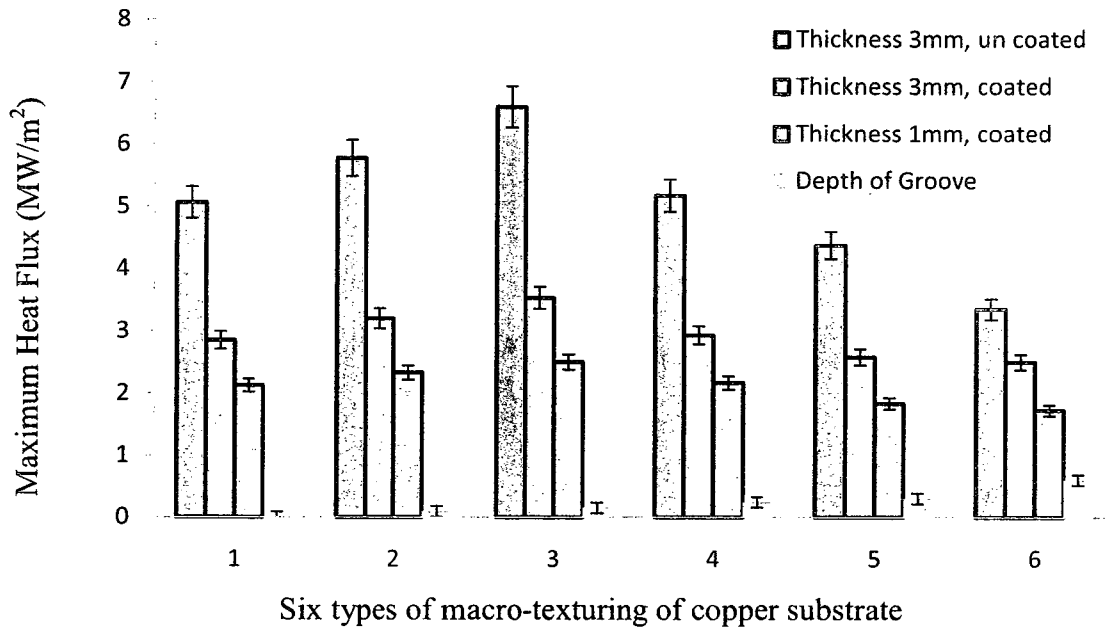
Figure 4.12 – Heat flux versus strip thickness and substrate textures

4.2. Macrostructure and surface quality:

4.2.1. Bottom surface quality of the strip:

AZ31-B melt was cast on smooth copper and steel substrates with and without graphite coatings. Figure 4.13 shows the bottom surface of the strip samples. It was found that there were many small pits or holes distributed on the strip's bottom surface for strips cast on steel substrate. Corresponding shrinkage marks were found on the strip's top surfaces vertically above the pitted regions. Because of low heat transfer in defects and air gaps, these are probably caused by delays in local solidification contact times forcing the melt above a pitted reign to feed liquid metal into regions where better heat extraction was acting.

4.2.1.1. The effect of the substrate material on bottom surface quality of the strip:

The pits and defects on Mg strips (Fig 4.13-a1 and a2) cast on the copper substrate were in more significant number compared with the case when the steel substrate (Fig 4.13-b1 and b2) was used. Then graphite was sprayed on the substrate surface to improve the melt's wettability with the substrate materials. However, Figures 4.13(a1) and (a2) show that the wettability of the melts was relatively increased. Then meniscus marks effects disappeared (Figure 4.13-a1) but number of air pocket defects was increased (Figure 4.13-a2).

However, the graphite coating led to a relatively improved bottom surface quality, for both copper and steel substrates with smooth surfaces.

Smooth Copper substrate product   Smooth Steel substrate product

a1   b1

a2   b2
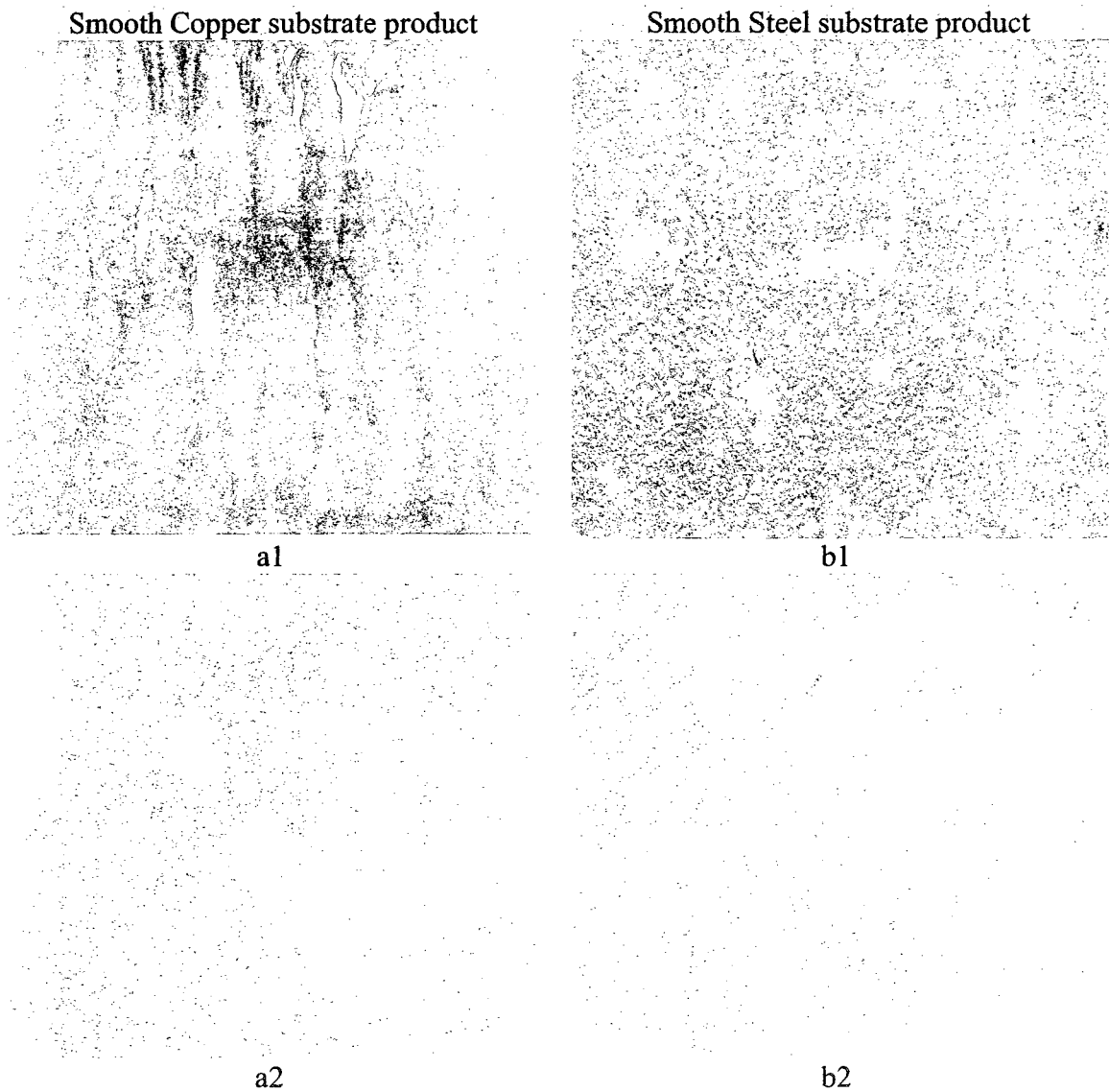
Figure 4.13 - Bottom surface quality of strip, casted on smooth substrates
a1) Bottom surface of strip casted on non- coated copper substrate
a2) Bottom surface of strip casted on coated copper substrate
b1) Bottom surface of strip casted on non-coated steel substrate
b2) Bottom surface of strip casted on coated steel substrate

4.2.1.2. The effects of the texture of the substrate on the bottom surface quality of the Strip:

Figure 4.14 (a1-a6 and b1-b6) illustrates the bottom surface quality of strips cast on copper substrates having different roughnesses, with and without graphite coating. According to the explanation in Chapter 3, section 3.2, the substrate texture was changed from smooth to 600µm in the groove (Figure 4.14). Clearly, as the roughness of substrate increased, the bottom surface qualities of strips improved. Defects were reduced by using both non-coated and graphite coated substrates.

Comparing a and b series, in Figure 4.14, it is found that the graphite coating did not help improve significantly the quality of the bottom surface with high roughness of the substrate. According to Figure 4.14, graphite powder reduced the roughness of the copper substrate in more rigid areas, the air pockets were trapped in the interface of melt/substrate. Values of heat flux in different areas of the substrate show that the amount of air pockets are high in rigid areas, but these were so fine and there were not big enough to affect the macrostructure of the strips.

Bottom surface with non-coated substrate   Bottom surface with graphite coated substrate

a1   b1
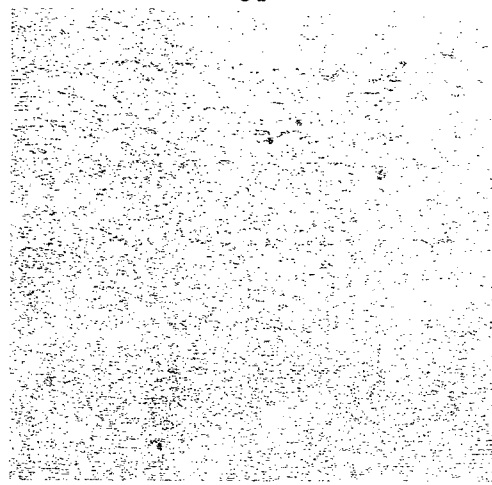
a2   b2

a3   b3

Figure 4.14-Bottom surface of strip with non coated and coated surface produced using different substrate textures

Bottom surface with non-coated substrate   Bottom surface with graphite coated substrate

a4

B4

a5

B5
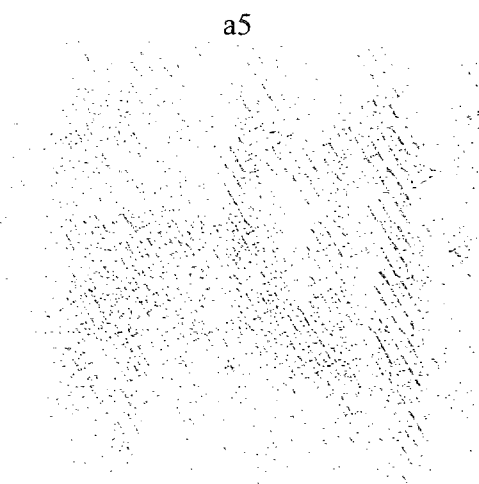
a6

B6

Figure 4.14 continued - Bottom surface of strip produced with non coated and coated surface using different substrate textures

4.2.2. Top surface quality of the strip:

According to the previous research conducted by Mahallawy and Assar[57], the origin of top surface quality during casting is thought to be the movement of liquid on solid within the semi-solid zone. Since highly segregated phases are present within this zone during casting, the physical displacement of these phases leads to the "poor quality" of the top surface of the strip. This may occur because of the movement of liquid within the solid-liquid zone as a result of thermal contractions, of solidification shrinkage, or of density differences in the interdendritic liquid. Also, the differences in density of the liquid ahead of the advancing solid and convection currents driven by temperature-induced density differences in the fluid may contribute to the poor surface quality. These factors can reduce the quality of the top surface by causing a mass flow over large distances during solidification[58].

Direction of moving melt

Semi solid layer

First solid layer

Substrate
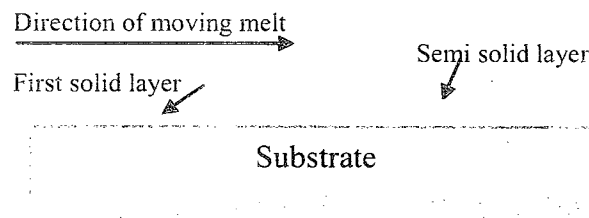
Figure 4.15 – Moving melt on surface of first layer of solid

Clearly, the top surface quality depends strongly on the sudden deceleration of the system at the end of casting, while the strip moves in a semi-solid state near the top surface. As a consequence of high heat flow on the surface of the substrate, the first layer of melt solidifies immediately after pouring more melt from the tundish on the substrate.

For this reason, semi solid layers move on the surface of the solid layer and reduced the quality of the top surface of the strip, as shown in Figure 4.15[48].

Figure 4.16 shows that, with an increase in the heat flux, the surface quality was modified. Therefore, the surface quality of magnesium alloy strip cast using copper substrate is better than that using steel substrate. Also, the heat flux was reduced in the case of coated substrates because of the poor thermal conductivity of the graphite layer, so the time difference between the solidification of the first layer and other layers of the melt was increased. Consequently, the semi solid layers had more time to move, and the top surface quality of the strip was significantly reduced.

As shown in Figure 4.16, because of high heat fluxes at the interface of melt/mould, the quality of strips top surface cast on the uncoated copper substrate (Figure 4.16a) were significantly better than the others.
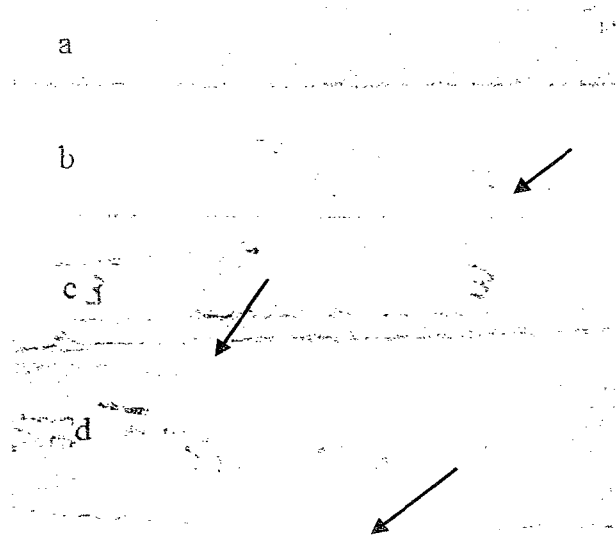
Figure 4.16 – Top surface quality of strip on different substrates. a) Non coated copper substrate product. b) Graphite coated copper substrate product. c) Non coated steel substrate product. d) Graphite coated steel substrate product.

4.3. Microstructure of cast AZ31-B strip:

4.3.1. Microstructural analysis:

Figure 4.17 shows a typical microstructure of the magnesium AZ31-B alloy strips. The grains and secondary phases were easily observed.
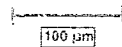
Figure 4.17 – Typical microstructure of magnesium AZ31-B alloys in X100

It has been claimed by Rappaz and Gandin[100] that the direction of the fluid flow directly influences the growth direction of dendrites at the melt/substrate interface. They showed that while the flow direction is upstream, the dendrites originate from substrate and at the

vicinity of the substrate are inclined towards the upstream direction[100]. However, in the work presented in this research the substrate was chosen to be perfectly horizontal. The investigation of the dendrite growth pattern for the horizontal substrate is shown in Figure 4.18. The dendrites initiate from the substrate, similarly to observations reported by Rappaz and Gandin[100]. However, the growth of the dendrites initiated at the substrate manifest no inclination and the growth direction is vertical.
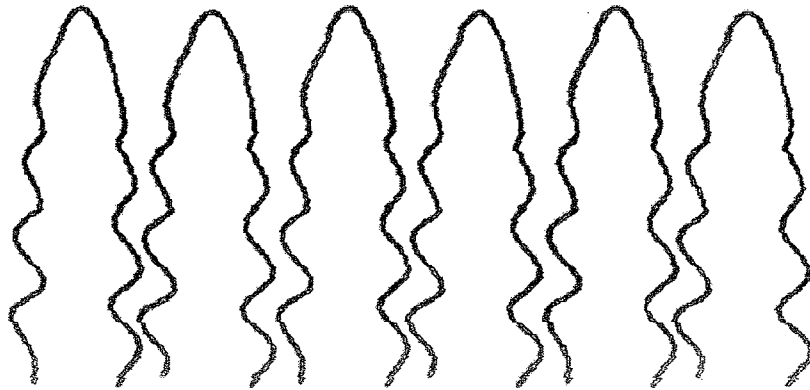
Figure 4.18 - Schematic diagram showing the influence of the fluid flow on dendritic growth[100]

The dendritic growth mechanism in magnesium AZ31-B alloys has been elaborated by Vander[101]. It is concluded that a similar principle governs the dendritic growth for magnesium AZ31-B alloy investigated in this work. During the solidification of the alloy, a symmetrical solute field at the dendrite tip is established. Accordingly, the solute gradient is uniform on both sides of the dendrite tip during the growth. Thus the main origin of the dendrite growth direction is deemed to be the solute distribution.

The non-homogeneous distribution of solute atoms between arms in a magnesium AZ31-B alloy is mainly due to the fact, that the dendritic solidification takes place over a range of temperatures. In fact there is insufficient time for atomic diffusion to redistribute the solute both within the liquid in the vicinity of the solid-liquid interface and within the solid, since cooling occurs rapidly through the two-phase (L+S) regime[58.91].

This creates gradients in the solute concentration through the thickness direction of a given dendrite arm with the likelihood of non-equilibrium phases forming in the last remaining liquid as shown in Figure 4.19. Similar observations have been reported in the literature[91].

Substrate movement direction
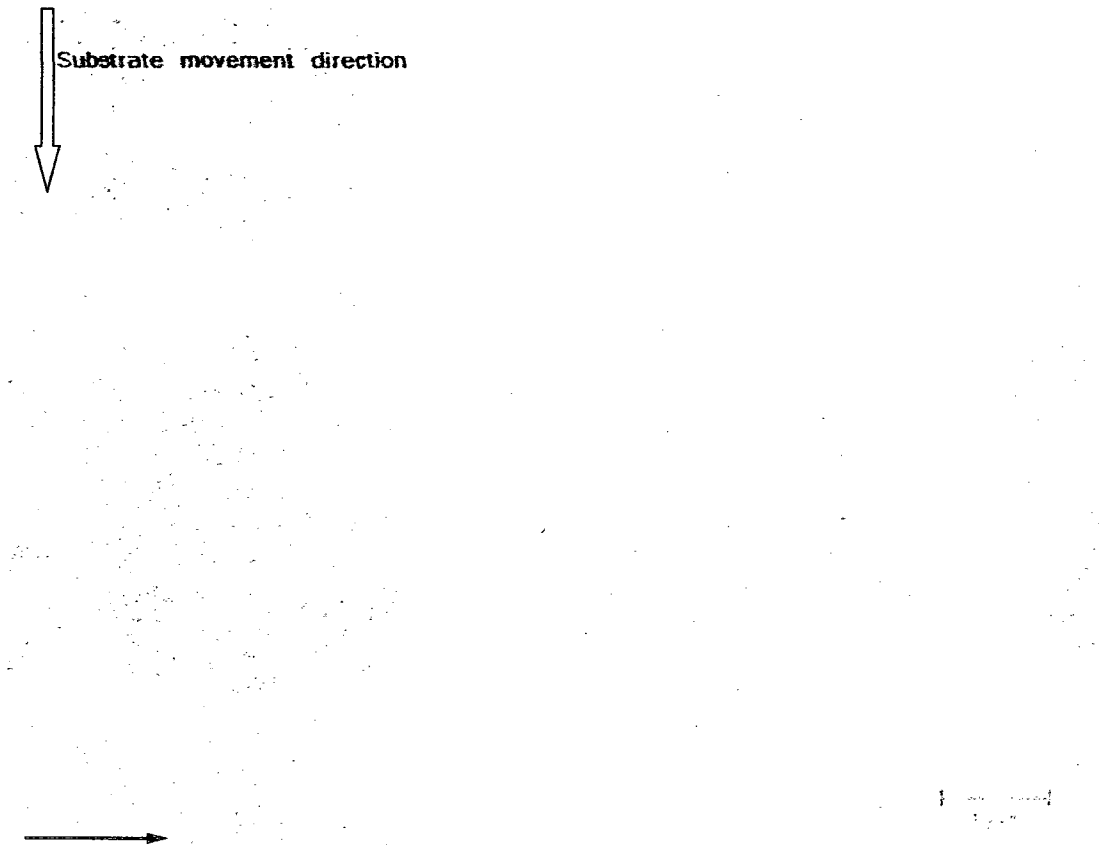
Figure 4.19 – Dendritic structure of magnesium AZ31-B alloy

Figure 4.20 (a) shows the microstructure of the bottom surface of AZ31-B that was cast on the segment with 0.15mm groove, with maximum heat flux (i.e. on a copper substrate). In addition, Figure 4.20 (b) illustrates the microstructure of the bottom surface of a strip that was cast with a minimum heat flux (i.e. on a smooth steel coated with graphite substrate).

a) Copper substrate

b) Steel substrate
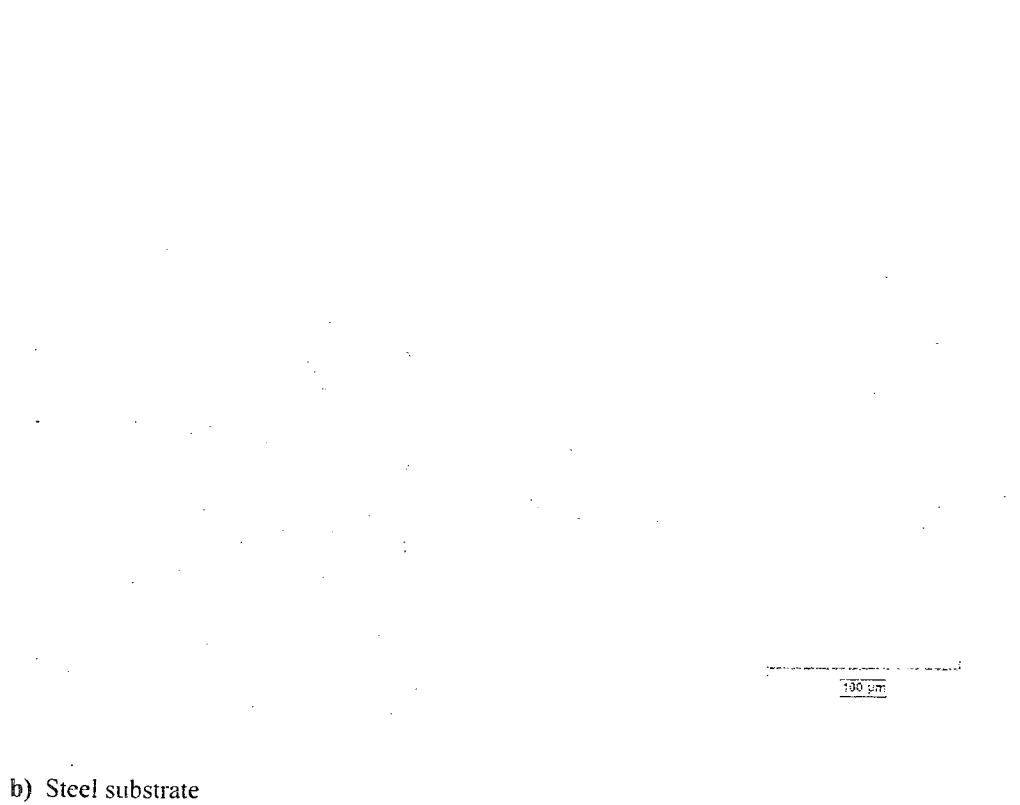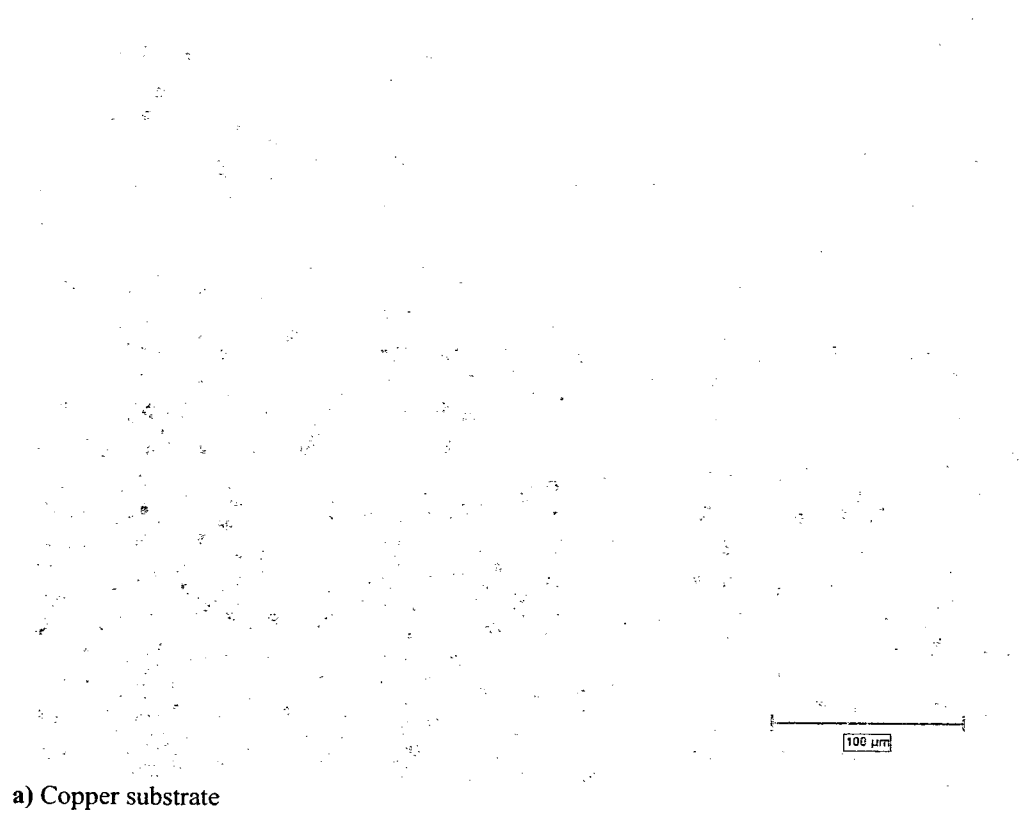
Figure 4.20 – Microstructure of bottom side of AZ31-B strip for different substrates; X200

95

By comparing the microstructures of the bottom surfaces of strips, it can be concluded that the grain size depends significantly on the heat flux. The results of the microstructural analysis of all samples are summarized in Table 4.4.

Table 4.4. Microstructure analyses of strips.

Depth of groove	Thickness	Coating	Heat Flux	R_c W/m² °C ×10⁻⁴	Grain Size Bottom	Grain Size Top	SDAS Bottom	SDAS Top
0.15	3mm	No	6.6	4.545	35	100	5.39	6.1
0.09	3mm	No	5.775	5.195	64	110	7.7	6.14
0.24	3mm	No	5.175	5.797	70	117	8.5	7.15
0	3mm	No	5.062	5.927	77	121	8.6	9.2
0.3	3mm	No	4.375	6.857	91	136	8.9	10
0.6	3mm	No	3.35	8.955	92	138	9.02	10.5
0.15	3mm	Yes	3.5	8.571	103	110	8.5	9.1
0.09	3mm	Yes	3.2	9.375	108	120	10.04	11.8
0.24	3mm	Yes	2.9	10.345	110	127	10.8	12.4
0	3mm	Yes	2.85	10.526	115	129	11.5	12.8
0.3	3mm	Yes	2.58	11.628	132	137	11.58	13.5
0.6	3mm	Yes	2.5	12.000	134	140	11.91	13.8
0.15	1mm	Yes	2.5	4.000	108	132	8.2	9.8
0.09	1mm	Yes	2.33	4.292	125	135	10.5	11
0.24	1mm	Yes	2.166	4.617	138	142	11.7	12.4
0	1mm	Yes	2.12	4.717	140	150	12.2	14
0.3	1mm	Yes	1.83	5.464	150	162	12.4	15.6
0.6	1mm	Yes	1.72	5.814	155	175	13	17
0 (Steel)	3mm	No	1.2	25.000	157	225	14	18
0 (Steel)	3mm	Yes	0.71	42.254	350	470	20	25

As shown in the microstructure of in Figure 4.20, with decreasing heat flux and increasing thermal heat resistance between the substrate and strip, the precipitation of second phases increases.

Obviously, with increasing heat flux, the grain size decreases. The grain size of the top surface is larger than that at the bottom surface because of solidification delay and smaller heat fluxes at the top surface.

Secondary dendrite arm spacing, (SDAS) are found to be directly related to heat flux and thermal contact resistance. As presented in Table 4.4, as the heat flux increase, the SDAS decreases

As explained earlier in section 2.5.3, air pockets are generally trapped at the substrate/melt interface, which dramatically reduces the heat flux. The occurrence of these air pockets can subsequently influence the microstructure of the strips. Consequently, the grains tend to grow up from the bottom surface to the top surface resulting in a columnar pattern of grain growth. The effect of these air pockets on the grain structure is clearly shown in Figure 4.21 presented at two different magnifications. Similar observation pertaining to the effect of air pocket formation on the strip's microstructure has been reported by Dube and Couture[78].
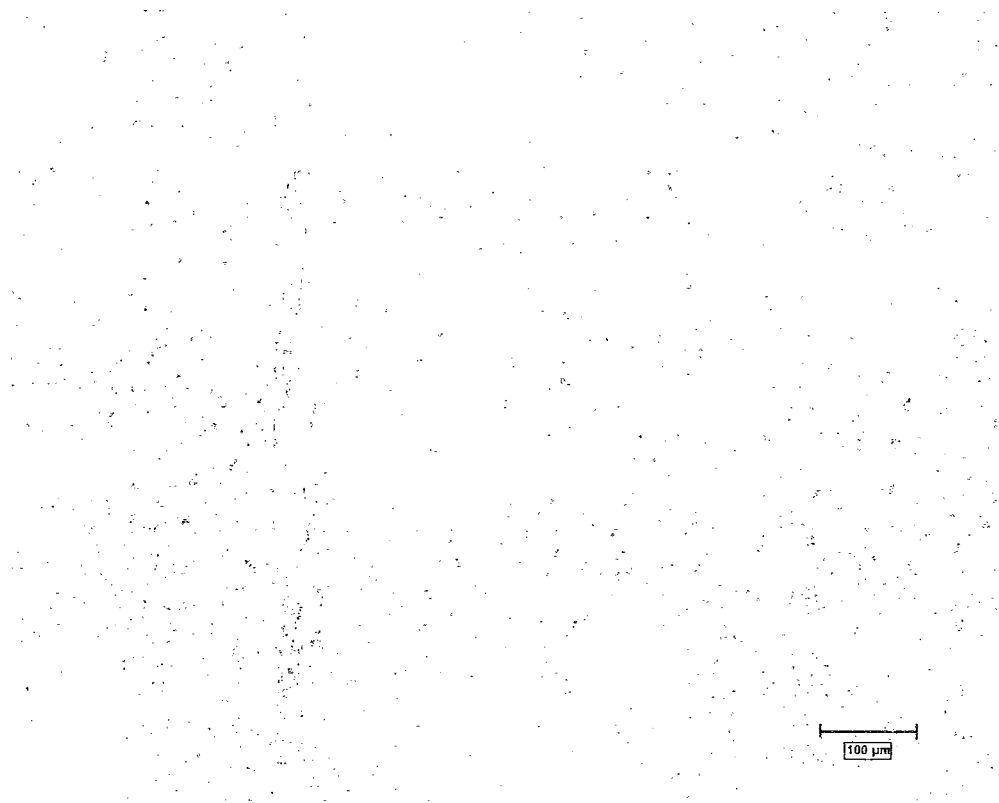
a) Directional grain growth because of air packet, X100
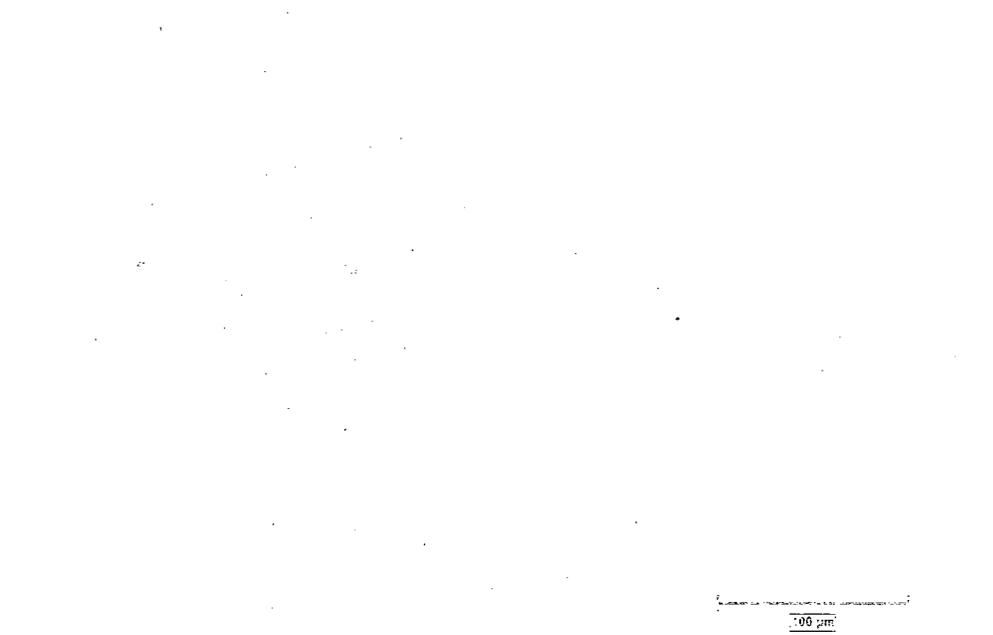
b) Directional grain growth because of air packet, X200

Figure 4.21 – Effect of trapped air pocket, at the interface of melt/mould

4.3.2. Phase analysis:

Secondary phases were precipitated onto secondary arms of dendrites shown in two

magnifications in Figure 4.22.
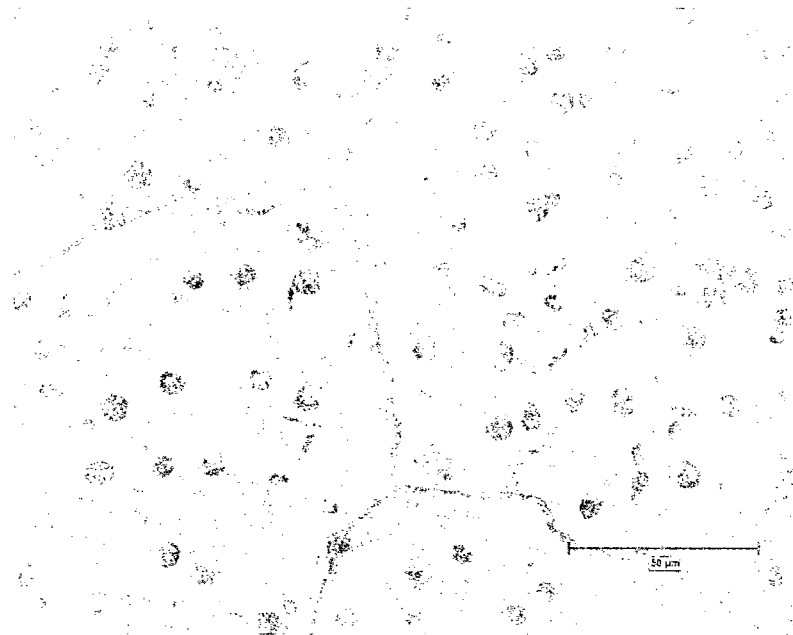
a) Precipitation of second phase in AZ31-B, X500

b) Precipitation of second phase in AZ31-B, X1000

Figure 4.22 – Precipitation of second phase in AZ31-B at different magnification

99

Scanning Electron Microscopy was used to obtain the chemistry and morphologies of the secondary phases as shown in Figure 4.23.
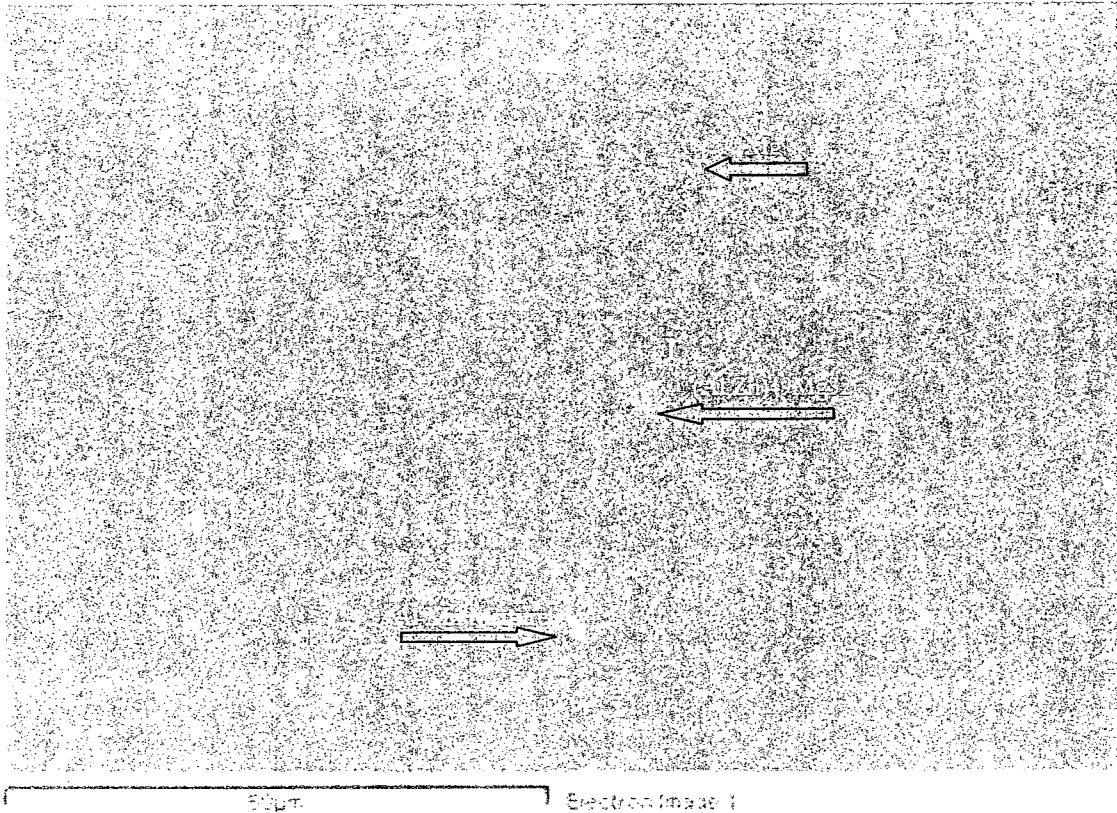
Figure 4.23 – SEM image of AZ31-B strip

The microanalyses using EDX technique was performed on the intermetallics marked in Figure 4.23, in order to identify their composition. An example of the X-Ray spectrum of the observed intermetallics is presented in Figure 4.24.
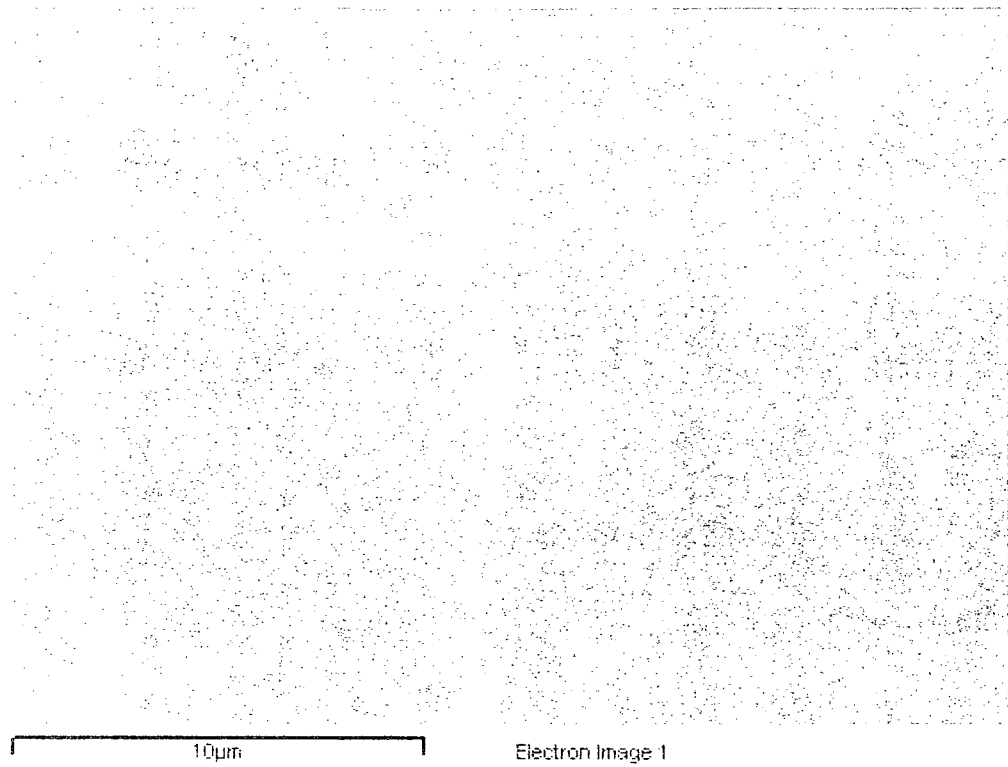
a) Image of focus on point 2 of Figure 4.23
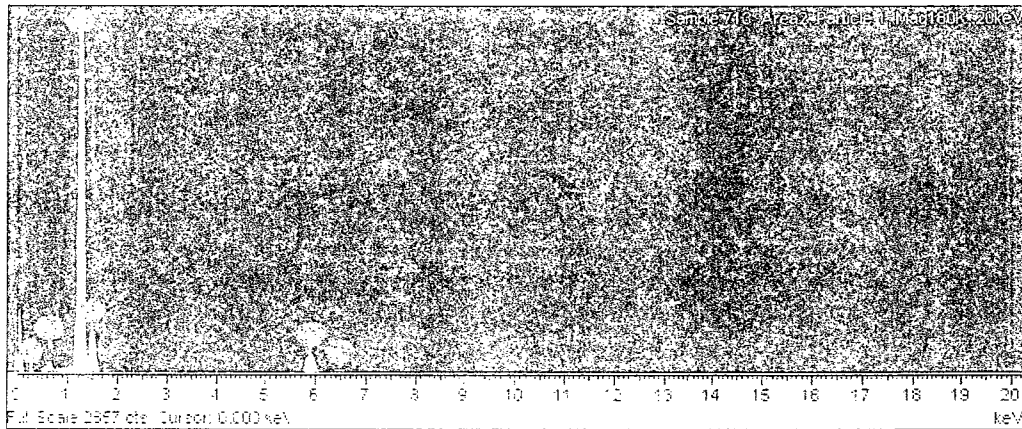
b) EDX analyses of point 2 of Figure 4.23

Figure 4.24 - SEM micrograph and EDX analysis of intermetallics in AZ31-B strip

EDX analysis demonstrated in the associated spectra indicates that the phases contain Mg, Zn, Al and Mn. The presence of magnesium in the spectra could originate from either the matrix or the intermetallics.

Based on the information from phase diagram the matrix is α-Mg, and the particles are Mg-Al-Zn phase (mostly likely $(Al,Zn)_{49}Mg_{32}$) and Al-Mn (it could be a mixture of $Al_{11}Mn_4$, Al_8Mn_5, Al_9Mn_{11} and β-Mn(Al)) intermetallics. However, α-Mg is Mg-Al-Zn-Mn solid solution. The above phases have been previously reported by Cao et al.[102]. To identify these phase precisely, further investigations using X-Ray techniques are necessary.

4.4. Mechanical properties:

According to the explanation given in the microstructure section 4.3, as the heat flux increases the proportion of secondary phase decreases. As the flux decreases, the secondary phases have more time to precipitate and grow.

Figure 4.25 and Table 4.5 summarize the mechanical properties of the AZ31-B strips. The tensile and yield strength are calculated using equations 3.1 and 3.4.

Vickers hardness was obtained for all cross section areas. The hardness of the top and bottom surfaces was the same because of the small thickness of the strips.

102
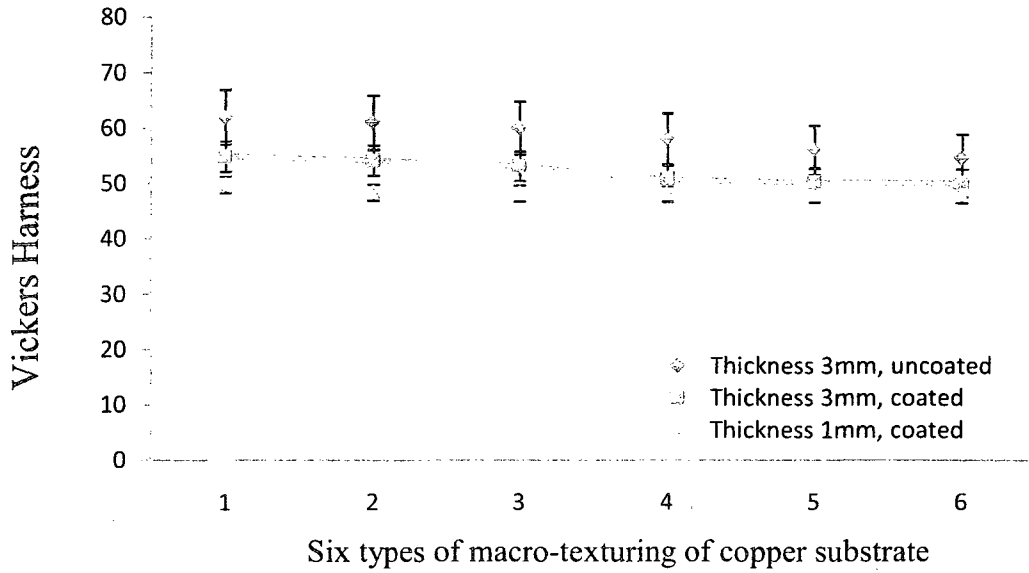
Figure 4.25 – The effect of heat flux on the mechanical properties of AZ31-B strips in different heat flux.

Table 4.5. Mechanical properties of AZ31-B strips.

Substrate No	Depth of Groove (mm)	Thickness	Coating	Heat Flux	R_c W/m² °C ×10⁻⁴	HV	YS MPa	TS MPa
III (c)	0.15	3mm	No	6.6	4.545	62	147	166.6
II (b)	0.09	3mm	No	5.77	5.195	61	144	163.2
IV (d)	0.24	3mm	No	5.17	5.797	60	144	163.2
I (a)	0	3mm	No	5.06	5.927	58	141	159.8
V (e)	0.3	3mm	No	4.37	6.857	56	138	156.4
VI (f)	0.6	3mm	No	3.35	8.955	54.5	135	153
III (c)	0.15	3mm	Yes	3.5	8.571	54.9	135	153
II (b)	0.09	3mm	Yes	3.2	9.375	54.2	135	153
IV (d)	0.24	3mm	Yes	2.9	10.345	53.1	132	149.6
I (a)	0	3mm	Yes	2.85	10.526	50.7	141	159.8
V (e)	0.3	3mm	Yes	2.5	11.628	50.2	141	159.8
VI (f)	0.6	3mm	Yes	2.5	12.000	50	141	159.8
III (c)	0.15	1mm	Yes	2.5	4.000	49.8	126	142.8
II (b)	0.09	1mm	Yes	2.33	4.292	48.4	126	142.8
IV (d)	0.24	1mm	Yes	2.16	4.617	48.2	126	142.8
I (a)	0	1mm	Yes	2.12	4.717	48.1	126	142.8
V (e)	0.3	1mm	Yes	1.83	5.464	48	126	142.8
VI (f)	0.6	1mm	Yes	1.72	5.814	47.9	123	139.4
I	0 (Steel)	3mm	No	1.2	25.000	47.5	123	139.4
I	0 (Steel)	3mm	Yes	0.71	42.254	47	123	139.4

Based on the experimental results presented above, as the heat flux increases and decreasing thermal contact resistance between the strip and substrate, the hardness and other mechanical properties were slightly reduced.

In the case of 1m thickness, because of small amount of the weight pressure of the strip on the substrate, thickness of air gap between strip and substrate was increased and heat transfer rate from strip to substrate was decreased.

Based on the less global heat fluxes which represent as an area under the curve, in strips with 1 mm thickness grain sizes were big and mechanical properties were lower than the cases which have small grain size. This issue was presented in detail in section 4.3.1.

4.5. Evaluation of black surface layer on the strips:

To protect the magnesium alloys from oxidation during casting, a mixture of CO_2 and SF_6 is usually used. Otherwise, a layer of black coating forms on the surface of the strip as shown in Figure 4.26.

Figure 4.26 - Black layer of coating on strip cast without protective atmosphere.

To evaluate this layer, it was collected and analyzed by the XRD as shown in Figure 4.27.
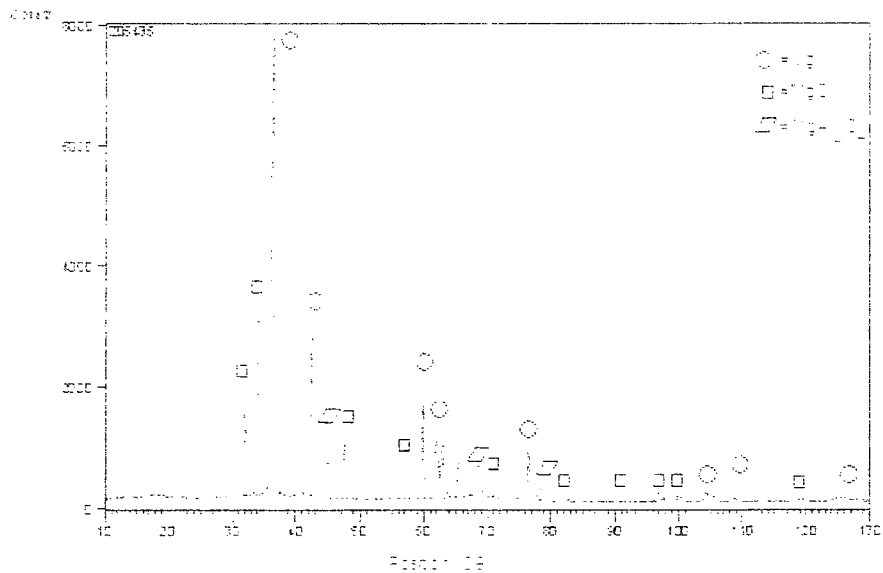
Figure 4.27- XRD pattern of black layer

Also Figure 4.28(a,b) illustrates SEM and EDX analysis of this layer.
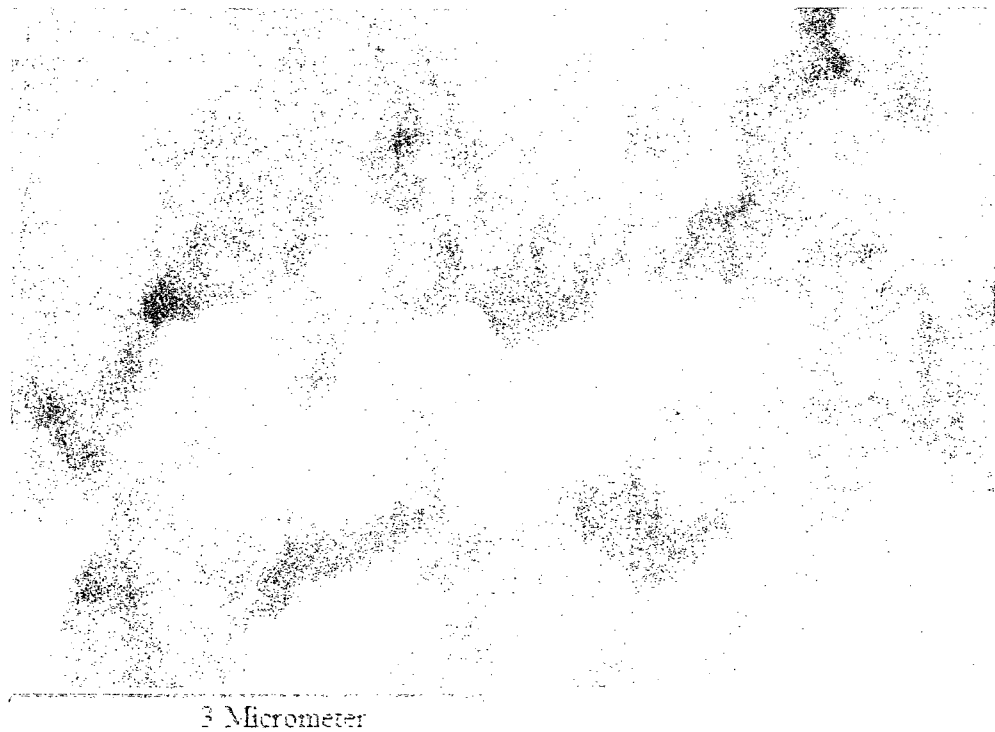
a) SEM image of the black layer
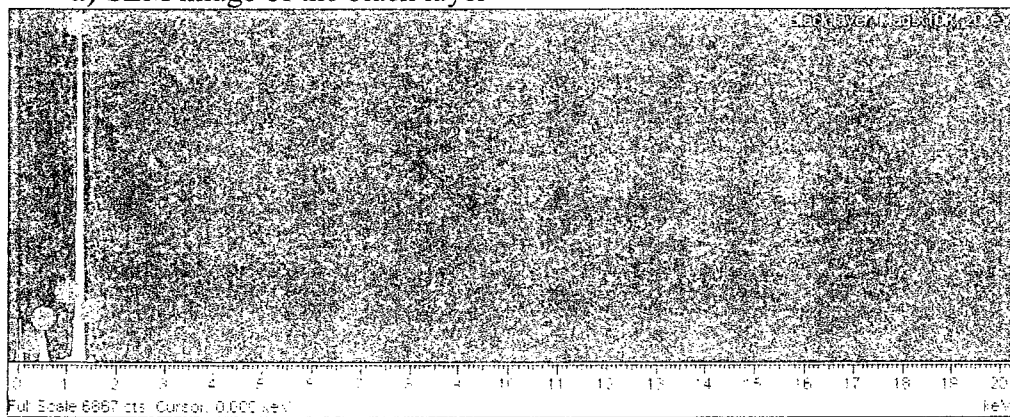
b) EDX analysis of the black layer

Figure 4.28 – SEM and EDX analysis of the black layer

It is well known that, in normal conditions, MgO is white and $MgAl_2O_4$ is colorless.

According to XRD and EDX patterns, the major component of the layer on the strip is

106

MgO. As shown in the SEM image, the particle sizes of MgO are around 0.1 μm. The particle size of the oxide is so small that it acts as a light trap and appears black[103-106].

It should be noted that Mg peaks in the XRD and EDX patterns emanated from the base metal, not from the thin black layer of MgO particles forming on top of the cast strip.

CONCLUSIONS

The heat transfer and parameters related to solidification have a great effect on the quality of strips cast on the horizontal single belt casting simulator. In the present study, the effects of different parameters on the properties of strips of AZ31-B alloy have been investigated. The effect of heat flux on the microstructure and mechanical properties was studied. The following conclusions can be drawn:

> Heat flux into the copper substrates were higher than that into steel substrates.

> Heat fluxes into coated substrates were lower than that into non-coated substrates.

> As substrate roughnesses increased beyond 0.15 mm for grooved substrates, thermal contact resistance increased while heat fluxes decreased.

> Because of low thermal contact resistance in the 0.15 mm grooved substrate, highest heat flux was recorded in this area.

> Increasing thickness of strip developed contact surface between substrate and strip due to the increasing weight pressure of the strip on substrate. Heat flux into substrates was increased by developing contact between strip and substrate.

> As the interfacial heat flux increased, the grain size decreased.

> As the interfacial heat flux increased, the SDAS through the strip decreased.

➤ Decreasing the interfacial heat flux reduced the quality of the top surface of strip cast on the HSBC simulator, owing to deceleration and movement of semi-solid material remaining at end of stroke.

➤ As the roughness of the grooved substrates increased, the quality of the bottom surface of the strips was improved.

➤ Microhardness of the top and bottom of the strip have not changed significantly. Consequently, heat flux was uniform through the strip thickness, due to the small thickness of the strips. This resulted in nearly uniform mechanical properties across the strips' thickness.

➤ As the heat flux increased, the mechanical properties, TS, YS and HV increased due to the reducing grain size.

➤ The black layer on the strips is composed of small-particles of MgO (in the 100nm range).

Finally, strip casting of magnesium AZ31-B can be successfully achieved, if the parameters given above are taken into account.

CONTRIBUTIONS

This main goal of the research work was to investigate the effect of different parameters on heat flux at the melt/substrate interface for magnesium AZ31-B alloy using horizontal single belt casting simulator. The following is the main contributions to the knowledge made by this work:

- Effect of the substrate roughness and the top and bottom surface quality was established.

- The dependence of heat flux and subsequently physical and mechanical properties of strips on the surface roughness were also evaluated.

- Effect of strip thickness as well as graphite coating on the heat flux were established.

- The effect of heat flux on the surface quality and mechanical behavior of the strip were established.

- It was revealed that the black film formed coating without protective atmosphere on the strip top surface was MgO with fine particles size.

FUTURE WORK

More experimental work can be done to study:

- ➢ The effect of casting speed on heat flux for substrates with different roughnesses

- ➢ The effect of different coating on surface quality of cast strips.

- ➢ The effects of grain refinement on strips properties.

- ➢ The effect of the quality of the protective gas on surface quality.

- ➢ The effect of nozzle design on strip quality.

- ➢ The effect of coating thickness on heat flux.

REFERENCE:

[1].K.Schwerdtfeger: Benefitis,challenges and limits in new routes for hot strip production, ISIJ International 38, 1998, pp. 852-861

[2].C.Jeffeies: Modelling a novel thin strip continuous steel caster delivery system, PhD. Thesis, Mcgill University, 1998, pp. 1-15

[3].K.H.Spitzer, K.Schwerdtfeger: Production of steel strip with a single belt process, Iron and Steel Making, 1995, pp. 47-53

[4].W.R.Irving: Continuous casting of steel, The Institute of Material, Cambridge University press, 1993

[5].F.Horst, M.Barry: Magnesium technology, Springer-Verlag Berlin Heidelberg, 2006

[6].R.Guthrie, M.Isac: Steel in the context of near net shape casting production. Process Metallurgy, 2000, pp.1-8

[7].W.Rechelt, W.Kapellner: Near net shape casting of flat products, Metallurgical Plant and Technology, 1998, pp. 18-35

[8].B.Colleen, M.Gibson: Current wrought magnesium, JOM, Vol. 57, 2005, pp. 46-51

[9].I.Polmear: Light Alloys. Metallurgy of the light metals, 3rd Edition, Arnold, 1995

[10].A.Sean,Wrought magnesium: A 21st century outlook, JOM , 2004, pp. 20-21

[11].P.Chevalier: Canadian minerals yearbook, 1994, pp. 29.1-29.13

[12].W.Shair, K.McBeth: China's magnesium ingot prices drop below cost level-producers: Journal Platts Metals Week, Vol. 79, No. 44, 2008, pp. 2-3.

[13].W.Shair, K.McBeth: Chinese magnesium ingot slides further on falling demand: Journal Platts Metals Week, Vol. 79, No. 42, 2008, pp. 12-13.

[14].R.L.Edgar, Hydro magnesium, Brussels: Global overview on demand and applications for magnesium alloys, Magnesium alloys and their applications, Edited by K. U. Kainer, Wiley-Vch Verlag GmbH, 2000, pp. 3-9

[15].H.Westengen: Current trends in magnesium alloy development, Science and Engineering of Light Metals. Japan Institute of Light Metals, Tokyo, 1991, pp. 77–84

[16].K.U.Kainer: Magnesium alloys and technology, Willey–Vch Verlag GmbH & Co. Weinheim, 2003

[17].F.Czerwinski: Magnesium Injection Moulding, Springer Science, 2008, pp.6-9

[18].W.Lingyun, L.Zhiwen, Z.Yazhong, Q.Xiaogang: The formablity of AZ31B magnesium alloy sheet, Journal of Wuhan University of Technology - Mater. Sci. Ed., Vol. 21, No.2, 2006, pp. 25-27

[19].B.L.Mordike, T.Ebert: Magnesium properties–applications-potential, Mater. Sci. Eng., A302, 2001, pp. 37–45.

[20].I.Jung, W.Bang, I.Kim, I.Sung, P.Hwan-Jin, C.Woo-Jin, S. Aim: Mg coil production via strip casting and coil rolling technologies: Magnesium Technology 2007 as held at the 2007 TMS Annual Meeting, 2007, pp. 85-88

[21].H.Friedrich, S.Schumann: Research for a new age of magnesium in the automotive industry, J. Mat. Pro. Tech, No.17, 2001, pp. 276-281

[22].H.Hu, A.Yu, N.Li , J.Allison: Potential magnesium alloys for high temperature die cast automotive applications, a review. Mat. and Man. Proc., Vol.18, No.5, 2003, pp. 687-717.

[23].E.Vinarcik: Opportunities for magnesium sheet in automotive lightening, Light Metal Age. Vol. 62, 2004, pp. 56-57

[24].F.Hassan, B.Amrani: Structural electronic and thermodynamic properties of magnesium chalcogenide ternary alloys, J. Phys., 2007, pp. 9

[25].A.Stalmann, W.Sebastian, H.Friedrich, S.Schumann, K.Droder: Properties and processing of magnesium wrought products for automotive applications, Adv. Eng. Mat., Vol. 3, No.12, 2001, pp. 969-974.

[26].T.Kameko, M.Suzuki: Automotive Applications of magnesium alloys, Mat. Sci. Foru. Vol. 419-422, 2003, pp. 67-72

[27].A.Luo: Wrought Magnesium alloys and manufacturing processes for automotive applications, SAE Transactions: J. of Mat. and Man., Vol. 114, 2006, pp. 411-421

[28].A.Luo: Wrought magnesium alloys and manufacturing processes for automotive applications, Magnesium Technology 2007 as held at the 2007 TMS Annual Meeting 2006, pp. 333-339

[29].R.Gradinger, P.Stolfig: Magnesium wrought alloys for automotive applications, Magnesium Technology 2003 as held at the 2003 TMS Annual Meeting, pp. 231-236

[30].E.Doege, K.Droder: Sheet metal forming of magnesium wrought alloys formability and process technology, J. of Mat. Proc. Tech.,Vol,115, 2001, pp. 14–19

[31].S.Kruse: Fair fight for the light weights, Eng. Cast. Solut., 2006, pp. 24-28

[32].R.Gradinger, P.Stolfig: Magnesium wrought alloys for automotive applications., Magnesium Technology 2003, TMS Annual Meeting, San Diego, CA, USA, 2003, pp. 231-236S

[33].S.Park, J.Lee, H.Lee, N.Kim: Development of wrought Mg alloys via strip casting, Magnesium Technology 2004, TMS Annual Meeting, Charlotte, NC, USA, 2004, pp. 107-112

[34].J.Colleen: Current wrought magnesium alloys: Strengths and weaknesses, JOM., Vol. 57, No. 5, 2005, pp. 46-49

[35].J.Edward, C.Vinarcik: Opportunities for magnesium sheet in the automotive lightening, J.Light Met. Age , 2004, pp. 56-57

[36].S.Yogeshwar, G.Manish: Simulation and analysis of thin strip casting processes, International conference of IEEE, 1999, pp. 119-127

[37].B.Engl: A New Technology for magnesium sheet production, J.Light Met. Age, Vol. 63, 2005, pp. 14-19

[38].K.Kammer: Continuous casting of aluminium, TALAT lecture, European aluminium association, 1999, pp. 2-10

[39].L.Daniel: Magnesuim alloys sheet and its productions, AU patent 2003/001243, 2003

[40].N.Zapuskalov: Comparison of continuous strip casting with conventional production, ISIJ International, Vol. 43, 2003, pp. 1115-1127.

[41].J.Dong-ying, H.Xiao-dong: Effect of casting parameters and deformation on microstructure evolution of twin-roll casting magnesium alloy AZ31, Trans. Nonfer.Met.Soc. China, Vol. 16, 2006, pp. 874-877

[42].D.Liang, C.Cowley: The twin roll strip casting of magnesium, JOM, 2004, pp. 26-28

[43].D.Kim, H.Ryu, I.Kim, K.Cho, T.Nam, K.Kim, J.Ahn: Electrochemical properties of magnesium electrolyte with organic solvent, J.Phy. Sci, 2007, pp. 70-73

[44].K.Moon: Physical and mathematical modeling of a metal delivery system for a single belt caster, PhD thesis, McGill University, 2003

[45].S.Kiyoshi, O.Michiharu: Strip casting technology for steel, ISIJ International, Vol. 31, 1991, pp. 661-668

[46].W.Borbige, D.Liang: Magnesium alloy sheet and its production, AU patent, US2006231173, 2006

[47].P.Regan: Advances in aluminium strip casting and continuous rolling technology - implication for aluminium can body sheet production, J. Light Met, 1992, pp. 58-61

[48].H.Watari, T.Haga, Y.Shibue, K.Davey, N.Koga: Twin roll casting of magnesium alloys with high aluminium contents, J. of Ach. Mate. and Manuf. Eng. Vol.18, 2006, pp. 419-422

[49].George E. Totten, Kiyoshi Funatani, Lin Xie: Handbook of metallurgy process design, CRC, 2004

[50].K.Spitzer, F.Rappel, R.Viscoroval, R.Scholz, J.Flaxa: Direct strip casting (DSC) - an option for the production of new steel grades, Steel Research International, Vol. 74, No.11-12, 2003, pp. 724-731

[51].M.Isac, R.Tavares, P.Netto, R.Guthrie: The influence of solidification and heat transfer on microstructure for horizontal scrip casting of light metal alloys, Light Metals Conference, 1997, pp. 463473

[52].J.Kim, M.Isac, R.Guthrie, Casting strips of magnesium alloys AZ91 on a moving mould system, METSOC, 41 Annual Conference of Metallu. of CIM. Montreal, Ca, 2002, pp. 52-58

[53].K.Schwerdtfeger. H.Spitzer, J,Kroos. P.Funke. K.Hower: Further results from strip casting with the single-belt process, ISIJ International (Japan). Vol. 40, No. 8, 2000, pp. 756-764.

[54].J.Kim, M.Isac, R.Guthrie: Metal-mold heat transfer and solidification of magnesium alloys in belt casting processes, 2004 TMS Annual Meeting, Charlotte, NC, USA, 2004, pp. 247-255

[55].C.A.Muojekwu, I.V.Samarasekera, J.K.Brimacombe: Heat Transfer and microstructure during the early stages of metal solidification, Met.Trans., Vol.26B, No.2, 1995, pp. 361-382

[56].S.J.Chen, R.C.ren, A.A.Tesng: Interface heat transfer in metal casting on a moving substrate, J. Mat. Proc. and Manu. Sci, 1995, pp. 473-386.

[57].N.A.El Mahallawy, A.M.Assar: Effect of melt superheat on heat transfer coefficient for aluminum solidifying against copper chill, J . Mat. Sci. 1991, Vol.26, No.7, pp. 1729-1733

[58].M.Ferry: Direct strip casting of metals and alloys, Woodhead publication in materials, Cambridge, 2006. pp.137-142

115

[59].J.Campbell: Casting, Second edition, Elsevier Science, 2003, pp. 117-125

[60].P.Netto, R.Tavares, M.Isac, R.Guthrie: A technique for the evaluation of instantaneous heat fluxes for the horizontal strip casting of aluminum alloys, ISIJ Int., Vol. 41, No. 11, 2001, pp. 1340-1349.

[61].J.Kim: Interfacial heat transfer and solidification of Mg and Al alloys in single belt casting process, Ph.D Thesis, McGill University, Canada, 2006.

[62].J. Kim: Interfacial heat transfer of a single belt casting process, MEng. Thesis, McGill University, Canada, 2002.

[63].L.Strezov, J.Herberston, Experimental solidification studies of pertinent to interfacial strip heat transfer and initial casting, ISIJ International, Vol. 38,1998, No. 9, pp. 959-966

[64].Yunus A. Çengel, Heat and mass transfer a practical approach, McGraw-Hill College, 2006, pp 138-143

[65].K.Ho and R.D.Pehlke, Metal-mould interface heat transfer, Met. Trans. 16B, 1985, pp. 25-29

[66].S.J.Hitchcock, N.Carroll, M.Nicholas, Some effect of substrate roughness on wettability, J.Mate.Sci, 1981, Vol.16, No.3, pp. 714-23

[67].A.Ditze, K.Schwerdtfeger, Strip casting of magnesium with the single belt process, J.Metall.Scand, 2003. p.311-316

[68].J.V.Beck: Non liner estimation applied to the inverse heat transfer conduction problem, Int.J. Heat Mass Transfer 23, 1970, pp. 703-716

[69].M.Krishnan, D.G.R.Sharm: Detraction of the interfacial heat transfer coefficient h in unidirectional heat flow by Beck's nonlinear estimation produce, Int. Comm., Heat Transfer 23, 1996, pp. 203-214

[70].J.C.Hwang, H.T.Chuang, S.H.Jong, W.S.Hwang: Measurement of heat transfer coefficient at metal/mould interface during cating, AFS Trans. Vol.102, 1994, pp. 883-887

[71].P.Ashtari, K.Gatenby, M.Gallerneault: Influence of cooling rate on morphology and distribution of Fe-containing intel-metallic compounds in strip cast AA1100 type alloys, Mat. Sci. Foru. Vol. 519-521, 2006, pp. 1713-1720

[72].H.Palkowski, L.Wondraczek: Direct strip casting of magnesium, Zeitschrift fur Metallkunde. Vol. 95, No. 12. 2004, pp. 1080-1086

[73].H.Spitzer, K.Schwerdtfeger: Production of steel strip with a single belt process, Process Technology, Vol.13. 1995, pp. 20-26

[74].D.Li, S.Shabestari, M.Isac, M.Guthrie: Studies in the casting of AA6111 strip on a horizontal single belt, strip casting simulator, Conference of Light Metals 2006, pp. 851-857

[75].J.Kim, M.Isac, R. Guthrie, J.Byun: Studies of interfacial heat transfer resistances and characterization of strip microstructures for Al-Mg alloys cast on a single belt casting simulator, Canadian Metallurgical Quarterly, Vol. 41,No.1, 2002, pp. 87-96

[76].C.Hongmei, K.Suk, Y.Huashun, W.Hyoung, M.Guanghui: Microstructure and mechanical properties of Mg–4.5Al–1.0Zn alloy sheets produced by twin roll casting and sequential warm rolling, Mater. Sci. and Eng. A, Vol. 492, No.1,2008, pp. 317-326

[77].C.H.Caceres, J.Davidson, J.Griffiths, C.Netwon: Effect of solidification rate and aging on the microstructure and mechanical properties of AZ91 alloy, Material .Sci. and Eng., 2002,Vol.2, pp. 344-355

[78].D.Dube, A.Couture, Y.Carbonneau, M.fiset, R.Angers, R.Trembay: Secondary dendrite arm spacing in magnesium alloys AZ91D, Int, J.Cast Metals Res. 1998, pp.139-144

[79].W.Kurz, D.J.Fisher: Fundamental of solidification, Tras Tech Publications, 1989, pp. 257-259

[80].G.Dmitry: Physical metallurgy of direct chill casting of aluminium alloys, Taylor and Francis, 2008, pp.47-50

[81].K.Pettersern, O.lohne, N.Ryum: Dendritic solidification of magnesium alloy AZ91, J. of Metall. Mater. Trans.B, Vol.21, 1990, No.1, pp. 221-230

[82].R.Smallman, R. Bishop: Modern physical metallurgy and materials engineering, Butterworth-Heinemann, 1999, pp. 42-48

[83].H. Watari, T. Haga, N. Koga, K. Davey: Feasibility study of twin roll casting process for magnesium alloys, J. of Mat. Proc. Tech., Vol.192-193, 2007, pp. 300-305

[84].E.George, D.Totten, S.MacKenzie: Handbook of Aluminium, Vol.7, Physical Metallurgy and Processes, Willy, 2003

[85].ASM Handbook, Metallography and Microstructure, Vol. 9. ASM International, Materials Park, 1983

[86].D.Li, M.Isac, R.Guthrie: Improving the surface of AA6111 sheet materials cast at light speeds, roughness the use of macro quality textured substrate, 2009 TMS Conference , 2009, pp. 200-205

[87].D.Li, M.Isac, R.Guthire: Improving the surface of AA6111 sheet materials cast at light speeds, roughness the use of macro quality textured substrate, MMPC Annual report 2008. pp. 62-67

[88].K.Shae, J.Kim, Y.Lee: Development of AZ31 Mg alloy wrought process route without protective gas, J. of Mat. Proc. Tech., Vol.187-188, 2007, pp. 757-760

[89].E.Velasco, J.Talamantes, S.Cano, S.Valtierra, J.F.Mojica , R.Colas: Casting-Chill interface heat transfer during solidification of an aluminium alloy, Met. Trans, 1999, pp. 773-778.

[90].Metals Handbook, Mechanical Testing and Evaluation, ASM, Vol.8, 1992, pp. 109-110

[91].J.Wang, M.Liang, Q.Kuang, M.Gurvan, G.Chen, K.Xia: Microstructural and mechanical properties of alloy AZ31 equal channel angular pressing, Mat. Sci. Forum, Vol.29, No.2, 2005, pp. 370-375

[92].M.Ashby, R.David: Engineering materials, Butterworth-Heinemann, 2002, pp. 87-88

[93].G.Dieter, B.David: Mechanical metallurgy, McGraw Hill, 1998, pp. 330-331

[94].R.Samuel: Rockwell hardness measurement of metallic materials, NIST, 2003, pp. 12-15

[95].J.Karki: Active Low-Pass filter design, Application Report Texas Instrument, 2002, pp. 30-37

[96].Shlomo Engelberg: IIR Filter design using MATLAB ,Springer London, 2008, pp. 23-24

[97].J.P.Holman: Heat transfer, McGraw-Hill, 1986, first edition, pp. 10-20

[98].M.Warren, J.Rohsenow, Y.Hartnett, C.Cho: Handbook of heat transfer, McGraw Hill, 1998, pp. 99-100

[99].J.Lienhard: A heat transfer textbook, McGraw-Hill, New York, 3rd edition, 1998, pp. 12-15

[100].M.Rappaz, C.Gandin: Probability modeling of microstructure formation in solidification process, Acta Metall. Mater. Vol.41, 1993, pp. 345-360.

[101].F.Vander: Metallography and microstructures, Materials Park, Vol. 9, ASM International. 2004, pp. 300-302

[102].P.Cao, D.Stjohn, M.Qian: The effect of manganese on the grain size of commercial AZ31 alloy. Mat. Sci. Forum., 488-489, 2005, pp.139-142.

[103].I.Berman, V.i.Zalesskii, Kh.I.Imanov, V.A.Sheiamov: Effect of the degree of deformation the mechanical properties and structure of extruded semifinished products from granules of aluminum alloys of the system Al-Zn-Mg-Cu, J. of Powder Meta.and Metal. Ceramics, Vol.8, 1969, pp. 14-18

[104].I.K.Ludow: Symmetry of a color center in magnesium oxide, J. of Solid State Physics Division, Vol.88, No.3, 1966, pp. 763-770

[105].Mark A.Shand: The chemistry and technology of magnesia, John Wiley & Sons, 2006, pp. 201-202

[106].B.Haxby: A study of color centers in magnesium-oxide, Thesis PhD, University of Minnesota, 1957, pp. 50-57

```
      CHARACTER ARQ*30,XIMP*30
        DOUBLE PRECISION A(2001),B(2001),C(2001),D(2001),T(2001),
       *TUSE0(2001),
       *Q1R(2001),QR(2001),TUSE1(2001),TUSE2(2001),TUSE3(2001),
       *TRT1(2001),qcomp(2001),
       *TRT2(2001),TIME(2001),POS(2001),K,Q2(2001),Q1(2001),C1,C2,
       *C3,CR,CC,DC
        REAL TIMEX(2001)
        WRITE(*,1047)
 1047 FORMAT(5X,'ENTER THE NAMES OF THE FILES FOR :',/,8X,'-
 TEMPERATURE
       * READING ',//,8X,'- RESULTS : HEAT FLUX')
        READ(*,1048)ARQ
 1048 FORMAT(A30)
        READ(*,1048)XIMP
        write(*,1048)ximp
        OPEN(8,FILE='PROP.DAT',STATUS='unknown')
        WRITE(*,629)
 629  FORMAT(10X,'WHICH KIND OF COORDINATES DO YOU WANT TO USE
 ?',/,
       *15X,'[0]RECTANGULAR',/,15X,'[1]CYLINDRICAL',/,15X,'[2]ESPHERICAL'
       *)
        READ(*,*)S
        READ(8,*)RE,RI,CP,K,RO
        ENDFILE 8
        CLOSE(8,STATUS='KEEP')
        WRITE(*,1)RE,RI,CP,K,RO
```

```fortran
1    FORMAT(10X,'PROPERTIES AND CHARACTERISTICS OF THE
SYSTEM',//,10X,
     *'EXTERNAL RADIUS(M) = ',F7.5,/,10X,'INTERNAL RADIUS (M) = ',F7.5,
     */,10X,'SPECIFIC HEAT (J/KG.K) = ',F8.2,/,10X,'HEAT CONDUCTIVITY (
     *W/M.K.) = ',F8.2,/,10X,'DENSITY (KG/M3) = ',F8.2,//)
15   CONTINUE
     WRITE(*,2)
2    FORMAT(10X,'DO YOU WANT TO CHANGE ANY OF THESE DATA ? Y[1]
N[2]')
     READ(*,*)ICH
     IF(ICH .EQ. 1)GOTO 3
     IF(ICH .EQ. 2)GOTO 4
     GOTO 15
3    WRITE(*,5)
5    FORMAT(10X,'ENTER THE PROPERTIES ABOVE IN THE SAME SEQUENCE
AND SE
     *PARATED BY COMMA ')
     READ(*,*)RE,RI,CP,K,RO
     OPEN(8,FILE='PROP.DAT',STATUS='unknown')
     WRITE(8,*)RE,RI,CP,K,RO
     ENDFILE 8
     CLOSE(8,STATUS='KEEP')
4    CONTINUE
     WRITE(*,12)
12   FORMAT(/,10X,'ENTER THE NUMBER OF NODES N - UP TO 100')
     READ(*,*)N
     DO40I=1,N
     POS(I)=(FLOAT(I-1)*(RE-RI)/FLOAT(N-1)+RI)*1000.
40   CONTINUE
     WRITE(*,29)
```

```fortran
29  FORMAT(10X,'SELECT THE POSITION OF THE SECOND
THERMOCOUPLE',/,12X,
   *'ACCORDING TO THE FOLLOWING TABLE: ',/,10X,'NODE NUMBER-
DISTANCE
   *TO THE CENTER')
   WRITE(*,41)(I,POS(I),I=1,N)
41  FORMAT(5(3X,I3,2X,F8.4))
   READ(*,*)NTC2
   WRITE(*,13)
13  FORMAT(/,10X,'ENTER THE NUMBER OF TEMPERATURE READINGS')
   READ(*,*)NREAD
   WRITE(*,6)
6   FORMAT(/,10X,'ENTER THE NUMBER OF TIME STEPS BETWEEN TWO
READINGS'
   *)
   READ(*,*)NDIVT
   OPEN(7,FILE=ARQ,STATUS='unknown')
   DO7 I=1,NREAD
   READ(7,*)TIME(I),TRT1(I),TRT2(I),QR(I)
7   CONTINUE
      ENDFILE 7
   CLOSE(7,STATUS='KEEP')
   DELTAR=(RE-RI)/FLOAT(N-1)
   ALFA=K/(RO*CP)
   DO600I=1,N
   T(I)=TRT1(1)+(TRT2(1)-TRT1(1))/(POS(NTC2)-POS(1))*(POS(I)-POS(1)
   *)
600 CONTINUE
   TUSE1(1)=T(NTC2-1)
   TUSE0(1)=T(NTC2-2)
   TUSE2(1)=T(NTC2)
```

```
      DO9999J=2,NREAD
      DELTAT=(TIME(J)-TIME(J-1))/FLOAT(NDIVT)
      DO9999JX=1,NDIVT
      JCONT=(J-2)*NDIVT+JX
      TIMEX(JCONT+1)=TIME(J-1)+FLOAT(JX)*DELTAT
      Q1R(JCONT+1)=QR(J)
      FO=ALFA*DELTAT/(DELTAR*DELTAR)
      B(1)=(TRT1(J)*FLOAT(JX)+TRT1(J-1)*FLOAT(NDIVT-JX))/FLOAT(NDIVT)
      C(1)=0.
      D(1)=1.
      DO 16 I=2,NTC2
      D(I)=1.+2.*FO
      R=FLOAT(I-1)*DELTAR+RI
      A(I-1)=FO*(-1.+S*DELTAR/(2.*R))
      C(I)=-FO*(1.+S*DELTAR/(2.*R))
      B(I)=T(I)
   16 CONTINUE
      A(NTC2-1)=0.
      D(NTC2)=1.
      B(NTC2)=(TRT2(J)*FLOAT(JX)+TRT2(J-1)*FLOAT(NDIVT-
     JX))/FLOAT(NDIVT)
      CALL TRI(NTC2,A,D,C,B,T)
      TUSE2(JCONT+1)=T(NTC2)
      TUSE0(JCONT+1)=T(NTC2-2)
      TUSE1(JCONT+1)=T(NTC2-1)
 9999 CONTINUE
      DO50IM=1,JCONT
      Q1(IM)=-K*(3.*TUSE2(IM)-4.*TUSE1(IM)+TUSE0(IM))/(2.*DELTAR)
   50 CONTINUE
      DO2222I=NTC2,N-1
      JFIN=JCONT-(I-NTC2)-1
```

```
      DO1111JKK=2,JFIN
      JI=(JKK-2)/NDIVT+2
      JF=(JKK-1)/NDIVT+2
      DELTN=(TIME(JI)-TIME(JI-1))/FLOAT(NDIVT)
      DELTPO=(TIME(JF)-TIME(JF-1))/FLOAT(NDIVT)
      CC=DELTN/(DELTPO*(DELTN+DELTPO))
      DC=DELTPO/(DELTN*(DELTN+DELTPO))
      IF(S .NE. 0)GOTO 51
      CR=1.
      GOTO 52
 51   CONTINUE
      CR=((RI+FLOAT(I-1)*DELTAR)/(RI+FLOAT(I)*DELTAR))**(S)
 52   CONTINUE
      C1=DELTAR*CR/K
      C2=RO*CP*CR*DELTAR*DELTAR*CC/K
      C3=RO*CP*CR*DELTAR*DELTAR*DC/K
      Q2(JKK)=Q1(JKK)*CR-RO*CP*CR*DELTAR*(CC*(TUSE2(JKK+1)-
TUSE2(JKK))-
      *DC*(TUSE2(JKK-1)-TUSE2(JKK)))
      TUSE3(JKK)=TUSE2(JKK)*(1.-C2+C3)-C1*Q1(JKK)+C2*TUSE2(JKK+1)-
C3*TUS
      *E2(JKK-1)
1111 CONTINUE
      IF(I .EQ. N-1)GOTO 7777
      DO 555 JCA=2,JFIN
      TUSE2(JCA)=TUSE3(JCA)
      Q1(JCA)=Q2(JCA)
 555  CONTINUE
2222 CONTINUE
7777 CONTINUE
      DO556JCA=2,JFIN
```

124

```fortran
      Q2(JCA)=-Q2(JCA)
556   CONTINUE
      OPEN(15,FILE=XIMP,STATUS='unknown')
      DO 444 JCA=2,JCONT-(N-NTC2)
      WRITE(*,456)TIMEX(JCA),Q1R(JCA),Q2(JCA),TUSE3(JCA)
456   FORMAT(2X,F9.3,2X,2F14.2,2X,2F9.2)
      WRITE(15,456)TIMEX(JCA),Q1R(JCA),Q2(JCA),TUSE3(JCA)
444   CONTINUE
      ENDFILE 15
      CLOSE(15,STATUS='KEEP')
      END


      SUBROUTINE TRI(N,A,D,C,B,X)
      implicit DOUBLE PRECISION(a-h,o-z)
      dimension A(2001),D(2001),C(2001),B(2001),X(2001)
      DO2I=2,N
       XMULT=A(I-1)/D(I-1)
       D(I)=D(I)-XMULT*C(I-1)
       B(I)=B(I)-XMULT*B(I-1)
2     CONTINUE
      X(N)=B(N)/D(N)
      DO3I=N-1,1,-1
       X(I)=(B(I)-C(I)*X(I+1))/D(I)
3     CONTINUE
      RETURN
      END
```

```
%%%%%%%%%%%%%%%%%%%%%%%%%%%%%%%%%%%%%%%%%%
%      Low-Pass Filter Using in Materials Engineering Application      %
%         Ahmad Changizi ©, Mechanical Engineering Department      %
%            Concordia University, Montreal, Qc, Canada            %
%                     Version 1.0 - Oct.2008                       %
%%%%%%%%%%%%%%%%%%%%%%%%%%%%%%%%%%%%%%%%%%
y = importdata('data.txt');
t=size(y,1);
p=t+30;
i = 1:1:p;
x = 1:1:t;
b = 0.2*sinc(0.2*(-15:15));
z = b.*hamming(31);
u = conv(z,y);
for w=1:15
    u(w)=0;
end
for h=1:size(u,1)
    l=h+15;
    e(h)=u(h);
end
figure(1);
plot(x,y)
figure(2);
plot(i,e)
fid = fopen('filter.xls','w');
    fprintf(fid,'%6.2f \n',e);
    fclose(fid);
```